Scholars' Mine

Spring 2015

Dissolution of borate glasses and precipitation of phosphate compounds

Jaime Lynn George

DISSOLUTION BEHAVIOR OF BORATE GLASSES AND PRECIPITATION OF
PHOSPHATE COMPOUNDS

by

JAIME LYNN GEORGE

A DISSERTATION

Presented to the Faculty of the Graduate School of the

MISSOURI UNIVERSITY OF SCIENCE AND TECHNOLOGY

In Partial Fulfillment of the Requirements for the Degree

DOCTOR OF PHILOSOPHY
in
MATERIALS SCIENCE AND ENGINEERING
2015

Approved by

Richard K. Brow, Advisor
Delbert E. Day
William G. Fahrenholtz
Mark E. Schlesinger
David J. Wronkiewicz

PUBLICATION DISSERTATION OPTION

This dissertation is compiled in the format that consists of four papers for publication in peer-reviewed journals. A statement of research objective and a review of the literature are included as a foreword. A statement on the impact of the work and suggestions for future work are included as an afterword. The first paper, "In-situ characterization of borate glass dissolution kinetics by μ-Raman spectroscopy," will be submitted for publication in the *Journal of Non-Crystalline Solids*. The second paper, "Dissolution of a bioactive borate glass under static conditions," and the third paper, "*In-vitro* dissolution of a bioactive borate glass under dynamic conditions," will be submitted for publication in the *Journal of Non-Crystalline Solids*. The fourth paper, "Nanocrystalline rare earth phosphates from glass dissolution and precipitation reactions," has appeared in the *Journal of the American Ceramic Society*, volume 97, issue 7, pages 1-7, April 2014.

ABSTRACT

Borate glasses have been developed for biomedical applications such as scaffolds for soft tissue and bone repair. The dissolution processes of borate glasses in phosphate-containing aqueous solutions were studied by μ-Raman spectroscopy which provided information about the types and concentrations of borate species released into the solution as a function of time and characterized the formation of calcium phosphate reaction products on the glass surface. Boric acid molecules (H_3BO_3) and borate anions ($B(OH)_4^-$) can be detected in solution and their relative concentrations depend on the solution pH.

Static and dynamic single-pass flow-through experiments were employed to study the dissolution kinetics of a borate bioactive glass 13-93B3 in water, simulated body fluid (SBF), and other solutions. As the glasses react, B-, Ca-, Na-, K-, Mg-, and P-species were released from the glass and a magnesium-containing amorphous calcium phosphate (ACP) or hydroxyapatite (HAP) layer formed on the surface of the glass. The formation of crystalline hydroxyapatite was favored with faster flow rates, longer reaction times, and increased phosphate concentration in solution. Under static conditions, the dissolution rates are initially described by a reaction-controlled model (linear kinetics), but after the glass is ~25-30% reacted, a diffusion-controlled model (parabolic kinetics) better describes the dissolution rates. The change in reaction mechanism is attributed to the diffusion of species from the glass through the ACP layer. The activation energy for the reaction-controlled process is 41.1±0.6 kJ/mol, whereas the activation energy for the diffusion process is 32.3±0.1 kJ/mol. For the SPFT experiments, glasses dissolved faster under faster flow rates and smaller glass volumes. The ion release rate was calculated and found to range from $1.7x10^{-5}$ $g/m^2/s$ for slow flow rates to $1.1x10^{-3}$ $g/m^2/s$ for lower glass volumes.

ACKNOWLEDGEMENTS

I'd like to thank my advisor, Dr. Richard K. Brow for his guidance and support throughout this entire process. He has given me so many opportunities to learn about glass science and provided me with everything I need to succeed.

This work would not have been possible without the help of several undergraduate students: Colin Ryan, Michaela Kuzara, and Angela Grueninger are thanked for their role in this work. I'd also like to thank the members of the glass group, current and former, for being there to help in the lab and provide useful discussions. Lina, Xiaoming, Katie, Ali, Erica, Zea, Parker, Christian, Luciana, Raphael, and Rick, thank you for your friendship.

Finally, I'd like to help Eric Bohannan, Clarissa Wisner, Jessica Terbush, Brian Porter, and Ron Hass for the services and utilities they have provided to make my research possible.

TABLE OF CONTENTS

LIST OF ILLUSTRATIONS

BACKGROUND

PAPER I

LIST OF TABLES

1. RESEARCH OBJECTIVE

Borate glasses have been studied for biomedical applications such as scaffolds for soft tissue[1] or bone repair[2]. Some of these borate glasses have been shown to promote angiogenesis *in-vivo*, which assists with soft tissue repair.[3] It has been shown that boron plays a positive role in wound healing[4] and that boron coordination can have an effect on biological reactions,[5-7] but there is little information about the behavior of borate species released to solution following the dissolution of borate glasses. The goal of this work is to characterize the mechanisms and kinetics of the dissolution of borate glasses, including the nature of borate species in aqueous solutions, and understand the precipitation of phosphates on the surfaces.

Relatively little is known about the dissolution behavior of borate glasses, compared with the many studies of silicate glasses. Previous dissolution studies of borate bioactive glasses in phosphate solutions focused on weight loss rather than ion release,[8-10] and had to account for the simultaneous processes of glass dissolution and the precipitation of calcium phosphate reaction layer. Characterizing the release of ions into solution could be a better approach for a kinetic analysis of the dissolution of the glass network. Additionally, it is difficult to compare results between previous dissolution studies due to wide variance in experimental conditions.[11-21] This work will highlight how variations of experimental conditions can affect dissolution kinetics and reaction product formation.

The nature of the solution as borate glasses dissolve has received little attention. At biological pH (7.4 ± 0.2)[22], $B(OH)_3$ is the stable species in aqueous solution, and HPO_4^{2-} and $H_2PO_4^-$ are the stable phosphate species. As borate bioactive glasses dissolve,

for example in simulated body fluid, the solution pH increases, which would lead to greater amounts of HPO_4^{2-} and $B(OH)_4^-$.[23, 24] This work will address how borate and phosphate speciation changes with solution pH or glass composition.

In-vitro studies of the dissolution behavior of borate glasses have typically been analyzed independently of biological processes. In this study, a method has been developed to characterize dissolution of borate glasses *in-situ* with Raman spectroscopy. The technique allows for quantification of the type and concentration of borate and phosphate species as well as a spatially and temporally sensitive evaluation of pH as a function of distance from the glass surface or dissolution time. The technique can also be used to monitor formation of reaction products on the glass surface or changes in the glass structure. This method can be used in conjunction with other Raman techniques to evaluate cell health *in-vitro*[25, 26] or bone growth *in-vivo*[27].

Characterization of the formation of phosphate compounds from dissolving borate glasses in phosphate-containing solutions is also a focus of the current work. It has been shown that Ca-containing borate glasses that dissolve in phosphate-containing aqueous solutions will precipitate calcium phosphate reaction layers.[9, 28] Fu showed that by adjusting the glass composition or reaction parameters, the size and thickness of the resulting calcium phosphate layer could be controlled.[20] Conzone was able to precipitate $DyPO_4$ microspheres from a Dy_2O_3-Li_2O-B_2O_3 glass reacted in a phosphate solution.[18] In the present work, glasses containing Ca and P are dissolved in water and it is shown that an amorphous calcium phosphate (ACP) layer precipitates on the glass surface, even without phosphate anions initially present in the reaction solution. The development of this ACP layer changes the reaction kinetics from reaction-controlled (linear with time) to

diffusion-controlled (linear with the square root of time) under static conditoins. Additionally, lanthanide solid solutions have been formed from a glass containing two lanthanide elements, La and Eu, using Conzone's method.

2.   BACKGROUND INFORMATION

Hench originally demonstrated the ability of a Ca-containing silicate glass to bond to tissue, leading to the development of a new class of bioactive materials.[29] Since then, borate glasses, which are known to have faster dissolution rates than silicate and borosilicate glasses, have been investigated for biomedical applications ranging from arthritis treatments to promoting bone growth to wound healing.[1, 3, 9, 30, 31]

2.1.   DISSOLUTION OF SILICATE AND BOROSILICATE GLASSES

In silicate glasses, the addition of modifying oxides such as Na_2O breaks the cross-linked silicate network and creates non-bridging oxygens (NBOs). The silicate network is resistant to attack against water, hydrolysis, which breaks network bonds (Equation 1).

$$\equiv Si\text{-}O\text{-}Si\equiv + H_2O \rightarrow \equiv Si\text{-}OH + HO\text{-}Si\equiv \tag{1}$$
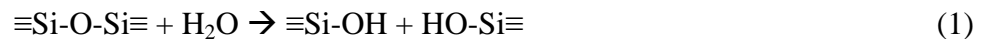
As modifiers are incorporated into the glass network, hydration, or leaching of modifying ions out of the glass occurs (Equation 2).

$$\equiv Si\text{-}O^- Na^+ + H_2O \rightarrow \equiv Si\text{-}OH + Na^+ + OH^- \tag{2}$$
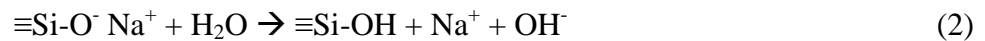
The overall dissolution is accompanied by diffusion of water into the glass, hydration of metal-ion bonds, diffusion of metal-ions out of the glass, and hydrolysis of network bonds. For silicate glasses, ion-exchange, or hydration, occurs faster than network hydrolysis, which leads to selective leaching of the modifier ions out of the glass and hydrogen ions into the glass. The selective leaching can lead to a concentration

gradient of modifier cations at the glass surface, shown in Figure 2.1.[32] The leaching rate depends on the type of modifier. In alkali silicate glasses, chemical durability increases in the order of $K^+<Na^+<Li^+$, suggesting that field strength and free energy of hydration affect glass dissolution rates.[33, 34] Alkaline earth cations increase the durability due to their high field strength and lower mobility than alkali ions.[33] The addition of Al_2O_3 reduces the number of NBO, increasing the network connectivity and increasing durability due to a decrease in the hydrolysis rate.[35]

Additionally, the alkali-depleted hydration layer can repolymerize to form a silica gel layer made of siloxane groups, shown in Equation 3.

$$\equiv Si\text{-}OH + HO\text{-}Si\equiv \rightarrow \equiv Si\text{-}O\text{-}Si\equiv + H2O \tag{3}$$
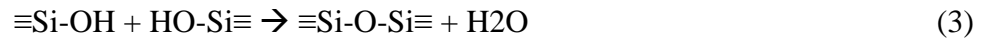
This gel layer can provide some corrosion resistance, which has been observed in silicate bioglasses.[15] In silicate glasses, the release of silicate species into solution increases as pH increases, shown in Figure 2.2.[33] As the [OH⁻] in solution increases, repolymerization of the siloxanes is less favorable, so the protective silica gel layer is no longer forming at high pH. Additionally, the solubility limit of silica increases at higher pH, leading to a decrease in glass durability at basic pH values.[36]
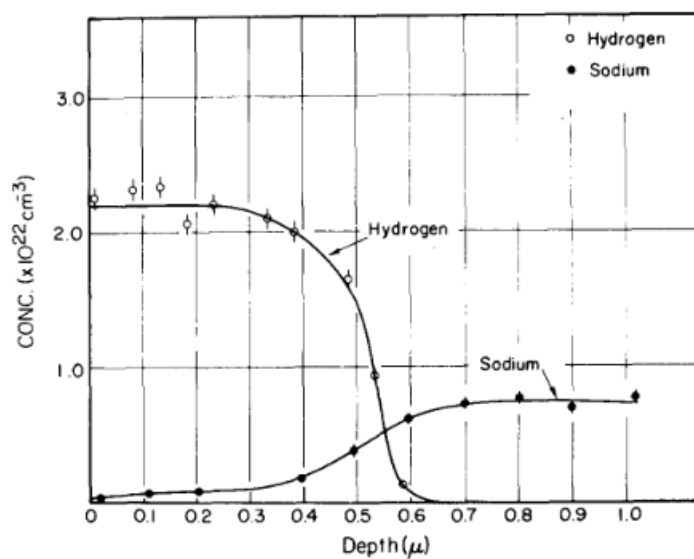
Figure 2.1. Concentrations of hydrogen and sodium near the glass surface of soda lime silicate after dissolution in water at 90°C for 560 h.[32]
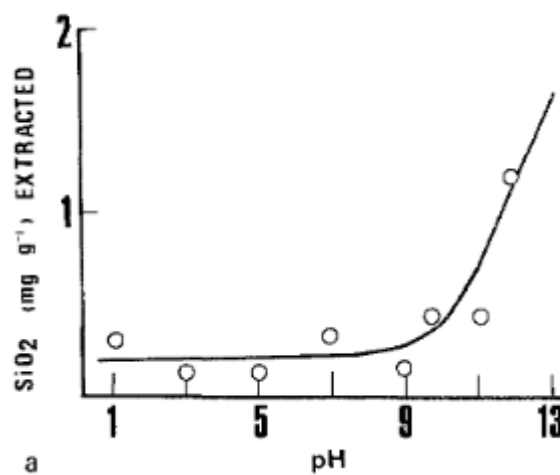
Figure 2.2. Effect of pH on the rate of extraction of SiO_2 from fused silica powder at 90°C.[33]

In borosilicate glasses, chemical durability decreases as (Na+B)/Si content of the glass increases.[37] Bunker et al. studied the relationship between structure and dissolution rate for sodium borosilicate glasses where the soda and borate contents were systematically varied.[38] In high-alkali borosilicate glasses, the formation of NBOs on the silicate network decreases durability in the same manner as they do for alkali silicate glasses. For the glasses studied by Bunker, et al., when the B_2O_3 content is high (B:Na>2), the glasses will phase separate into a sodium borate phase and a silica-rich phase. The sodium borate phase readily dissolves in water, resulting in faster glass dissolution.[38] Borosilicate glasses with greater fractions of 4-coordinated boron incorporated into the silicate structure have the lowest dissolution rates in water.[38] Density functional theory and molecular dynamics have been used to study reactions between water and borate units in borosilicate glasses.[39, 40] When a proton replaces a Na^+ ion on a $B\emptyset_4^-$ site, the 4-coordinated borate unit becomes unstable and a bridging oxygen (Ø) is broken to form a trigonal borate unit, shown in Equation 4.[40]

$$Na^+ [B\emptyset_4]^- + H_2O \rightarrow H^+ [B\emptyset_4]^- + NaOH \rightarrow B\emptyset_2OH + Na^+ + OH^- \qquad (4)$$

Both tetrahedral and trigonal borate sites in borosilicate networks are more susceptible to attack in acidic (protonated) environments than in neutral or basic environments.[39] Borosilicate glasses dissolved in acidic solutions release Na and B to solution at faster rates than Si, whereas borosilicate glasses dissolved in basic solutions exhibit more uniform (congruent) ion release behavior. Since borate glass corrosion rates increases as pH decreases and silicate glass corrosion rates decreases as pH decreases, it is consistent that borosilicate glasses selectively leach Na and B at low pH but dissolve more congruently at high pH.[37]

2.2.   DISSOLUTION OF BULK BORATE GLASSES

Velez studied the dissolution kinetics of binary lithium borate glasses in water and pH = 7 buffer solution.[41] Weight loss measurements indicated that the dissolution of these borate glasses was linear with respect to time. In water and the K_2HPO_4/NaOH buffer solution, dissolution rates were lowest for glasses with 25-30% mole Li_2O, consistent with compositions with the greatest fraction of four-coordinated boron. In water, the glass with 30 mole% Li_2O had the slowest dissolution rate, followed by the glass with 20 mole% Li_2O, then the glass with 40 mole% Li_2O. The 40 mole% Li_2O glass dissolved fastest of the three, presumably due to the high number of non-bridging oxygens in the glass network. In buffered solution, the glasses with 20-25 mole % Li_2O had the slowest dissolution rate, shown in Figure 2.3. There was no effect of stirring the solution on the dissolution rate. The authors also found that dissolution rate is pH dependent. Glasses dissolved in water, which quickly buffer to pH=9-10 as the glasses dissolve, had a slower dissolution rate than glasses dissolved in pH-7 buffered solution. Therefore as the pH increases, glass durability also increases, which is consistent with Zapol's first principle calculations, where protonated attack of borate sites has a lower activation energy than neutral or deprotonated attack.[39] This is opposite of the effect that was seen in silicate glass corrosion studies where corrosion rates increase in more basic solutions.[42, 43] This difference is partially due to the inability of hydrolysis products in borate glasses to polymerize and form gels on the glass surface as they do in silicate glasses below a pH ~9 (Equation 3).
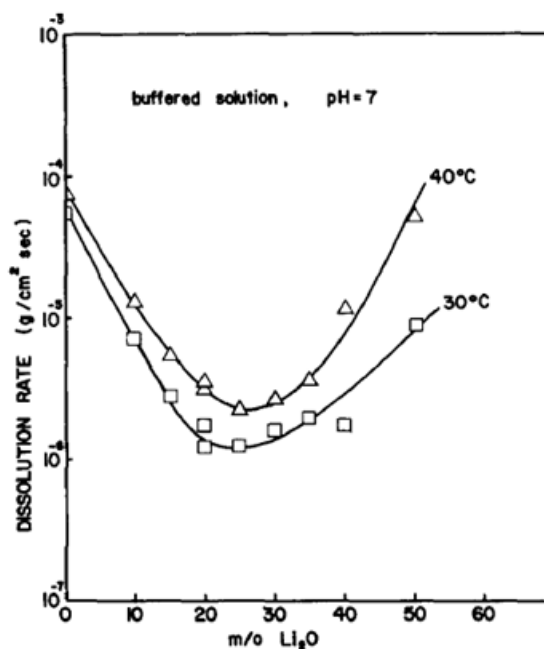
Figure 2.3. Dissolution rate of binary Li$_2$O-B$_2$O$_3$ glasses in buffered pH=7 solution at 30 or 40 °C, as reported by Velez *et al*.[41]

Lowry studied dissolution of calcium-containing alkali borate glasses in various solutions.[44] In that study, it was also found that the most durable glasses were those with the highest fraction of 4-coordinated boron in the structure. At short times (t < 120 min), weight loss is linear with respect to time for glasses with the molar compositions xNa$_2$O–xCaO–(100-2x)B$_2$O$_3$ (5 ≤ x ≤ 20) in water and in pH 4, pH 7, and pH 10 buffer solutions. For glasses where x ≤ 15, glasses dissolved faster at lower pH values, consistent with the results of Velez, et al.[41]

For Na-Ca-borate glasses, 60 mole% B_2O_3 glass dissolves more slowly than 80% B_2O_3 glass,[44] but in Li_2O-B_2O_3 glasses in water, 60% B_2O_3 dissolves faster than 80% B_2O_3.[41] This is likely due to greater amount of calcium in the 60 mole% B_2O_3 glass, which has a higher activation energy for hydration than lithium oxide.[45]

2.3. KINETIC ANALYSIS OF DISSOLUTION BEHAVIOR

The contracting volume model (CVM) and 3D diffusion models can be used to determine reaction rates of spherical particles in aqueous environments.[46] The CVM assumes a surface reaction-controlled mechanism where particles react with their surroundings and as the reaction progresses, the unreacted (untransformed) material uniformly decreases in size. The kinetic equation for the CVM is given in Equation 5,

$$k_{cvm}t = 1-(1-\alpha)^{1/3} \tag{5}$$

where α is the fraction of glass dissolved, t is time, and k_{cvm} is the reaction constant. The Jander 3D diffusion model assumes that the transformation reaction is limited by the diffusion of a species through a reaction product on the surface of the sphere, with a thicker reaction film producing a longer diffusion path. The equation for the 3D diffusion model is given in Equation 6, where k_{dm} is the diffusion-model reaction constant.

$$k_{dm}t = [1-(1-\alpha)^{1/3}]^2 \tag{6}$$

Kinetic analyses of the dissolution of the silicate bioactive glass 45S5 ($24.5Na_2O$-$24.5CaO$-$45SiO_2$-$6P_2O_5$, wt%) and three borosilicate and borate analogues, where 1/3, 2/3, and 3/3 of the SiO_2 mass in the base composition was replaced with B_2O_3, were

reported by Jung et al.[8]. Glasses were dissolved in 0.02 M phosphate solution at 37°C for times up to 1800 h[9] and reaction completion was determined by comparing observed weight losses to those expected if all the calcium in the glass reacted with phosphate in the solution to form hydroxyapatite. It was found that the borate analogue reached completion in 30h, whereas the silicate glass and borosilicate analogues reached a final weight loss less than the predicted theoretical weight loss. Each of the borosilicate samples had an unreacted core of silica remaining at the end of the experiments.

The dissolution of the borate analogue of 45S5 was found to follow the reaction-controlled CVM (Equation 5) over the entire reaction time. The borosilicate and silicate glasses followed the CVM through the first 30 hours and then deviated to the diffusion-controlled mechanism (Equation 6) for the remainder of the experiment. This change in mechanism was attributed to the diffusion of sodium and calcium ions through the silica gel layer that formed on the glass particles (Equation 3). These glasses were assumed for the kinetic analysis to dissolve congruently, but the unreacted glass core was Na- and Ca-depleted and Si-rich, indicating preferential release of certain species.[9] An additional complication associated with the weight loss analysis is the simultaneous formation of calcium phosphate and silica reaction layers.

A study of the conversion of Na_2O-CaO-B_2O_3 glasses to hydroxyapatite in 0.25 K_2HPO_4 was performed by Gu *et al.* at temperatures of 10-70 °C. A kinetic analysis was performed using weight loss measurements.[10] The $20Na_2O$-$20CaO$-$60B_2O_3$ (mole%) glass followed the CVM at 10, 22, and 37 °C, but at 70 °C, the reaction began with CVM kinetics and then at 70% completion, the dissolution kinetics were better described by the 3D diffusion model. Activation energies for dissolution of the glasses ranged from 32±8

to 36±5 kJ/mol, which are similar to activation energies measured for hydration of borate minerals.[47, 48]

2.4. DISSOLUTION BEHAVIOR IN DYNAMIC ENVIRONMENTS

The single-pass flow-through (SPFT) technique has been used to describe dissolution behavior of nuclear waste glasses in continuously flowing environments.[49-52] In an SPFT experiment, fresh media is flowed continuously over glass samples to study dissolution processes while reducing the effects of evolving solution conditions.[53] The experimental setup is shown in Figure 2.4.
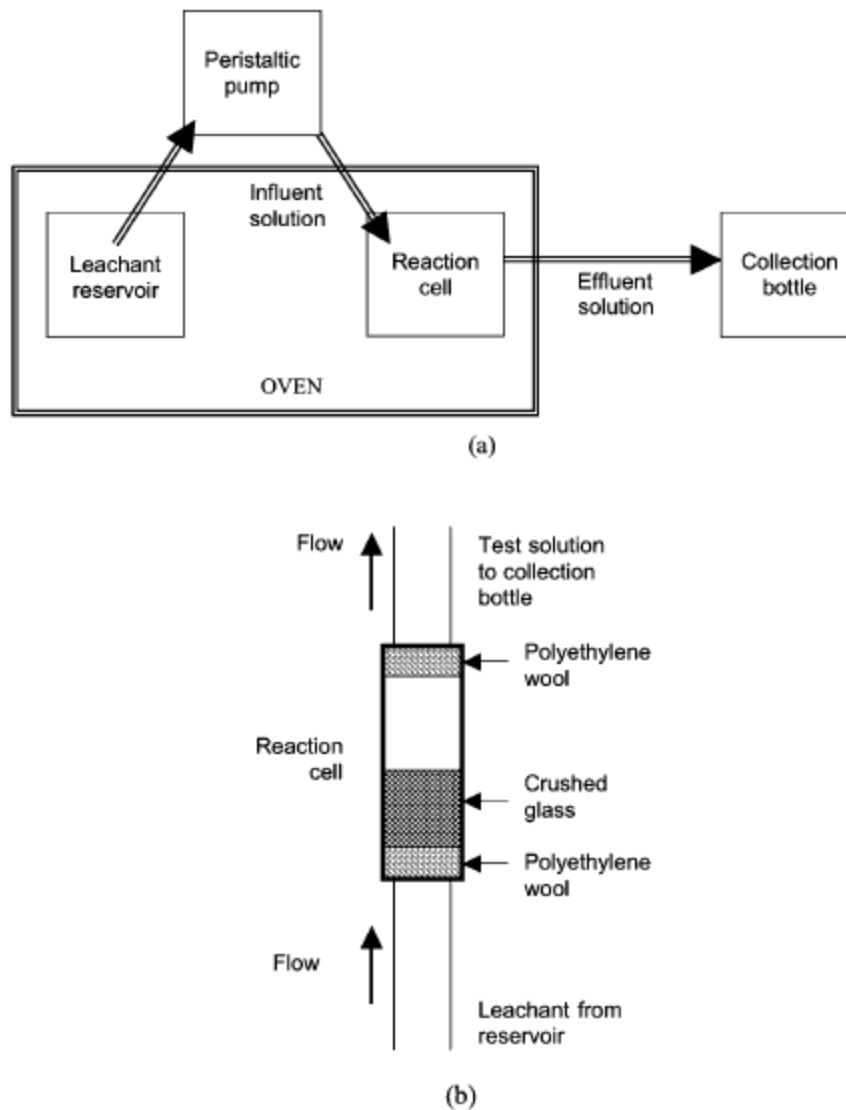
Figure 2.4. Single-pass flow-through experimental setup. (a) Schematic design of the experiment and (b) column reactor design[53]

SPFT studies measure an elemental release rate rather than an absolute

concentration, which then provides a prediction of long-term glass dissolution rates. The

measured concentration of a species in solution (c_i) can is normalized to the flow rate (q),

surface area (S), and fraction of the component i in the glass, x_i, to provide the elemental

release rate (r_i) as shown in Equation (7)[53]

$$r_i = \frac{c_i\left(\frac{q}{S}\right)}{x_i} \tag{7}$$

If the release rate for each element is constant with respect to time, then the glass

is dissolving by the same mechanism over the course of the entire dissolution test.

Additionally, if the release rates for all elements are equivalent, the glass is dissolving

congruently. The SPFT test is designed for glasses which are durable and do not dissolve

more than 5% of the original material over the course of the experiment,[53] and therefore

the controlling equations do not account for changes in the surface area of the dissolving

particles. To use this test for fast-reacting glasses like the bioactive borate glasses, rate

equations like that in Equation 7 must be modified to account for the decreasing surface

area.

The effect of ion concentrations (salinity) in solution is considered particularly

important for dissolution of silicate glasses because of the low solubility of silicate

species (~112 ppm)[36] in most acidic to near-neutral aqueous solutions.[52] Figure 2.5

shows that the borosilicate glass dissolution rate decreases as the [Si] concentration in tris

hydroxymethyl aminomethane (THAM) + HNO_3 solution increases. The effects of alkali

and borate anions in solution are generally disregarded in these studies because they have

much higher solubilities (57 g/L for H_3BO_3, 112 ppm for Si). For borosilicate glasses, the

extent of glass dissolution is measured from boron release rates.[52, 54]
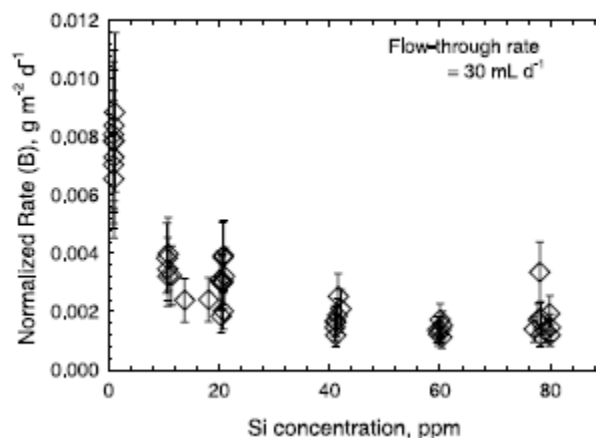
Figure 2.5. Effect of [Si] in solution in dissolution rate of a borosilicate glass.[54]

For SPFT studies, experimental conditions can be changed to decrease ion concentration in solution. Faster flow rates and lower glass particle surface areas lead to a decrease in ion concentration and solution and therefore a faster glass dissolution rate, shown in Figure 2.6 [47]. At a high enough flow rate or low enough particle surface area, the solution concentrations are sufficiently low that ion release rates are no longer affected by the concentrations of solution species. This is shown in Figure 2.6 where the release rates level off with increased q/S. This maximum in release rate is referred to as the forward dissolution rate. Forward dissolution rates are used to compare the compositional-dependences of corrosion rates after eliminating the effects of solution-surface interactions or precipitation layer formation.[49, 50, 52, 54]
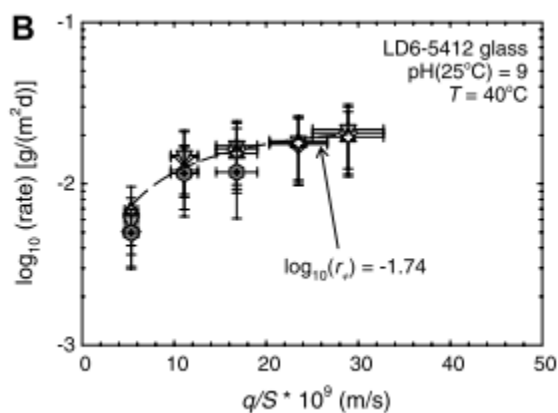
Figure 2.6. Effect of flow rate (q) and surface area (S) on glass dissolution rate.[50]

2.5.   NATURE OF BORATE AND PHOSPHATE ANIONS IN SOLUTION

Two predominant borate species are stable in solution, boric acid ($B(OH)_3$) and tetrahydroxyl borate anions ($B(OH)_4^-$). The pK_a value for the equilibrium between $B(OH)_3$ and $B(OH)_4^-$ is 9.24. For phosphate solutions, PO_4^{3-}, HPO_4^{2-}, $H_2PO_4^-$, and H_3PO_4 are stable in solution. The pKa values are 12.67 ($PO_4^{3-} + H^+ \longleftrightarrow HPO_4^{2-}$), 7.21($HPO_4^{2-} + H^+ \longleftrightarrow H_2PO_4^-$), and 2.21($H_2PO_4^- + H^+ \longleftrightarrow H_3PO_4$).[23] The pH of the plasma fluid in the body is 7.4±0.2 this is partially maintained by the $HPO_4^{2-} + H^+ \longleftrightarrow H_2PO_4^-$ equilibrium reaction.

As borate bioactive glasses dissolve, they buffer in aqueous solutions to a pH in the range 8-10.[9, 12, 21, 55] This means that if a borate glass scaffold dissolves in simulated body fluid (SBF), two solution reactions become important in the pH range of 7.2-10,

$$B(OH)_3 + OH^- \leftrightarrow B(OH)_4^- \qquad (pK_a=9.24) \qquad (8)$$

$$HPO_4^{2-} + H^+ \leftrightarrow H_2PO_4^- \qquad (pK_a=7.21) \qquad (9)$$

As borate glass particles or scaffolds dissolve and the pH increases, the concentrations of the predominant species in solution will vary according to the pH.

In solution, $B(OH)_3$ molecules and $B(OH)_4^-$ anions have unique Raman shift frequencies for their respective B-O symmetric stretching modes.[56-58] Each of the phosphate species also each have unique Raman shifts for their P-O$^-$ and P-O-H symmetric stretching modes.[59] Figure 2.7 shows spectra for H_3PO_4 and $H_2PO_4^-$ species in solution.[60] Cherif *et al.* investigated the effect of concentration on peak area and found that the integrated peak area increased linearly with phosphate concentration.[61] Preston investigated the effect of soluble cations on the peak position and found no significant changes in peak position for HPO_4^{2-} or $H_2PO_4^-$ with ammonium, sodium, or potassium ions.[59]
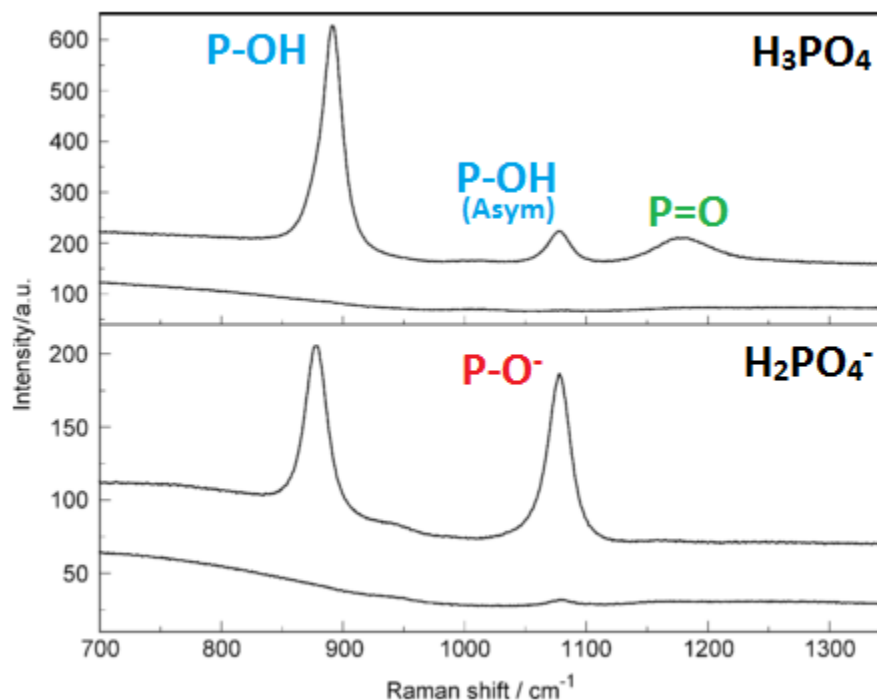
Figure 2.7. Raman spectra for H_3PO_4 and $H_2PO_4^-$ in solution.[60]

When phosphate glasses dissolve in aqueous solutions, phosphate anions that constitute the glass structure are released intact into solution.[62] The anions are temporarily stable, particularly in neutral solutions, prior to hydrolyzing and reaching equilibrium conditions.[62] No studies have investigated whether similar phenomena exist for borate glasses. If the predominant borate species released to solution only depend on solution pH, predictions can be made about pH based on the relative fractions of species present in the solution. Apart from pH, concentration plays a role in which borate species are stable. At high B concentrations (0.4 M), polyborate anion complexes become more stable, shown in Figure 2.8.[63] The fractional concentrations of each borate specie is

given by the vertical distance between two lines. These polyborate anion complexes are

also identifiable by Raman spectroscopy.[56, 64] The relative amounts of the polyborate

species in solution depend on the pH of the solution, shown in Figure 2.8.[56, 63]
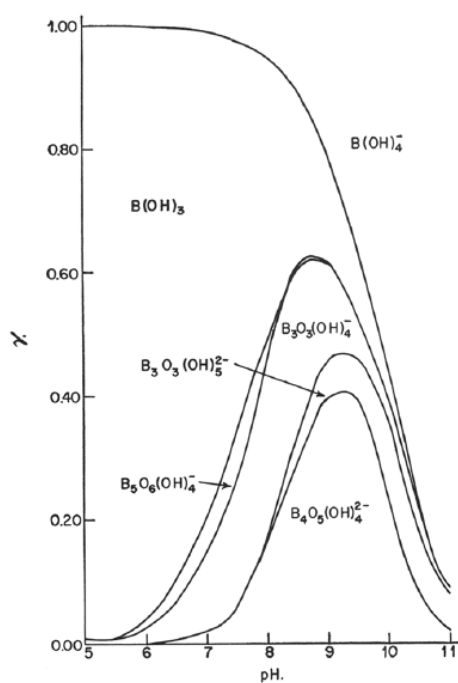
Figure 2.8. Fractional borate units as a function of pH when [B] = 0.4M.[63]

2.6.   PRECIPITATION OF PHOSPHATE COMPOUNDS

Dissolution of borate and silicate glasses in phosphate solutions leads to the

formation of crystalline and amorphous phosphates on the glass surface. Conzone

precipitated x-ray amorphous $DyPO_4$ on the surface of lithium borate microspheres which transitioned to hollow or solid spheres as the glass dissolved.[65] For Ca-containing glasses reacting in a phosphate solution, amorphous calcium phosphate (ACP) first forms on the glass surface and as the reaction time increases, the ACP transforms to crystalline hydroxyapatite (HAP).[66, 67] Dissolution of Ca-containing borate glasses in phosphate-containing solutions such as simulated body fluid (SBF) or K_2HPO_4 (*aq*) are reported to precipitate HAP or carbonate-substituted apatite on the surface.[9, 13, 28, 45, 68, 69] Room temperature dissolution of sodium calcium borate glasses in 0.1 M K_2HPO_4 solution (pH=8.8) led to the formation of amorphous calcium phosphate reaction layers on the glass surfaces.[44] Vanderspiegel found that microspheres of $16K_2O$-$12CaO$-$73B_2O_3$ and $14K_2O$-$21CaO$-$65B_2O_3$ glasses (mol%) glasses reacted in 0.25 M K_2HPO_4 solution at 37 °C formed a partially crystalline hydroxyapatite reaction layer in as little as three hours.[28] Glasses reacted at higher temperatures and in solutions with greater phosphate concentrations form hydroxyapatite in shorter times than reactions at lower temperatures or with less phosphate in solution.[10, 28, 44] Fears studied the effect of calcium content in lithium calcium borate glasses on the reaction product formation.[70] The initial reaction product precipitated on the glass surface and as the glass further reacted, the reaction product increased in thickness from the outer surface toward the center of the original glass particle. Glasses with $\leq$ 40 wt% CaO formed hollow HAP microspheres whereas glasses with $>$ 40 wt% CaO formed solid HAP microspheres. Gu *et al.* studied the effect of calcium content on the reaction product morphology.[10] As the calcium content of the glass increased from 10 mol% to 20 mol% in a soda lime borate system, the particle size of the hydroxyapatite particles decreased from 6 μm to 2 μm. The glass with higher

calcium content formed more nuclei, which led to the formation of more particles of a smaller size. It was also observed that the glasses with the lowest calcium content formed hollow hydroxyapatite particles, consistent with the results observed by Fears.[10, 70]

The nature of the calcium phosphate phase that precipitates is dependent on solution pH. Hydroxyapaite (HAP) is the stable crystalline phase in the $6 \leq pH \leq 11$ neutral-basic regime whereas other phosphate phases such as dicalcium phosphate dihydrate ($CaHPO_4 \bullet 2H_2O$) and octacalcium phosphate ($Ca_8H_2(PO_4)_6 \bullet 5H_2O$) are stable below pH 5.[71, 72] Calcium-containing glasses that were dissolved in acidic pH conditions precipitate dicalcium phosphate dihydrate on the glass surface.[28] The rate of transition from ACP to HAP was found to increase as pH decreased from 10 to 6.[72] Additionally, the calcium to phosphorus ratio (Ca/P) for ACP is ~1.5 and is lower than that of stoichiometric HAP (Ca/P = 1.67).

The goal of this work was to quantitatively describe the borate glass dissolution processes and to characterize the precipitation of phosphate phases on the surfaces of these glasses. A bioactive borate glass was dissolved in water under static conditions to gather information about the formation of calcium phosphate phases from a solution that was initially devoid of calcium and phosphate species. Additionally this work provided a kinetic description of glass dissolution based on ion release rather than weight loss measurements. Single-pass flow-through dynamic studies were employed to gain a better understanding of how solution concentrations affect dissolution rate. This work also provides information regarding how solution chemistry affects the crystallinity and morphology of the calcium phosphate layers forming on glass surfaces. Raman

spectroscopy was used to measure boron release from glasses and dissolution constants were determined for various glasses within the sodium calcium borate system. The trends between dissolution constants and composition allowed for understanding the relationship between hydration and hydrolysis in borate glasses. Finally, glass dissolution-precipitations were employed to prepare rare earth phosphate solid solutions, providing an understanding for the structure and chemistry of as-reacted phosphate precipitates.

REFERENCES

[1]   S. B. Jung, "Bioactive Borate Glasses"; chapter in Bio-Glasses: An Introduction; Edited by J. R. Jones and A. G. Clare. John Wiley & Sons, Ltd., 2012.

[2]   L. Bi, M. Rahaman, D. Day, Z. Brown, C. Samujh, X. Liu, A. Mohammadkhah, V. Dusevich, J. D. Eick and L. Bonewald, "Effect of Bioactive Borate Glass Microstructure on Bone Regeneration, Angiogenesis, and Hydroxyapatite Conversion in a Rat Calvarial Defect Model," *Acta Biomater.*, **9** [8] 8015-26 (2013).

[3]   M. Rahaman, D. Day, S. Bal, Q. Fu, S. Jung, L. Bonewald and A. Tomsia, "Bioactive Glass in Tissue Engineering," *Acta Biomater.*, **7** [6] 2355-73 (2011).

[4]   R. M. Nzietchueng, B. Dousset, P. Franck, M. Benderdour, P. Nabet and K. Hess, "Mechanisms Implicated in the Effects of Boron on Wound Healing," *J. Trace Elem. Med. Biol.*, **16** 239-44 (2002).

[5]   C. D. Hunt, "Biochemical Effects of Physiological Amounts of Dietary Boron," *J. Trace Elem. Exp. Med.*, **9** 185-213 (1996).

[6]   F. Nielsen, "Ultratrace Elements in Nutrition: Current Knowledge and Speculation," *J. Trace Elem. Exp. Med.*, **11** 251-74 (1998).

[7]   D. H. Kim, B. N. Marbois and C. D. Eckhert, "Esterification of Borate with NAD^{+} and Nadh as Studied by Electrospray Ionization Mass Spectrometry and ^{11}B NMR Spectroscopy," *J. Mass Spectrom.*, **38** [6] 632-40 (2003).

[8]   S. Jung and D. Day, "Conversion Kinetics of Silicate, Borosilicate, and Borate Bioactive Glasses to Hydroxyapatite," *Phys. Chem. Glasses: Eur.J. Glass Sci. Technol. B*, **50** [2] 85-8 (2009).

[9]   W. Huang, M. Rahaman, D. Day and Y. Li, "Mechanisms for Converting Bioative Silicate, Borate, and Borosilicate Glasses to Hydroxyapatite in Dilute Phosphate Solution," *Phys. Chem. Glasses: Eur.J. Glass Sci. Technol. B*, **47** [6] 647-58 (2006).

[10]   Y. Gu, W. Xiao, L. Lu, W. Huang, M. Rahaman and D. Wang, "Kinetics and Mechanisms of Converting Bioactive Borate Glasses to Hydroxyapatite in Aqueous Phosphate Solutions," *J. Mater. Sci.*, **46** [1] 47-54 (2011).

[11]   Q. Fu, M. N. Rahaman, B. S. Bal, L. F. Bonewald, K. Kuroki and R. F. Brown, "Silicate, Borosilicate, and Borate Bioactive Glass Scaffolds with Controllable

Degradation Rate for Bone Tissue Engineering Applications. II. In Vitro and in Vivo Biological Evaluation," *J. Biomed. Mater. Res. A*, **95A** [1] 172-9 (2010).

[12]   Q. Fu, M. N. Rahaman, H. Fu and X. Liu, "Silicate, Borosilicate, and Borate Bioactive Glass Scaffolds with Controllable Degradation Rate for Bone Tissue Engineering Applications. I. Preparation and in Vitro Degradation," *J. Biomed. Mater. Res. A*, **95A** [1] 164-71 (2010).

[13]   Y. Gu, W. Xiao, L. Lu, W. Huang, M. Rahaman and D. Wang, "Kinetics and Mechanisms of Converting Bioactive Borate Glasses to Hydroxyapatite in Aqueous Phosphate Solution," *J. Mater. Sci.*, **46** [1] 47-54 (2011).

[14]   X. Han and D. Day, "Reaction of Sodium Calcium Borate Glasses to Form Hydroxyapatite," *J. Mater. Sci.: Mater. Med.*, **18** [9] 1837-47 (2007).

[15]   S. B. Jung and D. E. Day, "Conversion Kinetics of Silicate, Borosilicate, and Borate Bioactive Glasses to Hydroxyapatite," *Physics and Chemistry of Glasses - European Journal of Glass Science and Technology Part B*, **50** [2] 85-8 (2009).

[16]   Y. Li, M. N. Rahaman, Q. Fu, B. S. Bal, A. Yao and D. E. Day, "Conversion of Bioactive Borosilicate Glass to Multilayered Hydroxyapatite in Dilute Phosphate Solution," *J. Am. Ceram. Soc.*, **90** [12] 3804-10 (2007).

[17]   X. Liu, Z. Xie, C. Zhang, H. Pan, M. Rahaman, X. Zhang, Q. Fu and W. Huang, "Bioactive Borate Glass Scaffolds: In Vitro and in Vivo Evaluation for Use as a Drug Delivery System in the Treatment of Bone Infection," *J. Mater. Sci.: Mater. Med.*, **21** [2] 575-82 (2010).

[18]   S. D. Conzone and D. E. Day, "Preparation and Properties of Porous Microspheres Made from Borate Glass," *Journal of Biomedical Materials Research, Part A*, **88A** [2] 531-42 (2009).

[19]   H. Fu, M. Rahaman, D. Day and W. Huang, "Effect of Pyrophosphate Ions on the Conversion of Calcium–Lithium–Borate Glass to Hydroxyapatite in Aqueous Phosphate Solution," *J. Mater. Sci.: Mater. Med.*, **21** [10] 2733-41 (2010).

[20]   H. Fu, M. N. Rahaman and D. E. Day, "Effect of Process Variables on the Microstructure of Hollow Hydroxyapatite Microspheres Prepared by a Glass Conversion Method," *J. Am. Ceram. Soc.*, **93** [10] 3116-23 (2010).

[21]   Y. Li, M. Rahaman, Q. Fu, B. S. Bal, A. Yao and D. Day, "Conversion of Bioactive Borosolicate Glass to Multilayered Hydroxyapatite in Dilute Phosphate Solution," *J. Am. Ceram. Soc.*, **90** [12] 3804-10 (2007).

[22]   D. J. Voet, J. G. Voet and C. W. Pratt, *Principles of Biochemistry*, Third ed., Edited by John Wiley & Sons, Inc., 2008.

[23]   D. D. Perrin, *Ionization Constants of Inorganic Acids and Bases in Aqueous Solutions*, Second ed., Edited by Pergamon, Oxford, 1982.

[24]   Y. Zhou, C. Fang, Y. Fang, F. Zhu and L. Cao, "Polyborates in Aqueous Sodium Borate Solution at 298.15 K," *Asian J. Chem.*, **24** [1] 29-32 (2012).

[25]   J. Jones, A. Vats, I. Notingher, J. Gough, N. Tolley, J. Polak and L. Hench, "*In Situ* Monitoring of Chondrocyte Response to Bioactive Scaffolds Using Raman Spectroscopy," *Key Eng. Mater.*, **284-286** 623-6 (2005).

[26]   I. Notingher, S. Verrier, H. Romanska, A. Bishop, J. Polak and L. Hench, "*In Situ* Characterization of Living Cells by Raman Spectroscopy," *Spectrosc.*, **16** 43-51 (2002).

[27]   G. Penel, C. Delfosse, M. Descamps and G. Leroy, "Composition of Bone and Apatitic Biomaterials as Revealed by Intravital Raman Microspectroscopy," *Bone*, **36** 893-901 (2005).

[28]   N. Vanderspiegel, "Reaction of Potassium Calcium Borate Glasses to Form Apatite and Dicalcium Phosphate Dihydrate"; Master of Science Thesis. University of Missouri - Rolla, Rolla, MO, 2004.

[29]   L. L. Hench, R. J. Splinter, W. C. Allen and T. K. Greenlee, "Bonding Mechanisms at the Interface of Ceramic Prosthetic Materials," *J. Biomed. Mater. Res.*, **5** [6] 117-41 (1971).

[30]   D. E. Day, J. E. White, R. F. Brown and K. D. McMenamin, "Transformation of Borate Glasses into Biologically Useful Materials," *Glass Technol.*, **44** [2] 75-81 (2003).

[31]   P. Wray, "Wound Healing Borate Glass Nanofibers," ACerS Bulletin, (2011).

[32]   C. A. Houser, J. S. Herman, I. S. T. Tsong, W. B. White and W. A. Lanford, "Sodium-Hydrogen Interdiffusion in Sodium Silicate Glasses," *J. Non-Cryst. Solids*, **41** [1] 89-98 (1980).

[33]   A. Paul, "Chemical Durability of Glasses; a Thermodynamic Approach," *J. Mater. Sci.*, **12** [11] 2246-68 (1977).

[34]   R. Conradt, "Chemical Durability of Oxide Glasses in Aqueous Solutions: A Review," *J. Am. Ceram. Soc.*, **91** [3] 728-35 (2008).

[35] B. C. Bunker, "Molecular Mechanisms for Corrosion of Silica and Silicate Glasses," *J. Non-Cryst. Solids*, **179** 300-8 (1994).

[36] G. B. Alexander, W. M. Heston and R. K. Iler, "The Solubility of Amorphous Silica in Water," *The Journal of Physical Chemistry*, **58** [6] 453-5 (1954).

[37] A. Ledieu, F. Devreux, P. Barboux, L. Sicard and O. Spalla, "Leaching of Borosilicate Glasses. I. Experiments," *J. Non-Cryst. Solids*, **343** [1–3] 3-12 (2004).

[38] B. C. Bunker, G. W. Arnold, D. E. Day and P. J. Bray, "The Effect of Molecular Structure on Borosilicate Glass Leaching," *J. Non-Cryst. Solids*, **87** [1–2] 226-53 (1986).

[39] P. Zapol, H. He, K. D. Kwon and L. J. Criscenti, "First-Principles Study of Hydrolysis Reaction Barriers in a Sodium Borosilicate Glass," *International Journal of Applied Glass Science*, **4** [4] 395-407 (2013).

[40] G. Geneste, F. Bouyer and S. Gin, "Hydrogen–Sodium Interdiffusion in Borosilicate Glasses Investigated from First Principles," *J. Non-Cryst. Solids*, **352** [28–29] 3147-52 (2006).

[41] M. H. Velez, H. L. Tuller and D. R. Uhlmann, "Chemical Durability of Lithium Borate Glasses," *J. Non-Cryst. Solids*, **49** 351-62 (1982).

[42] B. C. Bunker, G. W. Arnold and J. A. Wilder, "Phosphate Glass Dissolution in Aqueous Solutions," *J. Non-Cryst. Solids*, **64** [3] 291-316 (1984).

[43] J. J. Mazer and J. V. Walther, "Dissolution Kinetics of Silica Glass as a Function of pH between 40 and 85°C," *J. Non-Cryst. Solids*, **170** [1] 32-45 (1994).

[44] J. Lowry, "Dissolution Behavior of Alkali Borate Glasses"; Master of Science Thesis. University of Missouri - Rolla, Rolla, MO, 2002.

[45] K. L. Goetschius, "The Effect of Composition on the Viscosity, Crystallization, and Dissolution of Simple Borate Glasses and Compositional Design of Borate Based Bioactive Glasses"; Ph.D. Thesis. Missouri University of Science and Technology, Rolla, 2014.

[46] A. Khawam and D. R. Flanagan, "Solid-State Kinetic Models: Basics and Mathematical Fundamentals," *The Journal of Physical Chemistry B*, **110** [35] 17315-28 (2006).

[47]   S. Kuslu, F. C. Disli and S. Colak, "Leaching Kinetics of Ulexite in Borax Pentahydrate Solutions Saturated with Carbon Dioxide," *J. Ind. Eng. Chem.*, **16** 673-8 (2010).

[48]   H. Temur, A. Yatarsi, M. Copur and M. M. Kocakerim, "The Kinetics of Dissolution of Colemanite in H_3PO_4 Solutions," *Ind. Eng. Chem. Res.*, **39** 4114-9 (2000).

[49]   E. M. Pierce, E. A. Rodriguez, L. J. Calligan, W. J. Shaw and B. Pete McGrail, "An Experimental Study of the Dissolution Rates of Simulated Aluminoborosilicate Waste Glasses as a Function of pH and Temperature under Dilute Conditions," *Appl. Geochem.*, **23** [9] 2559-73 (2008).

[50]   J. P. Icenhower, B. P. McGrail, W. J. Shaw, E. M. Pierce, P. Nachimuthu, D. K. Shuh, E. A. Rodriguez and J. L. Steele, "Experimentally Determined Dissolution Kinetics of Na-Rich Borosilicate Glass at Far from Equilibrium Conditions: Implications for Transition State Theory," *Geochim. Cosmochim. Acta*, **72** [12] 2767-88 (2008).

[51]   B. P. McGrail, D. H. Bacon, J. P. Icenhower, F. M. Mann, R. J. Puigh, H. T. Schaef and S. V. Mattigod, "Near-Field Performance Assessment for a Low-Activity Waste Glass Disposal System: Laboratory Testing to Modeling Results," *J. Nucl. Mater.*, **198** 95-111 (2001).

[52]   B. P. McGrail, J. P. Icenhower, D. K. Shuh, P. Liu, J. G. Darab, D. R. Baer, S. Thevuthasen, V. Shutthanandan, M. H. Engelhard, C. H. Booth and P. Nachimuthu, "The Structure of $Na_2O–Al_2O_3–SiO_2$ Glass: Impact on Sodium Ion Exchange in H_2O and D_2O," *J. Non-Cryst. Solids*, **296** [1–2] 10-26 (2001).

[53]   ASTM Standard C1662-10, 2007, "Standard Practice for Measurement of the Glass Dissolution Rate Using the Single-Pass Flow-through Test Method," ASTM International, West Conshohocken, PA,

[54]   B. P. McGrail, D. H. Bacon, J. P. Icenhower, F. M. Mann, R. J. Puigh, H. T. Schaef and S. V. Mattigod, "Near-Field Performance Assessment for a Low-Activity Waste Glass Disposal System: Laboratory Testing to Modeling Results," *J. Nucl. Mater.*, **298** [1–2] 95-111 (2001).

[55]   A. Yao, D. Wang, W. Huang, Q. Fu, M. N. Rahaman and D. E. Day, "In Vitro Bioactive Characteristics of Borate-Based Glasses with Controllable Degradation Behavior," *J. Am. Ceram. Soc.*, **90** [1] 303-6 (2007).

[56]   L. Maya, "Identification of Polyborate and Fluoropolyborate Ions in Solution by Raman Spectroscopy," *Inorg. Chem.*, **15** [9] 2179-84 (1976).

[57] C. Schmidt, R. Thomas and W. Heinrich, "Boron Speciation in Aqueous Fluids at 22 to 600 °C and 0.1 MPa to 2 GPa," *Geochim. Cosmochim. Acta*, **69** [2] 275-81 (2005).

[58] L. Zhihong, G. Bo, L. Shuni, H. Mancheng and X. Shuping, "Raman Spectroscopic Analysis of Supersaturated Aqueous Solution of MgO-B_2O_3-32%$MgCl_2$-H_2O," *Spectrochim. Acta, Part A*, **60** 3125-8 (2004).

[59] C. Preston and W. A. Adams, "A Laser Raman Spectroscopic Study of Aqueous Orthophosphate Salts," *J. Phys. Chem. A*, **83** [7] 814-21 (1979).

[60] W. W. Rudolph, "Raman-and Infrared-Spectroscopic Investigations of Dilute Aqueous Phosphoric Acid Solutions," *Dalton Trans.*, **39** [40] 9642-53 (2010).

[61] M. Cherif, A. Mgaidi, N. Ammar, G. Vallée and W. Fürst, "A New Investigation of Aqueous Orthophosphoric Acid Speciation Using Raman Spectroscopy," *J. Solution Chem.*, **29** [3] 255-69 (2000).

[62] B. C. Tischendorf, "Interactions between Water and Phosphate Glsses"; Ph.D. Thesis. University of Missouri-Rolla, Rolla, 2005.

[63] J. L. Anderson, E. M. Eyring and M. P. Whittaker, "Temperature Jump Rate Studies of Polyborate Formation in Aqueous Boric Acid," *J. Phys. Chem. A*, **68** [5] 1128-32 (1964).

[64] M. Maeda, T. Hirao, M. Kotaka and H. Kakihana, "Raman Spectra of Polyborate Ions in Aqueous Solution," *J. Inorg. Nucl. Chem.*, **41** 1217-20 (1979).

[65] S. D. Conzone and D. E. Day, "Preparation and Properties of Porous Microspheres Made from Borate Glass," *J. Biomed. Mater. Res. A*, **88A** [2] 531-42 (2009).

[66] X. Liu, M. Rahaman and D. Day, "Conversion of Melt-Derived Microfibrous Borate (13-93b3) and Silicate (45S5) Bioactive Glass in a Simulated Body Fluid," *J. Mater. Sci.: Mater. Med.*, **24** [3] 583-95 (2013).

[67] W. Liang, M. N. Rahaman, D. E. Day, N. W. Marion, G. C. Riley and J. J. Mao, "Bioactive Borate Glass Scaffold for Bone Tissue Engineering," *J. Non-Cryst. Solids*, **354** [15−16] 1690-6 (2008).

[68] W. Huang, D. Day, K. Kittiratanapiboon and M. Rahaman, "Kinetics and Mechanisms of the Conversion of Silicate (45S5), Borate, and Borosilicate Glasses to Hydroxyapatite in Dilute Phosphate Solutions," *J. Mater. Sci.: Mater. Med.*, **17** [7] 583-96 (2006).

[69]   S. Jung, "Borate Based Bioactive Glass Scaffolds for Hard and Soft Tissue Engineering"; Ph.D. Thesis. Missouri University of Science and Technology, Rolla, MO, 2010.

[70]   K. P. Fears, "Formation of Hollow Hydroxyapatite Microspheres"; M.S. Thesis. University of Missouri-Rolla, Rolla, 2001.

[71]   M. H. Prado Da Silva, J. H. C. Lima, G. A. Soares, C. N. Elias, M. C. de Andrade, S. M. Best and I. R. Gibson, "Transformation of Monetite to Hydroxyapatite in Bioactive Coatings on Titanium," *Surf. Coat. Technol.*, **137** [2] 270-6 (2001).

[72]   A. L. Boskey and A. S. Posner, "Magnesium Stabilization of Amorphous Calcium Phosphate: A Kinetic Study," *Mater. Res. Bull.*, **9** [7] 907-16 (1974).

PAPER

I.   IN-SITU CHARACTERIZATION OF BORATE GLASS DISSOLUTION KINETICS BY M-RAMAN SPECTROSCOPY

AUTHORS:

Jaime L. George[a]
Richard K. Brow[a]

[a]Missouri University of Science and Technology
401 W. 16th St.
Rolla, MO
65409

ABSTRACT

The dissolution processes of alkali alkaline earth borate glasses in phosphate-containing aqueous solutions were studied by µ-Raman spectroscopy. Raman spectra provided measurements of the types and concentrations of borate anions released into the solution as a function of time and were collected to describe the formation of calcium phosphate reaction products, such as hydroxyapatite, on the glass surface. Boric acid molecules (H_3BO_3) and tetrahydroxyl borate anions ($B(OH)_4^-$) can be detected in solution and their relative concentrations depend on the solution pH. By monitoring the areas under peaks associated with these two species, the overall borate release rates and variations in solution pH were determined.

1. INTRODUCTION

Borate bioactive glasses have shown promise for biomedical applications such as bone repair[1] and wound healing.[2] As these bioactive glasses dissolve, they release calcium ions which react with the phosphate anions in the aqueous environment to form an hydroxyapatite-like calcium phosphate phase which can then bond to tissue *in-vivo*. The composition of the glass can affect how quickly the glasses dissolve and the calcium phosphate layers form.[3-5]

Raman spectroscopy has been used to analyze borate[6-10] and phosphate[11-14] speciation and concentrations in aqueous solutions. Preston and Adams found linear correlations between phosphate concentration and peak intensities of Raman P-O stretching modes.[12] The stable phosphate species are pH dependent and can be differentiated with Raman spectroscopy.[11] Similar analyses have been done on borate species in solution. At low (≤ 2000 ppm) concentrations of borate, there are two stable solution species, $B(OH)_3$, and $B(OH)_4^-$.[6, 15] The pK_a for the equilibrium between these species is 9.24, which is in the pH range where bioactive borate glasses buffer during dissolution.[4, 16] Raman spectroscopy thus can be used to characterize borate speciation in aqueous solutions in the vicinity of the glass during dissolution.

Raman spectroscopy can also be used to characterize borate glass structures[17, 18] and the formation of calcium phosphate reaction layers that form on bioactive glass surfaces.[19, 20] Formation of boric acid on the surface of alkali borate glasses has been observed following dissolution in an aqueous solution and exposure to air. [21] Formation of hydroxycarbonate apatite (HCA) on the surface of bio-active silicate glasses has been measured by an *in-situ* Raman spectroscopic technique.[22]

In this paper, micro-Raman spectroscopy was used to evaluate the dissolution kinetics of Na-Ca-borate glasses in phosphate solution and the precipitation of calcium phosphate layers on the glass surfaces. Changes in local pH conditions were characterized from the relative intensities of the Raman peaks of borate species in solution and related to boron coordination and glass composition.

2. EXPERIMENTAL METHODS

2.1. SOLUTION PREPARATION

Several series of aqueous solutions were prepared from deionized water and

K_2HPO_4 (Acros Organics, 99+%), H_3BO_3 (Alfa Aesar, 99.8%), NaOH (Mallinckrodt,

98.6%), and/or H_3PO_4 (Alfa Aesar, 85% aqueous solution). An Accumet pH electrode

was used to record pH values for the solutions. Boron and phosphorus concentrations

were measured by inductively coupled plasma – optical emission spectroscopy (ICP-

OES, Perkin Elmer Optima 2000 DV) for some solutions, with all measurements made in

triplicate.

2.2. GLASS PREPARATION

Glasses from the Na_2O-CaO-B_2O_3 system, with the molar compositions shown in

Figure 1, were prepared by traditional melt techniques. Compositions were batched from

reagent grade Na_2CO_3 (Alfa Aesar, 98%), $CaCO_3$ (Alfa Aesar, 98%), and H_3BO_3 (Alfa

Aesar, 99.8%), calcined at 600 °C overnight, and melted from 900-950 °C for 0.5-1 hour

in a Pt crucible. Glasses were cast into 1 cm diameter cylinders and annealed at their

respective glass transition temperatures (T_g) for two hours and allowed to cool. The

cylinders were cut into discs 5 mm in height and the discs were cut in half longitudinally

using a diamond saw. Prior to dissolution studies, glass surfaces were cleaned with

ethanol. Analyzed compositions of dissolved glasses were within 2% of their nominal

compositions, and so the latter are used in this paper.

2.3. RAMAN MEASUREMENTS

Raman measurements were made with a Horiba Jobin Yvon LabRAM Aramis μ-

Raman spectrometer. Solution samples were held in an aluminum vial (1.5 cm diameter,

2 cm height) and the laser was focused on the solution surface with a 10x objective.

Spectra were collected using a 632.8 nm HeNe laser with initial power of 17 mW. Silicon

was used as a calibration standard using the 520 cm-1 peak.

Bulk samples of Na_2O-B_2O_3 and Na_2O-CaO-B_2O_3 glasses were dissolved in 0.1

M K_2HPO_4 aqueous solution (glass surface area-to-solution volume ratio, SA/V = 33.5

m^{-1}) under static conditions at 20 °C in a polycarbonate cell. Spectra were collected from

the solution as a function of time, 30-1000 μm from the cut surface of each glass, with the

632.8 HeNe laser described above. Additionally, spectra were collected from the top

surface of the glass as a function of time using a 785 nm diode laser with initial power of

100 mW. Independent weight loss measurements were made in triplicate on glasses

dissolved under identical experimental conditions. Samples were dried by blotting on a

paper towel prior to weighing and pH was measured on with the pH electrode.

3.   RESULTS

3.1. BORATE AND PHOSPHATE SOLUTIONS

A series of solutions containing 0.1 M K_2HPO_4 and up to 7000 ppm B, with a pH of 8.78±0.03, adjusted with NaOH, were prepared. The Raman spectra from several of these solutions are shown in Figure 2. The 0.1 M K_2HPO_4 solution containing no borate has a sharp peak at 989 cm^{-1} and a broad peak at 850 cm^{-1}, assigned to the PO_3 and P-O-H symmetric stretching modes of the HPO_4^{2-} anion, respectively.[11] As borate is introduced to the solution, new peaks appear at 745 cm^{-1} and 876 cm^{-1} and these peaks increase in intensity relative to the dominant phosphate peak as the borate concentration increases. These new peaks are assigned to the B-O symmetric stretching modes of $B(OH)_4^-$ and $B(OH)_3$, respectively.[6, 7, 9] These borate peaks were detected as low as 50 ppm B in these experiments. At borate concentrations greater than 2000 ppm, a third peak appears at 610 cm^{-1}, and this peak is assigned to the ring breathing mode of the $B_3O_3(OH)_4^-$ anion.[6-9] A summary of peak assignments and references are shown in Table 1.

The areas of the $B(OH)_3$, and $B(OH)_4^-$ peaks were measured and normalized to the area of the phosphate peak at 989 cm^{-1} for each sample. The relative area of the $B(OH)_4^-$ peak to the total boron peak area remains constant at 0.157±0.020 for the eight measurements shown. These normalized peak areas are plotted in Figure 3 as a function of the [B]/[P] weight ratio, which was measured by ICP-OES. Additionally, the sum of both borate peak areas is plotted. A linear correlation is found between the ratio of the total borate-to-phosphate peak areas and ratio of boron-to-phosphorus solution concentration, described by Equation (1).

$$\frac{\left(A_{B(OH)_4^-} + A_{B(OH)_3}\right)}{A_{HPO_4^{2-}}} = 2.028 * [B]/[P] \tag{1}$$

By determining the peak areas of the borate species and the phosphate anion,

along with a known phosphorus concentration, the boron concentration of a solution can

be determined using Equation (1). The presence of $B_3O_3(OH)_4^-$ anions in the concentrated

solutions (3000-7000 ppm B) caused those data points to deviate from this line, so only

samples with boron concentrations at or below 3000 ppm are analyzed here. For

dissolution experiments with calcium-containing glasses, phosphate from the solution

reacts with calcium released by the dissolving glass to form a Ca-phosphate precipitating

phase and so depleting the phosphate concentration in solution. For the experiments

described below, the maximum depletion of phosphate was 3.6% and so this ignored

when using Equation 1 to calculate borate concentrations.

Raman spectra were collected from several series of solutions with different

concentrations of borate (300, 1000, or 2000 ppm) and phosphate ions (0 or 0.1M

K_2HPO_4), were prepared with pH values adjusted with NaOH or H_3PO_4/H_3BO_3 mixtures.

Figure 4 shows the spectra collected from solutions with 1000 ppm B added to deionized

water, and the pH then adjusted with NaOH. In acidic solutions (pH < 8), the only peak

present is that at 876 cm^{-1}, for $B(OH)_3$. In basic solutions (pH > 8.8), the peak at 745 cm^{-1}, due to $B(OH)_4^-$ ions, can be detected. The relative intensity of the $B(OH)_4^-$ peak

increases until a pH near 10.5, where it is the only peak present. The same trends were

seen for the other solutions, and are consistent with other studies of the pH dependence of

$B(OH)_3$ and $B(OH)_4^-$ species in solution.[23]

The areas of the $B(OH)_4^-$ and $B(OH)_3$ peaks at 745 cm^{-1} and 876 cm^{-1},
respectively, were measured for these different series of solutions and the area of the
$B(OH)_4^-$ peak was normalized to the sum of the area for both peaks and is plotted as a
function of pH in Figure 5. The sigmoidal trend shown is independent of boron
concentration and phosphorus concentration within the ranges studied. The empirically
derived equation for this fit is given by:

$$A_{745}/(A_{745}+A_{876}) = 1.046/(1 + 1.07 \times 10^9 * \exp(-2.196*pH)) \qquad (2)$$

Equation 2 can be used to calculate the pH of solutions where both borate species
are present in the range $8.0 \leq pH \leq 10.5$.

3.2. GLASS DISSOLUTION KINETICS

Figure 6 shows Raman spectra collected in a room temperature 0.1M K_2HPO_4
solution about 250 μm from the surfaces of the $20Na_2O-80B_2O_3$ and $5Na_2O-15CaO-$
$80B_2O_3$ glasses for times up to 210 minutes. The predominant borate species in solution
is $B(OH)_3$, indicated by the peak at 876 cm^{-1}. For longer reaction times, the area of this
peak increases relative to the phosphate peak at 989 cm^{-1}. The peak at 876 cm^{-1} increases
more rapidly when the $20Na_2O-80B_2O_3$ dissolves than when the $5Na_2O-15CaO-80B_2O_3$
glass dissolves. The relative areas of these peaks were measured and Equation 1 was used
to determine the boron concentration released to solution. Figure 7 shows a linear time
dependence for the release of boron into the phosphate solution from the $20Na_2O-80B_2O_3$
glass and a parabolic time dependence for the release of boron from the $5Na_2O-15CaO-$
$80B_2O_3$ glass and a $10Na_2O-30CaO-60B_2O_3$ glass.

Normalized weight loss ($[m_0-m_f]/m_0$, where m_o is the initial glass weight and m_f is
the glass weight after the designated dissolution time) data in room temperature 0.1 M

K_2HPO_4 aqueous solution are shown for all glasses in Figure 8. The time-dependence of the weight losses from the sodium borate glasses is linear (Figure 8a), with the $10Na_2O$-$90B_2O_3$ glass dissolving the fastest. The weight loss rates for glasses with 20-30 mol% Na_2O are similar and relatively low, and then increase for the glass with 35mol% Na_2O. The normalized weight loss data for the sodium calcium borate glasses are shown in Figure 8b. When CaO replaces Na_2O, the normalized weight loss decreases, and the $7.5Na_2O$-$22.5CaO$-$70B_2O_3$ and $10Na_2O$-$30CaO$-$60B_2O_3$ glasses have the lowest normalized weight loss.

Figure 9 shows Raman spectra of solutions following complete dissolution of xNa_2O-$(1-x)B_2O_3$ glasses in water (1 g glass/50 mL water). The spectra of solutions following dissolution of glasses with 0 and 0.1 Na_2O show predominantly $B(OH)_3$ species. As the soda content of the glass increases, the relative intensity of the peak for $B(OH)_4^-$ increases. Figure 10 shows the pH, measured by pH electrode, of room temperature 0.1M K_2HPO_4 solutions in which bulk binary sodium borate glasses have dissolved for the times indicated(initial SA/V=11.2) As the soda content of the glass increases, the pH of the solution increases. The pH of the solution with the $10Na_2O$-$90B_2O_3$ glass decreased with time.

A sample of $20Na_2O$-$80B_2O_3$ glass was dissolved in water and the pH was measured to be 8.50. The Raman spectrum of that solution is shown in Figure 11. Aliquots of the solution were adjust to pH = 11.53 with NaOH and pH = 6.89 with HCl. The original solution contained both $B(OH)_3$ and $B(OH)_4^-$ species, evidenced by the peaks at 876 cm^{-1} and 745 cm^{-1}, respectively. Using the respective peak areas and

Equation 2, the pH was calculated to be 8.46±0.06. The spectra with the adjusted pH values only contain $B(OH)_3$ for the acidic sample and $B(OH)_4^-$ for the basic sample.

3.3. CALCIUM PHOSPHATE PRECIPITATION.

Figure 12 shows Raman spectra collected from the surfaces of the $10Na_2O$-$90B_2O_3$, $5Na_2O$-$15CaO$-$80B_2O_3$, and $10Na_2O$-$30CaO$-$60B_2O_3$ glasses for different reaction times in 0.1M K_2HPO_4 solutions. The peaks in the 700-850 cm^{-1} region for all glasses are attributed to six-membered borate rings in the glass structure.[17] Peaks at 989 and 876 cm^{-1} are phosphate[11] and borate[6] species from the solution, respectively. There is no evidence for presence of a new phase precipitating on the surface of the $10Na_2O$-$90B_2O_3$ glass (Figure 12a). Additionally, the ratio of the intensity of the boroxol ring peak (806 cm^{-1}) to the intensity of the triborate ring peak (775 cm^{-1}) remains constant as the glass dissolves. Similar spectral observations were made for all of the binary sodium borate glasses. The spectra from the surface of the sodium calcium borate glasses show the formation of a new a peak at 960 cm^{-1}, attributed to the P-O symmetric stretching mode from a calcium phosphate layer that has formed on the surface of the glass.[19] The $5Na_2O$-$15CaO$-$80B_2O_3$ glass shows the presence of a calcium phosphate layer within two hours exposure to the phosphate solution, and by seven hours, the layer is thick enough to obscure the signal from the borate glass remaining underneath. The calcium phosphate peak can be detected on the surface of the $60B_2O_3$ glass within seven hours, but even after ten hours, the layer is not yet thick enough to obscure the glass signal underneath.

4.   DISCUSSION

As alkali and alkaline earth oxides are added to a B_2O_3 glass, the basicity of the glass increases. The modifying oxides (basic oxides) donate oxygen to the acidic glass network (B_2O_3). In the compositional range studied here, it is known that glasses with greater soda contents have greater fractions of four-coordinated borate species in the glass structure.[24] These structural changes will affect glass properties, including their dissolution rates in aqueous environments.

The boron release data for these Na-borate and Na-C-borate glasses can be compared with the respective dissolution reaction rates from the weight loss measurements. The weight of B_2O_3 lost from the glass was calculated from the B-concentrations measured by the Raman peak areas and the solution volume, using Equation (3). Earlier studies have shown that borate glasses dissolve congruently,[25-28] and if this is assumed here, then the concomitant weight losses of Na_2O and CaO can calculated from the measured B_2O_3 weight loss and from the weight ratios of the respective oxide components in the nominal glass compositions, according to Equations (4) and (5). The total weight of glass lost is then the sum of the weight loss of the individual components. For the Ca-containing glasses in phosphate solutions, a weight gain is calculated assuming that all of the calcium ions released from the dissolving glass react with phosphate anions in solution to form stoichiometric hydroxyapatite,[25, 26] according to Equation (6), with the calculated fractional weight loss shown in Equation (7).

$$w_{B_2O_3}(aq) = c_B * V * 3.201 \frac{g\ B_2O_3}{g\ B} \tag{3}$$

$$w_{Na_2O}\,(aq) = w_{B_2O_3}(aq) * \frac{x_{Na_2O}}{x_{B_2O_3}} \tag{4}$$

$$w_{CaO}\,(aq) = w_{B_2O_3}(aq) * \frac{x_{CaO}}{x_{B_2O_3}} \tag{5}$$

$$w_{HAP} = w_{CaO}(aq) * 1.798\,\frac{g\,HAP}{g\,CaO} \tag{6}$$

$$\frac{m_0 - m_f}{m_0} = \frac{m_0 - \left(w_{B_2O_3}(aq) + w_{Na_2O}\,(aq) + w_{CaO}\,(aq)\right) + w_{HAP}}{m_0} \tag{7}$$

where w_i is the weight of component i in solution (g), c_B is boron concentration (g/L), V is solution volume (L), m_0 is the initial weight of glass, and m_f is the final weight of glass.

The formation of a calcium phosphate phase on the surface of the glass causes a depletion of phosphate in the solution, which could affect boron concentration measurements, since the phosphate peak is used as a reference. Based on estimated Ca concentrations and stoichiometric hydroxyapatite formation, the phosphate concentration in solution is depleted by less than 5% for all experiments.

Using Equations (3)-(7) and the boron release rate equations from Figure 7, fractional weight loss can be predicted from the Raman spectra as a function of time for these glasses and are given by the solid lines in Figure 13, where they are shown to be in good agreement with the measured weight losses (closed data points),. A summary of the dissolution rates from all weight loss measurements and calculations from Raman experiments is provided in Figure 14. A linear kinetic model ($\Delta w = k_l \cdot t$) was used to fit the dissolution kinetics for the binary soda-borate glasses (Figure 14a), and a parabolic kinetic model ($\Delta w = k_p \cdot t^{1/2}$) was used to fit the dissolution kinetics of the calcium-containing glasses (Figure 14b) . The dissolution rates determined by Raman

measurements of borate release are consistent with those determined by weight loss measurements.

Glass dissolution may proceed by different processes. Hydration of metal cations results in the release of these cations to solution and their replacement by protons for charge balance. Hydrolysis results in the breaking of network bonds to form hydroxyls. Hydration of the modifying cations and hydrolysis of the borate network can be described by the following reactions, where $\emptyset$ represents a bridging oxygen.

Hydration

$$Na^+[\emptyset_3B]^--O-B\emptyset_2 + H_2O \rightarrow H^+[\emptyset_3B]^--O-B\emptyset_2 + Na^+ + OH^- \rightarrow HO-[\emptyset B]-O-B\emptyset_2 + Na^+ + OH^-$$

$$(8)$$

$$B\emptyset_2O^-Na^+ + H_2O \rightarrow B\emptyset_2(OH) + Na^+ + OH^- \qquad (9)$$
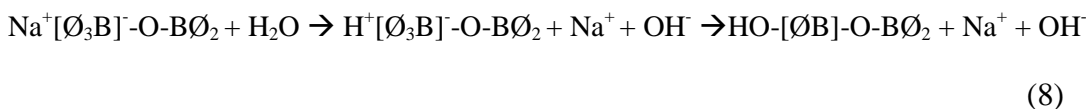
The replacement of an alkali ion associated with a four-coordinated boron with a proton in an initial hydration reaction creates an unstable four-coordinated borate unit, which must lower its coordination number to three to become stable.[29, 30] (Reaction 8) In this case, hydration of alkali ions in the borate glass structure is accompanied by the loss of a bridging oxygen bond between borate neighbors. The hydration of alkali ions on anionic three-coordinated borate units yields similar hydroxyl groups bonded to the borate units (Reaction 9). For both hydration reactions, solution pH will increase because of the consumption of protons.

During hydrolysis, water attacks the bridging bonds between neighboring three-coordinated borate units to eventually release boric acid to solution; two possible reactions are shown below, for the hydrolysis of hydrated borate sites formed by the

hydration reactions described above (Reaction 10) and for the hydrolysis trigonal sites in the original glass (Reaction 11) shown in Reaction 10.

Hydrolysis

$$B\emptyset_2OH + H_2O \rightarrow B(OH)_3 \text{ (aq)} \tag{10}$$

$$\emptyset_2B\text{-}O\text{-}B\emptyset_2 + 3H_2O \rightarrow 2B(OH)_3 \text{ (aq)} \tag{11}$$
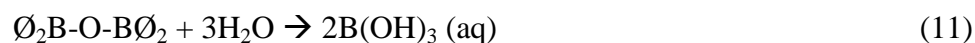
The release of boric acid to solution by the hydrolysis of the borate sites reaction would increase the pH of the solution.

The dissolution of borate glasses progresses by the simultaneous hydration of alkali (or alkaline earth) ions and hydrolysis of the borate network. A decrease in the rate of either reaction should decrease the dissolution rate of the glass. The net effect of glass dissolution on solution pH will depend on the relative concentrations of alkali and borate in the initial glass.

For the series of binary sodium borate glasses, the initial addition of Na_2O to B_2O_3 produces a significant decrease in the linear dissolution rate constants before reaching a broad minimum over the range of 20-30 mol% Na_2O (Figure 14), before increasing for the $35Na_2O\text{-}65B_2O_3$ glass Similar minima were observed by Velez, et al.[31] for the dissolution rates of $Li_2O\text{-}B_2O_3$ glasses in water. Nuclear magnetic resonance (NMR) studies have shown that additions of modifying oxides (alkalis and alkaline earths) to B_2O_3 glasses produce systematic increases in the fraction of tetrahedral borate units that constitute the glass structure, with anionic trigonal borate sites replacing the tetrahedral borate sites in the alkali- (or alkaline earth)-rich glasses. [24] Velez, et al. attributed the minimum in dissolution rates for their glasses to a maximum in network connectivity with the formation of four-coordinated boron in this compositional range.

Thus, in this compositional range, the slower hydration of the sodium ions associated with the tetrahedral sites (Reaction 8) controls the overall dissolution rates of these glasses. In the alkali-rich glasses, faster hydration of the alkalis associated with the anionic trigonal borate sites (reaction 11) accounts for the faster dissolution kinetics.

This simple dependence on structure, however, is not sufficient to explain the detailed dependence of dissolution rate on composition. For example, those NMR studies show that increasing the Na_2O-content of a binary Na-borate glass from 20 mole% to 30% mole% increases the fraction of four-coordinated boron from ~0.25 to ~0.42,[24] with no increase in dissolution rate (Figure 14). Likewise, Zhang, et al.[32] found that the dissolution rates in water decreased in densified low alkali Na_2O-B_2O_3 glasses that had smaller fractions of four-coordinated borate sites.[32] In addition to the relative hydration and hydrolysis rates, other factors, perhaps the transport of water into the glass structure, also affect the overall dissolution rates of these glasses..

The decrease in dissolution rate when CaO replaces Na_2O as the network modifier (Figure 14) indicates that the identity of the cation is also important for controlling the dissolution kinetics. This can be explained, for example, if the hydration reactions 8and 9 have different activation energies for the different alkali and alkaline earth ions. Slower hydration of Ca-ions would reduce the overall dissolution rates of the glasses.

The changes in solution pH with time (and with glass composition) can be understood in terms of the hydration reactions (8 and 9) and hydrolysis reactions (10 and 11) described above and will depend on the relative concentrations of NaOH (or $Ca(OH)_2$) and H_3BO_3 released to solution.. For example, as the alkali content of the glass increases, the phosphate solution will buffer to a higher pH following dissolution (Figure
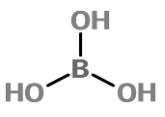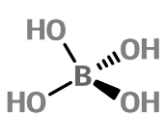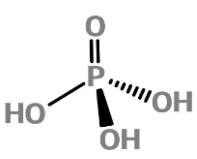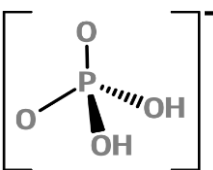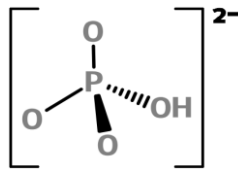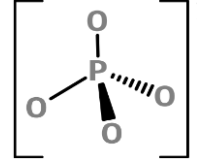
10). This in turn creates a higher concentration of four-coordinated boron in solution.

The increased proportion of $B(OH)_4^-$ in solution is not due to the greater fractions of

tetrahedral borates in the glasses with greater alkali oxide content (up to 33 mole%), but

is instead dependent only on the solution pH (Figure 11).

5.   CONCLUSIONS

Raman spectroscopy proved to be a useful tool for analyzing borate glass dissolution processes and kinetics. The type of borate species in solution was found to be dependent on pH and not the initial coordination of boron in the glass network. As a result, the fraction of four-coordinated boron in the solution could be used to measure solution pH. Boron release rates determined by increases in the intensities of Raman peaks in solution were in good agreement with those calculated from sample weight loss measurements. Additionally, calcium phosphate precipitation layers were characterized *in-situ* during the dissolution experiments.

TABLES AND FIGURES

Table 1. Raman peak assignments for borate and phosphate anionic species in solutions.

Species		Peak (cm^{-1})		Assignment		Ref
	B(OH)$_3$	sh, s	874-876	B3-O symmetric stretch	v_1	[10]
			495	B3-O bend	v_2	[10]
			1140-1155	B-O-H in-plane bend		[12]
	B(OH)$_4^-$	sh, s	745	B4-O symmetric stretch	v_1	[10]
			375	B4-O bend	v_2	[11]
			522		v_4	[11]
	H$_3$PO$_3$	sh, s	892	P-O-H symmetric stretch	v_1	[16]
		vb, w	1178	P=O symmetric stretch		[18]
			370			[16]
			498			[16]
			1010			[16]
			1080			[16]
	H$_2$PO$_4^-$	sh, s	874	P-O-H symmetric stretch	v_3	[15]
		sh, s	1074	PO2 symmetric stretch	v_1	[15]
		vb, m	380	bending mode		[15]
		b, m	514	bending mode		[15]
		vb, vw	1150	PO2 asymm stretch	v_6	[15]
	HPO$_4^{2-}$	sh, s	989	PO3 symmetric stretch	v_1	[15]
		b, m	850	P-O-H stretch	v_3	[15]
		b, m	390	O$_3$P(OH) bend	v_6	[15]
		b, m	530	PO3 deformation	v_2, v_5	[15]
		vb, w	1080	PO3 asymm stretch	v_4	[15]
	PO$_4^{3-}$	sh, s	934	PO4 symm stretch	v_1	[15]
		b, m	412	PO4 bending	v_2	[15]
		b, m	550	PO4 bending	v_4	[15]
		b, w	1007	PO4 asymm stretch	v_3	[15]

sh-sharp, b-broad, vb-very broad; s-strong, m-medium, w-weak
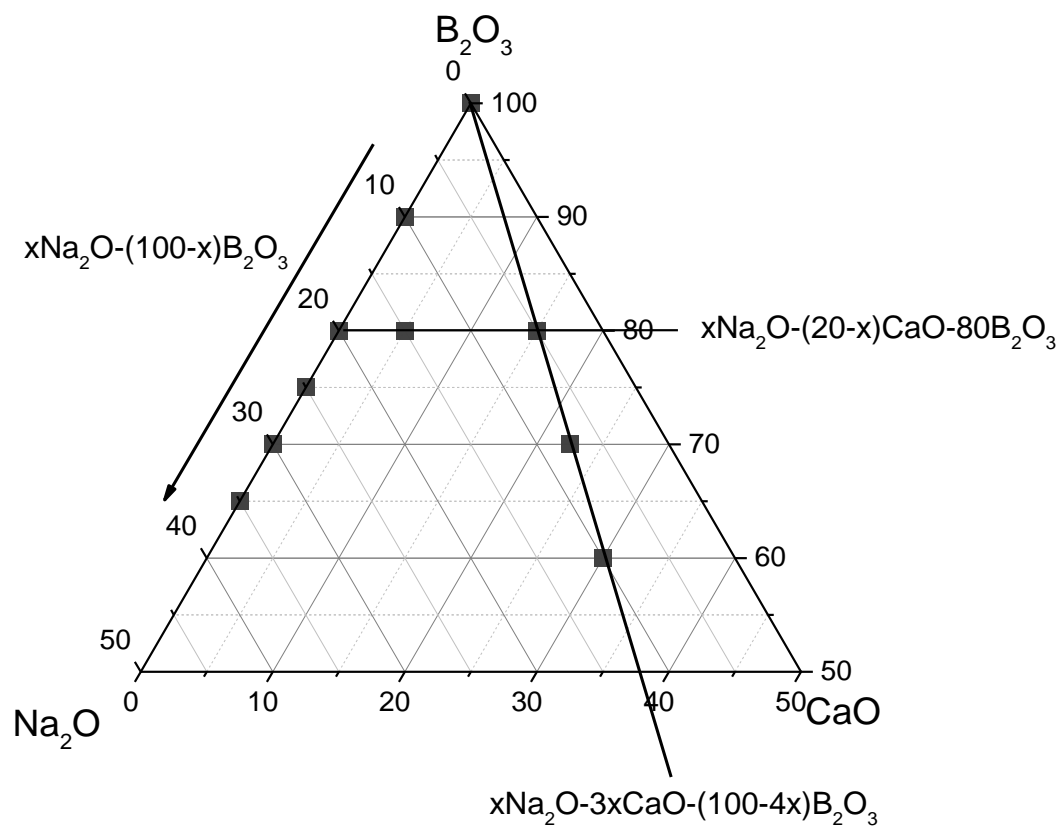
Figure 1. Molar compositions of the glasses investigated in this study.
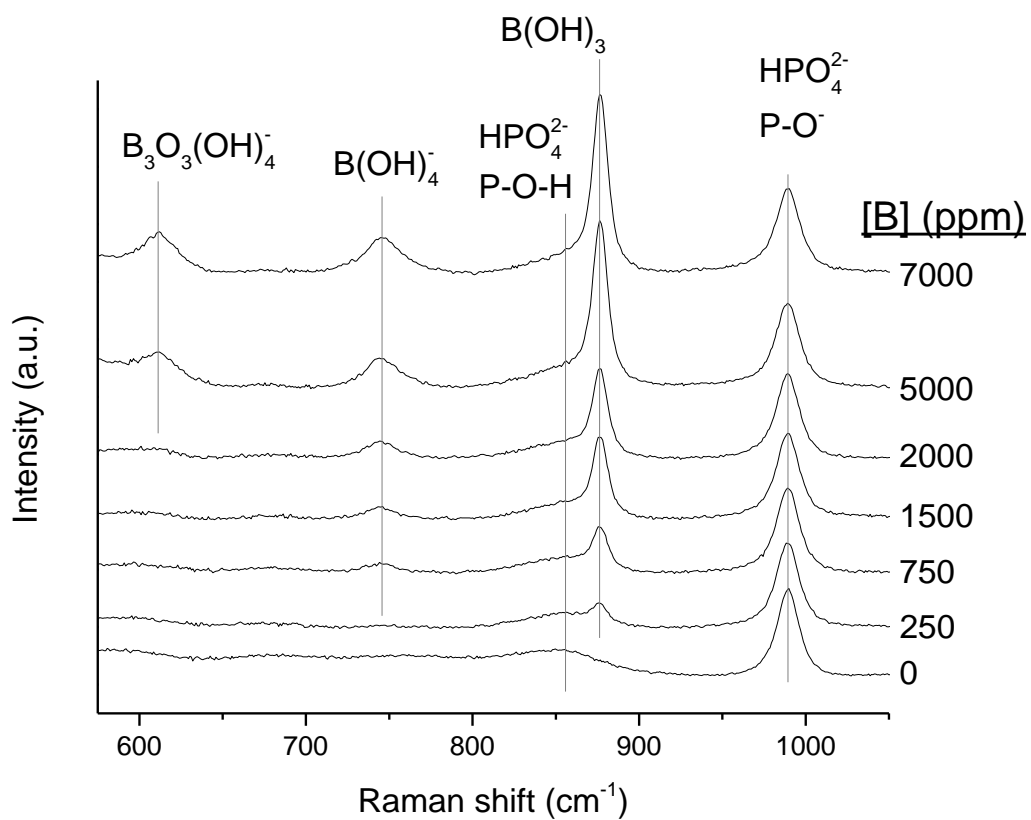
Figure 2. Raman spectra for 0.1 M K_2HPO_4 solutions with varying amounts H_3BO_3 added. The pH was adjusted to 8.78±0.03 with NaOH.
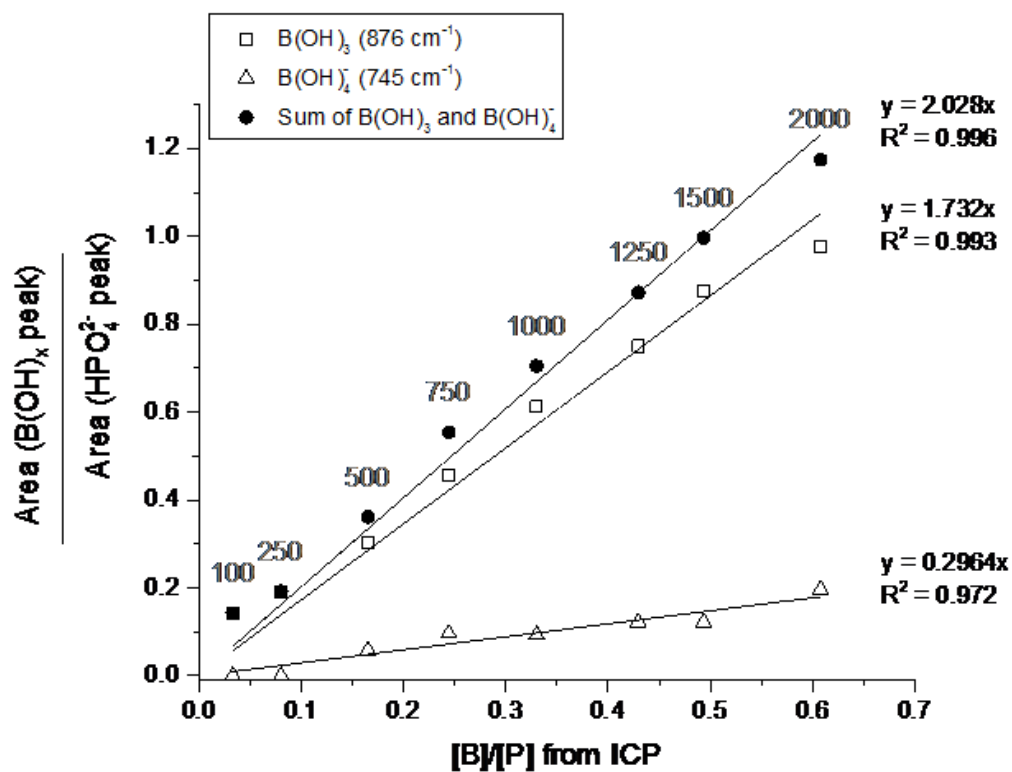
Figure 3. Areas of Raman peaks for B(OH)$_3$ and B(OH)$_4^-$ normalized to the P-O- peak area for HPO$_4^{2-}$ shown as a function of the analyzed [B]/[P]. The linear fit for each data set is shown on the right. The values above the data points are the approximate boron concentrations in ppm by weight.
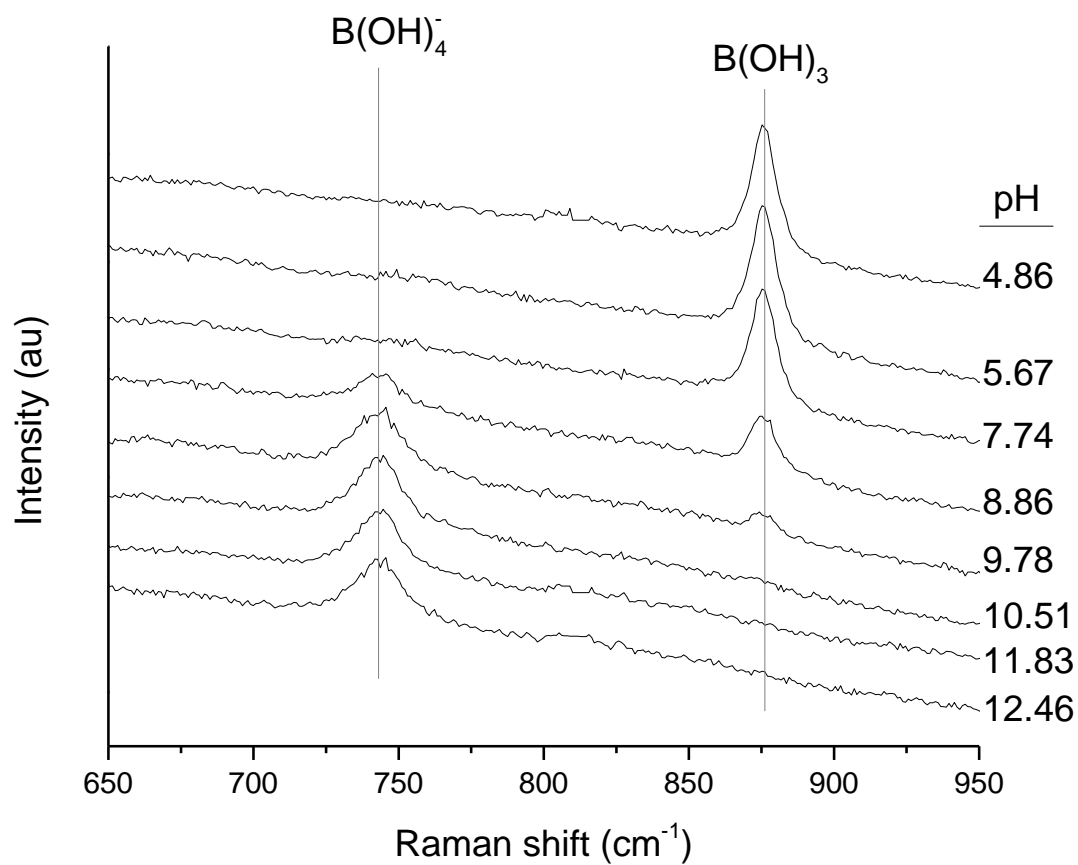
Figure 4. Raman spectra for solutions containing water and H_3BO_3, with pH adjusted as indicated with NaOH.
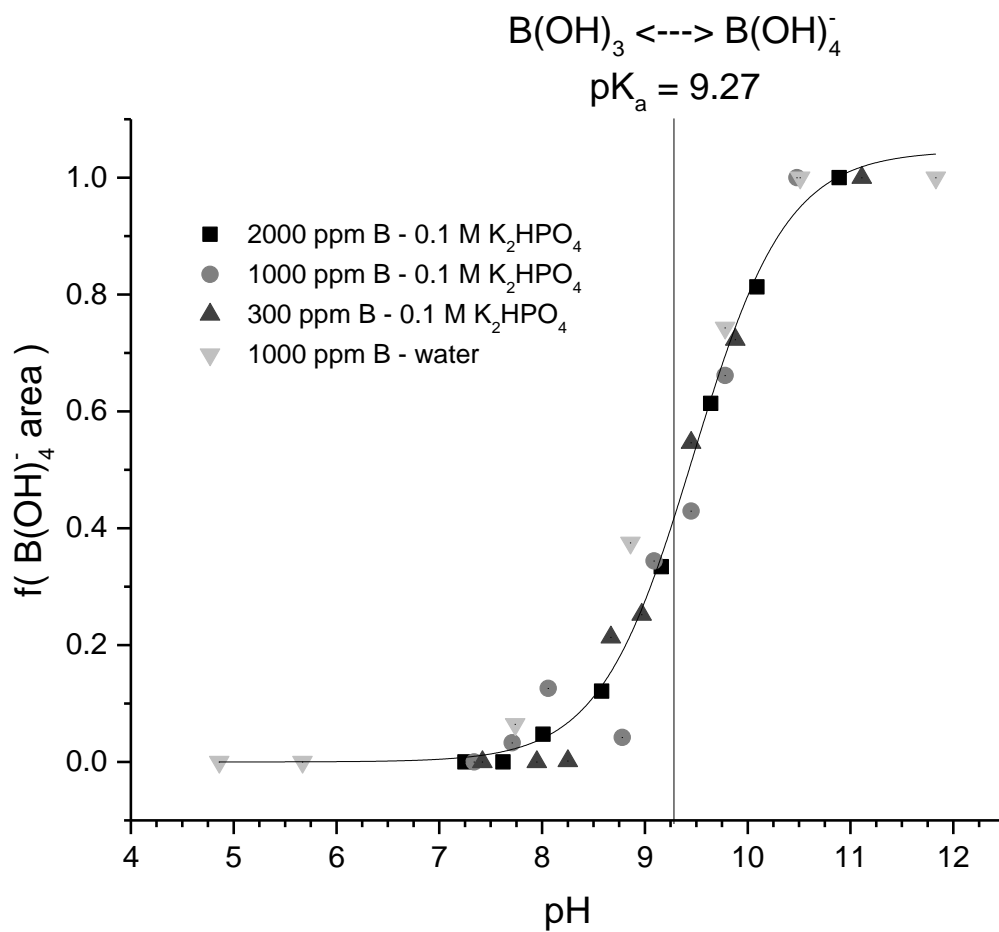
Figure 5. Fractional Raman peak area of $B(OH)_4^-$ relative to the total area for the $B(OH)_4^-$ and $B(OH)_3$ peaks as a function of pH, for several series of borate-phosphate solutions.
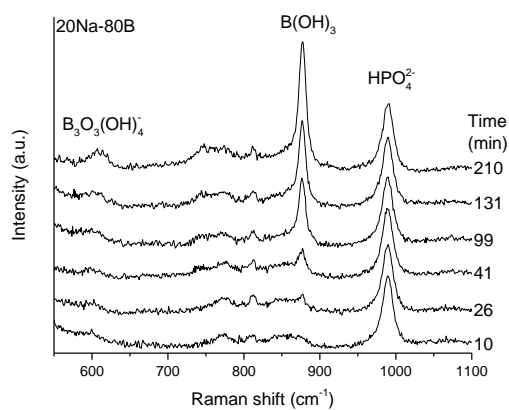
(a)
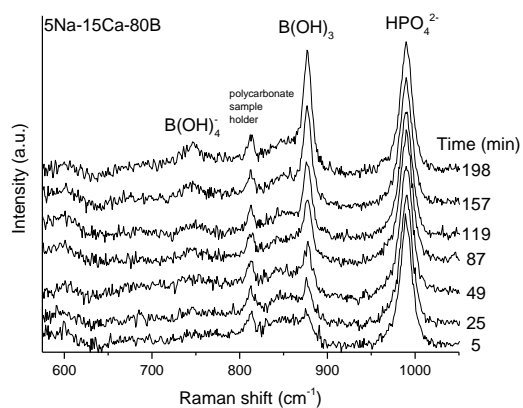
(b)

Figure 6. Raman spectra of room temperature 0.1 M K_2HPO_4 solutions in which (a) $20Na_2O\text{-}80B_2O_3$ and (b) $5Na_2O\text{-}15CaO\text{-}80B_2O_3$ glasses were dissolved for different times; spectra were collected 250 μm from the surface of each glass.
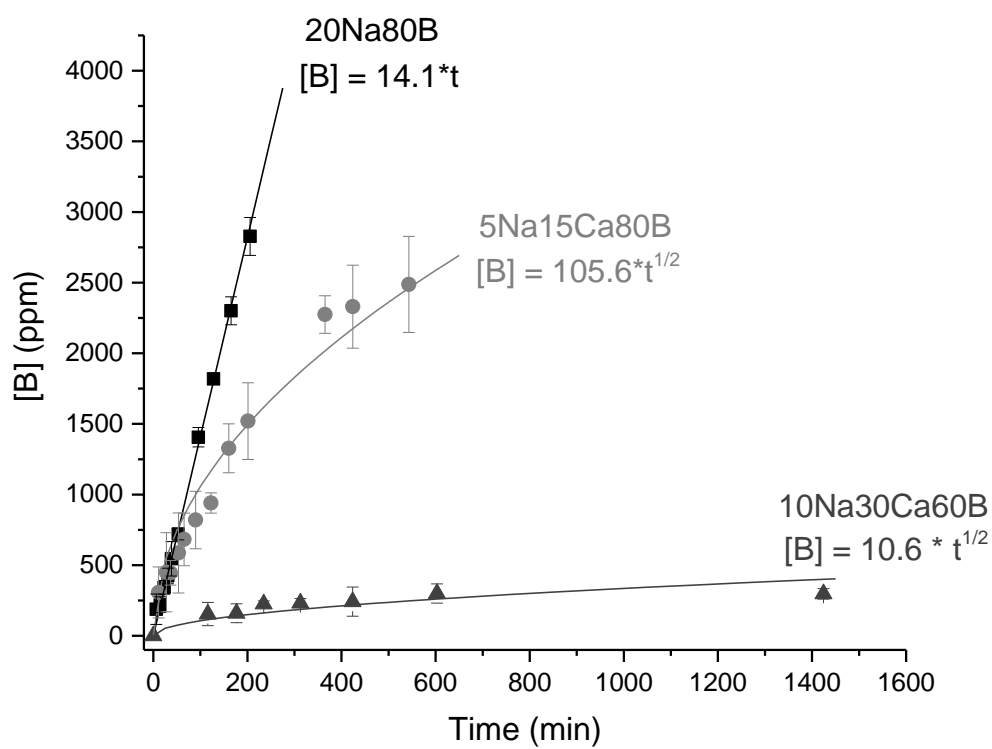
Figure 7. Boron release data from $20Na_2O-80B_2O_3$, $5Na_2O-15CaO-80B_2O_3$, and $10Na_2O-30CaO-60B_2O_3$ glasses in room temperature 0.1 M K_2HPO_4 aqueous solutions from Raman spectra; symbols are measured values and lines are linear or parabolic fits, as indicated.
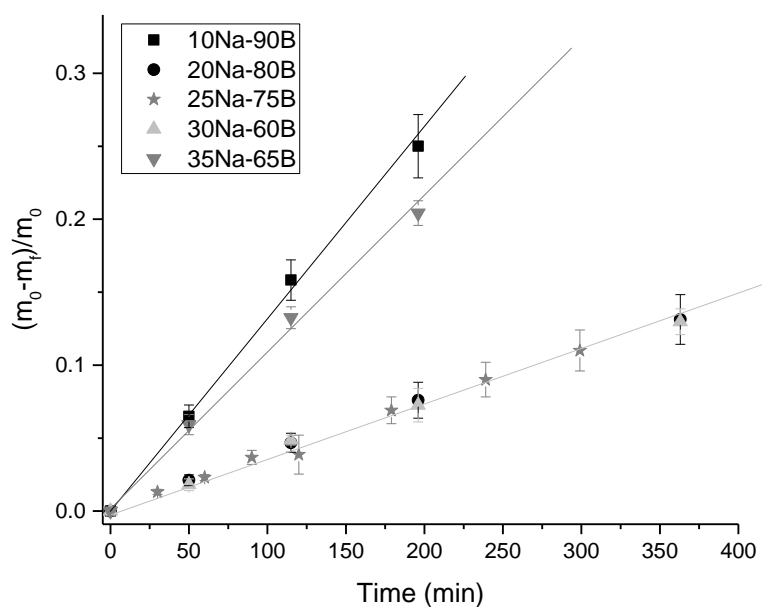
(a)
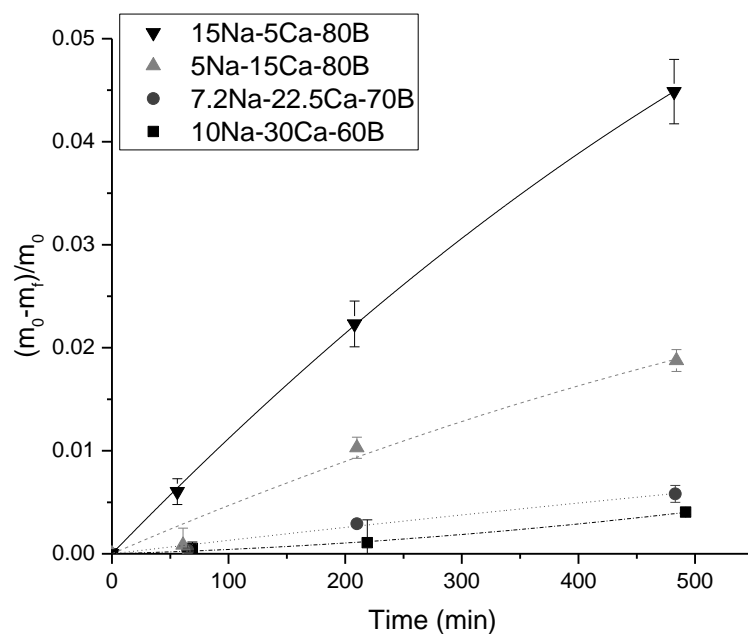
(b)

Figure 8. Normalized weight loss measurements for (a) sodium borate glasses and (b) sodium calcium borate glasses in room temperature 0.1 M K_2HPO_4 aqueous solution; symbols are measured values and lines are linear fits for the sodium borate glasses and parabolic fits for the sodium calcium borate glasses.
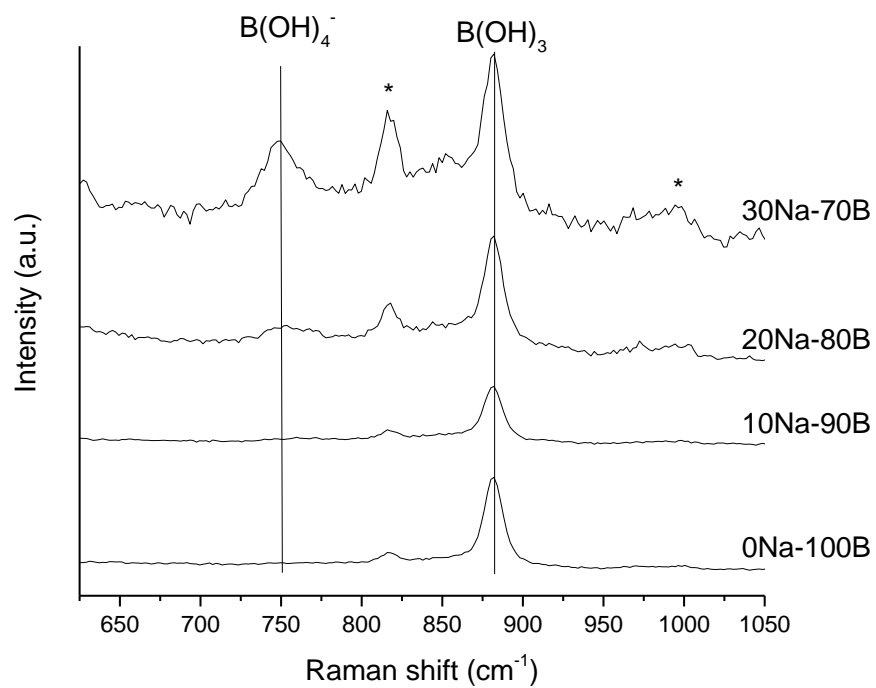
Figure 9. Raman spectra of solutions following dissolution of binary sodium borate glasses in water. The peaks with the asterisk (*) are from the polycarbonate sample holder.
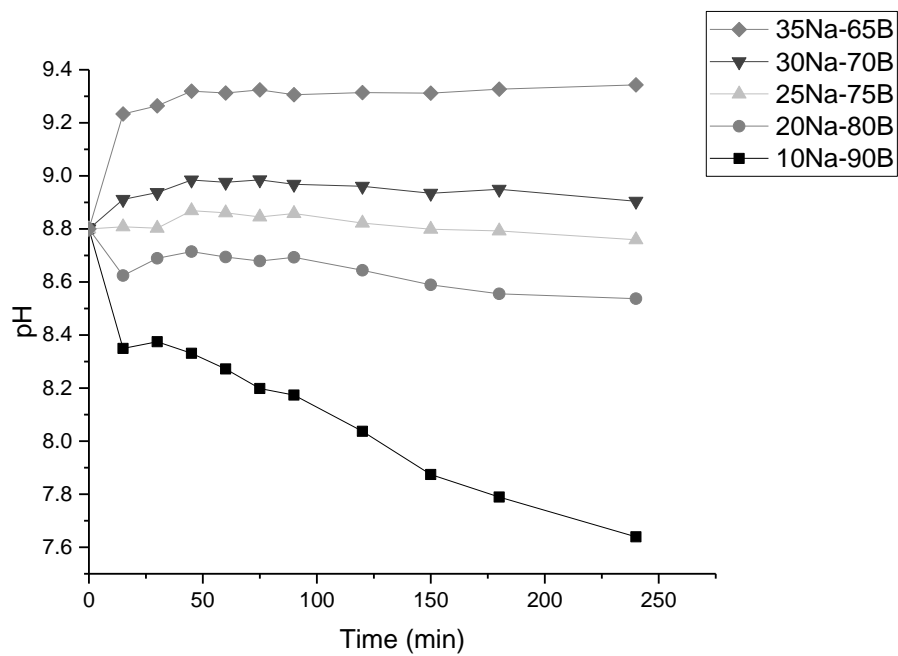
Figure 10. pH as a function of time as binary sodium borate glasses are dissolved in 0.1M K$_2$HPO$_4$ solution
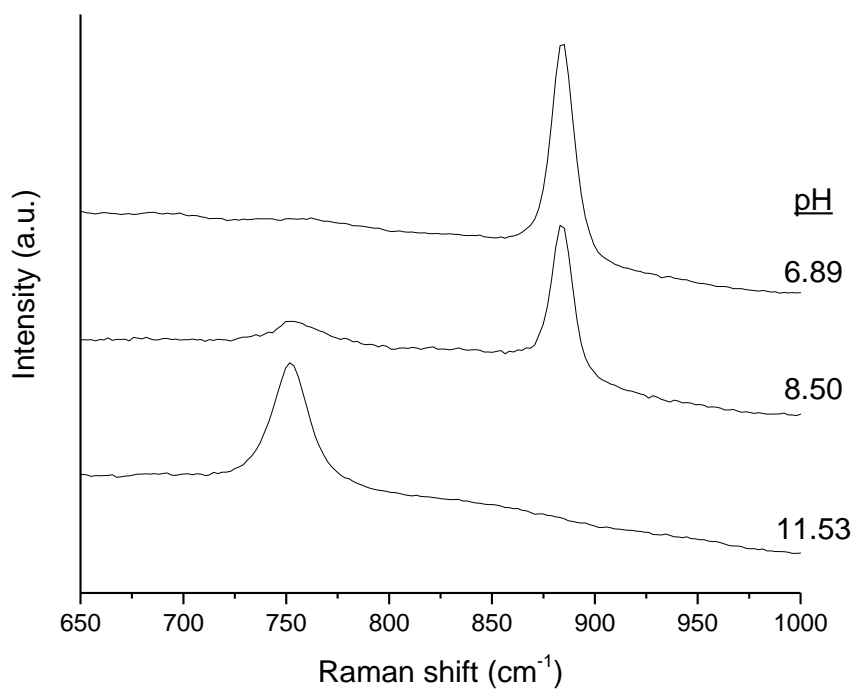
Figure 11. Raman spectra of different solutions following the dissolution of the $20Na_2O$-$80B_2O_3$ glass in water: as dissolved (pH=8.50), after adjusting to a lower pH with HCl (pH=6.89), and after adjusting to a higher pH with NaOH (pH=11.53).
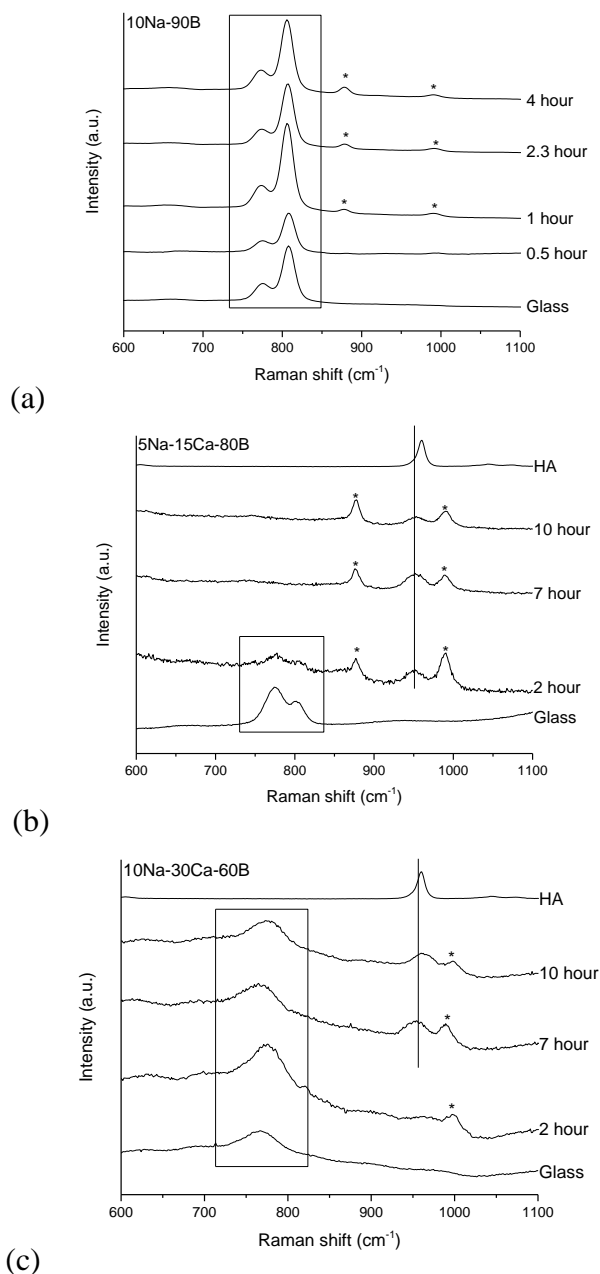
Figure 12. Raman spectra collected from the surfaces of the (a) $10Na_2O-90B_2O_3$, (b) $5Na_2O-15CaO-90B_2O_3$, and (c) $10Na_2O-30CaO-60B_2O_3$ glasses after reaction in room temperature 0.1 M K_2HPO_4 solution for the times indicated. Peaks encompassed by the box are assigned to six-membered borate rings in the glass structure. Peaks indicated by an asterisk (*) represent borate and phosphate species in solution. Peaks indicated by the vertical line represent the P-O symmetric stretch for the calcium phosphate reaction layer that formed on the glass surface. The spectrum for hydroxyapatite (HA) is shown for reference.
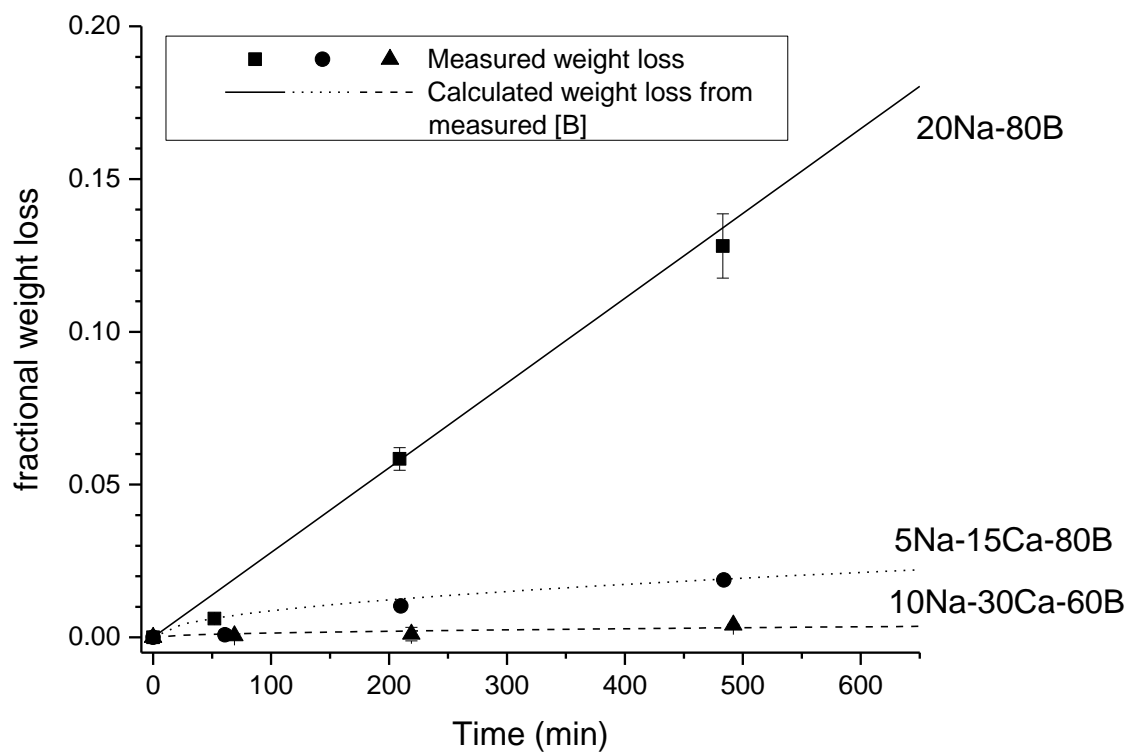
Figure 13. Fractional weight loss measurements (solid points) compared to weight losses calculated from boron concentration trends based on the Raman data (lines).
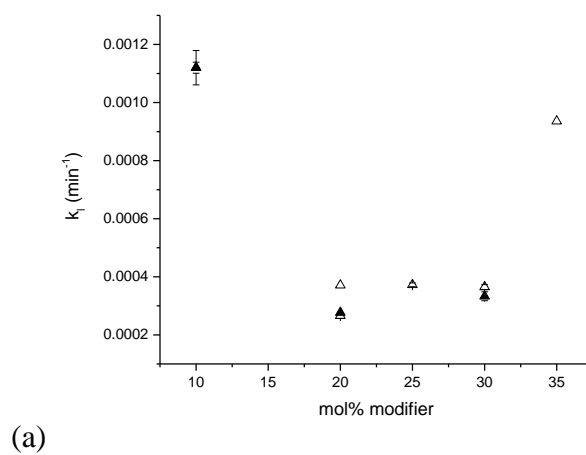
(a)
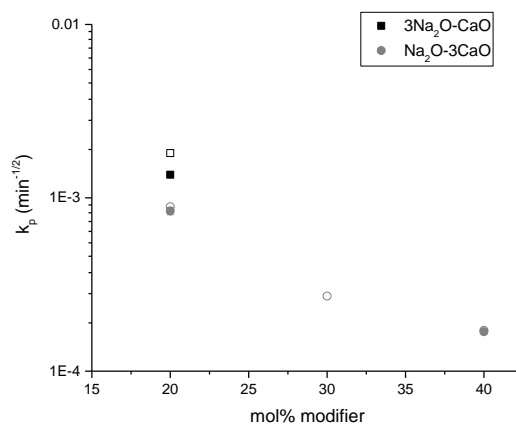
(b)

Figure 14. Dissolution constants for three series of glasses in room temperature 0.1M K$_2$HPO$_4$ solution, calculated from the weight loss (open symbols) and Raman (closed symbols) experiments. (a) Linear reaction constant (k$_l$) for the sodium borate glasses and (b) parabolic reaction constant (k$_p$) for sodium calcium borate glasses. Error bars not shown are within the size of the marker.

REFERENCES

[1] L. Bi, M. Rahaman, D. Day, Z. Brown, C. Samujh, X. Liu, A. Mohammadkhah, V. Dusevich, J. D. Eick and L. Bonewald, "Effect of Bioactive Borate Glass Microstructure on Bone Regeneration, Angiogenesis, and Hydroxyapatite Conversion in a Rat Calvarial Defect Model," *Acta Biomater.*, **9** [8] 8015-26 (2013).

[2] S. B. Jung, "Bioactive Borate Glasses"; chapter in Bio-Glasses: An Introduction; Edited by J. R. Jones and A. G. Clare. John Wiley & Sons, Ltd., 2012.

[3] M. Rahaman, D. Day, S. Bal, Q. Fu, S. Jung, L. Bonewald and A. Tomsia, "Bioactive Glass in Tissue Engineering," *Acta Biomater.*, **7** [6] 2355-73 (2011).

[4] W. Huang, M. Rahaman, D. Day and Y. Li, "Mechanisms for Converting Bioative Silicate, Borate, and Borosilicate Glasses to Hydroxyapatite in Dilute Phosphate Solution," *Phys. Chem. Glasses: Eur.J. Glass Sci. Technol. B*, **47** [6] 647-58 (2006).

[5] S. Jung and D. Day, "Conversion Kinetics of Silicate, Borosilicate, and Borate Bioactive Glasses to Hydroxyapatite," *Phys. Chem. Glasses: Eur.J. Glass Sci. Technol. B*, **50** [2] 85-8 (2009).

[6] L. Maya, "Identification of Polyborate and Fluoropolyborate Ions in Solution by Raman Spectroscopy," *Inorg. Chem.*, **15** [9] 2179-84 (1976).

[7] M. Maeda, T. Hirao, M. Kotaka and H. Kakihana, "Raman Spectra of Polyborate Ions in Aqueous Solution," *J. Inorg. Nucl. Chem.*, **41** 1217-20 (1979).

[8] L. Zhihong, G. Bo, L. Shuni, H. Mancheng and X. Shuping, "Raman Spectroscopic Analysis of Supersaturated Aqueous Solution of $MgO-B_2O_3$-$32\%MgCl_2-H_2O$," *Spectrochim. Acta, Part A*, **60** 3125-8 (2004).

[9] Y. Zhou, C. Fang, Y. Fang and F. Zhu, "Polyborates in Aqueous Borate Solution: A Raman and DFT Theory Investigation," *Spectrochimica Acta Part A: Molecular and Biomolecular Spectroscopy*, **83** [1] 82-7 (2011).

[10] C. Schmidt, R. Thomas and W. Heinrich, "Boron Speciation in Aqueous Fluids at 22 to 600 °C and 0.1 MPa to 2 GPa," *Geochim. Cosmochim. Acta*, **69** [2] 275-81 (2005).

[11] C. Preston and W. A. Adams, "A Laser Raman Spectroscopic Study of Aqueous Orthophosphate Salts," *J. Phys. Chem. A*, **83** [7] 814-21 (1979).

[12]   C. Preston and W. A. Adams, "A Laser Raman Spectroscopic Study of Aqueous Phophoric Acid," *Can. J. Spectrosc.*, **22** 125-36 (1977).

[13]   M. Cherif, A. Mgaidi, N. Ammar, G. Vallée and W. Fürst, "A New Investigation of Aqueous Orthophosphoric Acid Speciation Using Raman Spectroscopy," *J. Solution Chem.*, **29** [3] 255-69 (2000).

[14]   W. W. Rudolph, "Raman-and Infrared-Spectroscopic Investigations of Dilute Aqueous Phosphoric Acid Solutions," *Dalton Trans.*, **39** [40] 9642-53 (2010).

[15]   J. L. Anderson, E. M. Eyring and M. P. Whittaker, "Temperature Jump Rate Studies of Polyborate Formation in Aqueous Boric Acid," *J. Phys. Chem. A*, **68** [5] 1128-32 (1964).

[16]   Q. Fu, M. N. Rahaman, H. Fu and X. Liu, "Silicate, Borosilicate, and Borate Bioactive Glass Scaffolds with Controllable Degradation Rate for Bone Tissue Engineering Applications. I. Preparation and in Vitro Degradation," *J. Biomed. Mater. Res. A*, **95A** [1] 164-71 (2010).

[17]   W. L. Konijnendijk and J. M. Stevels, "The Structure of Borate Glasses Studied by Raman Scattering," *J. Non-Cryst. Solids*, **18** 301-31 (1975).

[18]   E. I. Kamitsos, M. A. Karakassides and G. D. Chryssikos, "Vibrational Spectra of Magnesium-Sodium-Borate Glasses. 2. Raman and Mid-Infrared Investigation of the Network Structure," *The Journal of Physical Chemistry*, **91** [5] 1073-9 (1987).

[19]   M. Kazanci, P. Fratzl, K. Klaushofer and E. P. Paschalis, "Complementary Information on in Vitro Conversion of Amorphous (Precursor) Calcium Phosphate to Hydroxyapatite from Raman Microspectroscopy and Wide-Angle X-Ray Scattering," *Calcif. Tissue Int.*, **79** [5] 354-9 (2006).

[20]   R. Cuscó, F. Guitián, S. d. Aza and L. Artús, "Differentiation between Hydroxyapatite and β-Tricalcium Phosphate by Means of μ-Raman Spectroscopy," *J. Eur. Ceram. Soc.*, **18** [9] 1301-5 (1998).

[21]   D. Leipply, B. A. Melhus, M. R. Leonardo, S. A. Feller and M. Affatigato, "Development of Functional Borate Glass Surfaces to Inhibit Bacterial Growth," *Glass Technology - European Journal of Glass Science and Technology Part A*, **47** [5] 127-32 (2006).

[22]   J. Jones, A. Vats, I. Notingher, J. Gough, N. Tolley, J. Polak and L. Hench, "*In Situ* Monitoring of Chondrocyte Response to Bioactive Scaffolds Using Raman Spectroscopy," *Key Eng. Mater.*, **284-286** 623-6 (2005).

[23]   R. E. Mesmer, J. C. F. Baes and F. H. Sweeton, "Acidity Measurements at Elevated Temperatures VI Boric Acid Equilibria," *Inorg. Chem.*, **11** [3] 537-43 (1971).

[24]   P. J. Bray and J. G. O'Keefe, "Nuclear Magnetic Resonance Investigations of the Structure of Alkali Borate Glasses," *Phys. Chem. Glasses*, **4** [2] 37-46 (1963).

[25]   N. Vanderspiegel, "Reaction of Potassium Calcium Borate Glasses to Form Apatite and Dicalcium Phosphate Dihydrate"; Master of Science Thesis. University of Missouri - Rolla, Rolla, MO, 2004.

[26]   J. Lowry, "Dissolution Behavior of Alkali Borate Glasses"; Master of Science Thesis. University of Missouri - Rolla, Rolla, MO, 2002.

[27]   Y. Gu, W. Xiao, L. Lu, W. Huang, M. Rahaman and D. Wang, "Kinetics and Mechanisms of Converting Bioactive Borate Glasses to Hydroxyapatite in Aqueous Phosphate Solution," *J. Mater. Sci.*, **46** [1] 47-54 (2011).

[28]   B. C. Bunker, G. W. Arnold, D. E. Day and P. J. Bray, "The Effect of Molecular Structure on Borosilicate Glass Leaching," *J. Non-Cryst. Solids*, **87** [1–2] 226-53 (1986).

[29]   P. Zapol, H. He, K. D. Kwon and L. J. Criscenti, "First-Principles Study of Hydrolysis Reaction Barriers in a Sodium Borosilicate Glass," *International Journal of Applied Glass Science*, **4** [4] 395-407 (2013).

[30]   G. Geneste, F. Bouyer and S. Gin, "Hydrogen–Sodium Interdiffusion in Borosilicate Glasses Investigated from First Principles," *J. Non-Cryst. Solids*, **352** [28–29] 3147-52 (2006).

[31]   M. H. Velez, H. L. Tuller and D. R. Uhlmann, "Chemical Durability of Lithium Borate Glasses," *J. Non-Cryst. Solids*, **49** 351-62 (1982).

[32]   Z. Zhang, K. Hirao and N. Soga, "Water Corrosion Behavior of Densified Glass. II. Borate Glasses," *J. Non-Cryst. Solids*, **135** [1] 62-6 (1991).

II.   DISSOLUTION OF A BIOACTIVE BORATE GLASS UNDER STATIC CONDITIONS

AUTHORS

Jaime L. George
Richard K. Brow

ABSTRACT

The dissolution kinetics in water of a borate glass developed for biomedical applications were studied at temperatures from 21-60°C. As the glasses react, B, Ca, Na, K, Mg, and P are released from the glass and Ca, Mg, and P precipitate to form a magnesium-containing amorphous calcium phosphate (ACP) layer on the surface of the glass. The dissolution rates are initially described by a reaction-controlled contracting volume model, but after the glass is ~25-30% reacted, a diffusion-controlled Jander three-dimension model better describes dissolution kinetics. The change in reaction model is attributed to the diffusion of species from the glass or solution through the ACP layer. The activation energy for the reaction-controlled process is 41.1±0.6 kJ/mol, whereas the activation energy for the diffusion process is 32.3±0.1 kJ/mol.

1.   INTRODUCTION

Bioactive glasses have been studied for hard and soft tissue repair since the 1970s when Hench first reported the efficacious effects of the silicate glass designated 45S5.[1] Other bioactive silicate glass compositions have been investigated, including 13-93 which is less likely to crystallize upon reheating than 45S5 and is therefore suited for making scaffolds by sintering particle and fibers.[2] Although silicate glasses have received the most attention for biomedical applications, borate glasses have recently been developed for similar applications.[3-7] Borate glasses react faster in aqueous environments than do silicate glasses, and this can lead to more rapid formation of calcium phosphate reaction products, and faster release of other ions, which may be beneficial for some medical treatments.[3, 6-8]

Reaction kinetics of the silicate glasses 45S5 and 13-93, along with borate and borosilicate analogues, have been previously studied in phosphate-containing solutions including simulated body fluid (SBF) and 0.02M K_2HPO_4 at 37°C.[6, 8] Linear dissolution kinetics of the borate analogue of 45S5 in 0.02M K_2HPO_4 were described by a reaction-controlled model, whereas the silicate and borosilicate analogues initially followed the linear reaction-controlled kinetic model and then transitioned to a parabolic, diffusion-controlled kinetic model after about 30h.[3] The change in kinetic behavior was attributed to the formation of a rate-controlling silica gel layer, through which reaction species diffused.[3] The dissolution behavior in SBF of scaffolds of the borate analogue of 13-93 (13-93B3) was described by a diffusion-controlled dissolution model.[6]

The dissolution of simple borate glasses in water has been described. Alkali borate glasses lose weight linearly with time[9, 10] and their dissolution rates increase as

pH decreases from 9-10 to 7.[9, 11] For binary alkali (M_2O) borate glasses, the dissolution

rates are lowest with M_2O contents in the range of 25-30 mol%; these glasses generally

have the largest fractions of tetrahedral borate sites.[9] First principles calculations

indicate that hydrolysis of borate sites in sodium borosilicate glasses are more likely in

acidic environments than basic environments,[11] which is in agreement with previous

experimental measurements.[9]

      In the present work, the dissolution kinetics of 13-93B3 glass particles in water at

temperatures ranging from 21°C to 60°C are reported and the effects of changing solution

conditions on the precipitation of amorphous calcium phosphate reaction products on

dissolution kinetics are discussed.

2.   EXPERIMENTAL PROCEDURE

2.1. GLASS PREPARATION

A glass, designated 13-93B3, with the nominal composition (wt%) 12 K2O – 6 Na2O – 20 CaO –5 MgO – 53 B_2O_3 –4 P_2O_5 was prepared by conventional melt quenching techniques. The raw materials, H_3BO_3 (98%, Alfa Aesar), $CaCO_3$, (98%, Alfa Aesar), K_2CO_3, (99%, Alfa Aesar), Na_2CO_3 (98%, Alfa Aesar), $MgCO_3$ (USP/FCC grade, Fisher Scientific), and $NH_2H_2PO_4$ (98%, Alfa Aesar), were mixed and melted in air for one hour at 1075°C in a Pt-Rh crucible. The melt was quenched between two steel plates to form glass that was stored in a desiccator prior to the dissolution experiments.

2.2. STATIC DISSOLUTION EXPERIMENTS

Glass particles with a weight of 200±5 mg were rinsed in ethanol to remove fines, added to a polypropylene conical tube with 50 mL of deionized water, and placed on their side in an oven at either 39, 50, or 60°C, or were stored on a lab bench at 21°C. Particles were distributed along the bottom of the container to ensure maximum exposure to solution and were agitated once a day to prevent agglomeration. Samples were removed from the oven and particles were collected with 8 μm filter paper from solutions at different times through 150 hr. Particles were rinsed twice with deionized water and twice with ethanol, then dried overnight at 100 °C before weighing. The pH of each solution was analyzed (Accumet pH electrode) at temperature, and the solution was then diluted 1:10-1:100 with 1 vol% HNO_3 for elemental analysis using inductively-coupled plasma optical emission spectroscopy (ICP-OES, PerkinElmer Optima 2000 DV, Norwalk, USA).

X-ray diffraction (XRD) was used to characterize the as-reacted particles using a

Philips X'pert multipurpose diffractometer with PIXcel detector, with Cu K_α radiation

and Ni filter, at 45 kV and 40 mA. Reacted particles were also mounted in epoxy,

polished to a 1200 grit, and then characterized with a scanning electron microscope

(SEM, Hitachi S4700, Hitachi High-Tech, Tokyo, Japan) and the attached energy

dispersive spectroscopy (EDS) system.

3.   RESULTS

Ion release data for 13-93 B3 in water at 39 °C is shown in Figure 1(a).

Horizontal lines are the solution concentrations expected after complete dissolution of the

glass. The concentrations of B, Ca, Mg, Na, and K increase with time for about 200 ks

(56 hrs) and then level off. About 80-90% of the total B, Na, and K are released from the

13-93B3 particles at the conclusion of the experiment, whereas less than 60% of the Ca

and Mg species, and less than 1% of the P-species, have been released. The ratios of each

species in solution, normalized to the respective B-concentrations are constant with

respect to time, as shown in Figure 1(b). Figure 1(c) shows the element-to-boron ratios at

the conclusion of this dissolution experiment, divided by the respective element-to-boron

ratio in the base glass. These ratios indicate that Na and K are released congruently with

respect to B, ratios equal 1, and that there are deficiencies of Ca, Mg, and P in the

solution, relative to their respective concentrations in the glass. Similar sets of data were

collected for dissolution experiments done at other temperatures.

Kinetic analyses of the dissolution processes were done using the B-release data.

To determine the extent of dissolution at a given time, α_t, the concentration of boron at

that time (B_t) was normalized to the concentration of boron in solution assuming

complete dissolution (B_{final}), given as,

$$\alpha_t = \frac{B_t}{B_{final}} \tag{1}$$

The fractions released to water at different temperatures are plotted a function of

dissolution time in Figure 2. The borate release rate increases at greater temperatures.

The α_t values shown in Figure 2 are analyzed using two models developed to describe the reactions of spherical particles.[12] The contracting volume model (CVM) assumes a reaction-controlled mechanism where particles react with their surroundings at their surfaces and as the reaction continues, the spheres systematically decrease in size. For spherical particles, the reacted fraction will depend on reaction time according to

$$1 - (1 - \alpha_t)^{1/3} = k_{CVM}t \tag{2}$$

where k_{CVM} is the contracting volume model reaction constant. The Jander 3D diffusion model assumes that diffusional process controls the rate at which the spherical particles will react, leading to the reaction rate equation

$$1 - (1 - \alpha_t)^{1/3} = k_{DM}t^{1/2} \tag{3}$$

where k_{DM} is the diffusion model reaction constant.

The boron release data were evaluated using both reaction models. For experiments done at each temperature, the contracting volume model initially provided the best fit to the boron release data, indicating that the glass dissolution processes were initially reaction-controlled. For example, the initial (t < 40ks,~11 hours) borate-release data for the 21°C experiments are shown in Figure 3(a) with a fit to the CVM (Equation 2). The data at longer times (t > 48 ks,~13 hours), however, are better fit to the 3D diffusion model (Equation 3), as shown in Figure 3(b). The reaction constants, k_{CVM} and k_{DM}, were determined from the slopes of the respective fits in Figure 3(a and b), and the resulting relationship between α_t dissolution time is shown Figure 3(c) along with the measured data. The two reaction rate constants for each experiment are given in Table 1. The transition from a reaction-controlled mechanism to a diffusion-controlled mechanism

was observed at every experimental temperature, with the transition decreasing with
increasing temperatures (Tables and Figures

Table 1). For each experiment, the transition occurs when approximately 25-30%
of the borate has been released.

The reaction constants were determined for both reaction mechanisms at all four
temperatures. The temperature dependence of the reaction constant can be described by
an Arrhenius model, shown in Equation (4),

$$\mathrm{k} = A \, exp\left(\frac{E_A}{RT}\right) \tag{4}$$

where E_A is the activation energy (kJ/mol), R is the gas constant (J mol^{-1} K^{-1}), T is the
temperature (K), and A is a constant (s^{-1}). The Arrhenius dependences of the two reaction
constants are shown in Figure 3(d). The activation energies, calculated from the slopes of
the lines, are 41.1±0.6 kJ/mol for the reaction-controlled regime and 32.3±0.1 kJ/mol for
the diffusion-controlled regime. The activation energy of the reaction-controlled regime
is similar to measured activation energy values for dissolution of ulexite in aqueous
EDTA solution, which is reported as 36 kJ/mol,[13] and within the range of 39-115 kJ/mol
as predicted by Zapol for the dissolution of borosilicate glass. [11]

Micrographs and micro-analyses of the cross-sections of a partially-reacted glass
particle (21°C, 4 days) are shown in Figure 4(a). The EDS analyses in Figure 4(b-g) show
that the unreacted glass (A) contains Na, K, Ca, Mg, and P, whereas the reaction layer
(B) is rich in Ca, Mg, and P; B could not be detected by this EDS system. There was no
trend between Ca/P ratio and temperature or reaction time. The Ca/P in the reaction
products is 2.23±0.4.

Figure 5 shows the cross-section of the microstructure of the reaction layer that formed on 13-93B3 particles after 4h, 16h, and 6d in 21 °C water. After 4h at 21°C, the layer is approximately 500nm thick and is discontinuous. After 16h, the layer thickness has increased to 1-1.5μm and is more continuous, and after six days, the reaction product is 10-15μm thick. The 6d reaction product is comprised of many layers that are less than 1 μm thick, but with thicker and more well-separated layers on the outside of the particle, near the solution, than on the inside, near the unreacted glass core. XRD diffraction patterns for a reaction product and for hydroxyapatite are shown in Figure 6. The reaction products are x-ray amorphous at all times up to 2 weeks for all experimental temperatures.

4.   DISCUSSION

Initially, the dissolution of 13-93 B3 glass is a reaction-controlled process at the surface of the particle. As the glass dissolves, B, Ca, Na, Mg, P, and K are released into solution. The P reacts with Ca and Mg to continuously form a magnesium-modified amorphous calcium phosphate (ACP) layer. At 21°C, the layer could be detected in SEM images as early as 4 hr, where it was 500nm in thickness (Figure 5a). The layer grows as the glass continues to dissolve and more ACP precipitates. The layers in the ACP layer indicate that when Ca and P are released, concentrations exceed the local solubility limit, which leads to precipitation of a thin layer at the glass surface. When ~25% of the glass is dissolved, the release kinetics change to a diffusion-controlled process. At this time, the ACP layer may reach a critical thickness that begins to contribute to diffusion.

The ACP layer that formed during these experiments remained amorphous over the entire two-week period of this experiment. Dissolution experiments of similar glasses in phosphate-containing solutions formed HAP.[8, 14] The most likely explanation for this is that the Ca/P ratio in solution for this set of experiments is much greater than previous studies, which leads to an ACP layer (Ca/P=2.23±0.4) with a higher Ca/P ratio than hydroxyapatite (Ca/P=1.67). The formation of the ACP layer rather than the HAP layer may be the contributor to diffusion.

The data presented here can provide insight into the nature of the precipitation phases formed on glass surfaces. Typically, ACP is the first calcium phosphate phase formed in both *in vivo* and *in vitro* experiments.[4, 15, 16] With time, the metastable ACP phase can recrystallize to form thermodynamically stable HAP or other crystalline calcium phosphate phases.[17] The mechanism for converting ACP to HAP is poorly

understood, but is proposed to involve a dissolution-precipitation reaction.[17] The ACP phase can be stabilized by ions such as magnesium[18], pyrophosphate[19], and carbonate.[17] Previous studies of dissolution behavior of borate glasses report the formation of HAP instead of ACP .[3, 6, 8, 20-23] The formation of HAP can be related to experimental conditions.

Lower Ca/P ratios in solution lead to a more favorable condition for HAP formation. A lower $[Ca^{2+}]$ in solution is favorable for ACP dissolution.[24] Higher phosphate concentrations in solution will lead to more calcium precipitating as ACP, thus lowering the $[Ca^{2+}]$.   To lower the $[Ca^{2+}]$, one could perform experiments with lower glass weights-to-solution volumes and lower surface areas to solution volumes. Additionally, a higher phosphate concentration solution such as 0.25M K_2HPO_4 will lead to HAP formation. Glasses with greater CaO-contents should release more Ca^{2+} to solution, but the glass will dissolve more slowly[23, 25], so the calcium content of the glass may not affect the results as strongly as the other factors outlined. Formation of hydroxyapatite is thermodynamically favored under basic pH conditions[18, 26] but the rate of the ACP-to-HAP transformation decreases as pH increases.[18] Therefore, HAP formation is more likely in simulated body fluid (pH=7.2) than in a K_2HPO_4 solution with a similar phosphate concentration (8.5≤pH≤9). Finally, stabilization of the ACP layer by cations such as Mg^{2+} suggest that glasses with a lower Mg/Ca ratio will be more likely to convert to HAP.

Glasses have been evaluated *in-vitro* for potential bioactivity performance by using static dissolution experiments. The parameters outlined above, such as glass volume to solution volume, glass surface area to solution volume, solution composition,

and pH, will greatly affect the composition and structure of the precipitated layer. The experimental conditions could be manipulated to achieve the desired results and may not accurately reflect the performance of a material *in-vivo*. A dynamic dissolution study which more accurately mimics the conditions of the body would be better indicator of bioactivity than static dissolution experiments.

5.   CONCLUSIONS

Dissolution processes of a borate bio-active glass were studied in water at several temperatures. The glass dissolution kinetics initially followed a reaction-controlled contracting volume model. As the glass dissolved, a Mg-substituted amorphous calcium phosphate layer precipitated on the glass surface. After the glass was ~25% reacted, the dissolution kinetics transitioned to follow a diffusion-controlled model. Both the reaction-controlled and diffusion-controlled kinetic reactions exhibited an Arrhenius relationship. The ACP layer had a greater Ca/P ratio than stoichiometric hydroxyapatite, which prevented the transition from ACP to HAP.

TABLES AND FIGURES

Table 1. Reaction rate constants for borate release at different temperatures, and times and α values for the transition from reaction-controlled to diffusion-controlled reaction mechanisms.

Temp (°C)	kCVM (s-1)	kDM (s-1)	α	Time (hr)
21	2.25E-6	3.00E-7	0.25	12
39	4.00E-6	7.59E-7	0.29	8
50	1.10E-5	6.60E-7	0.30	3
60	1.13E-5	1.41E-6	0.26	1.5
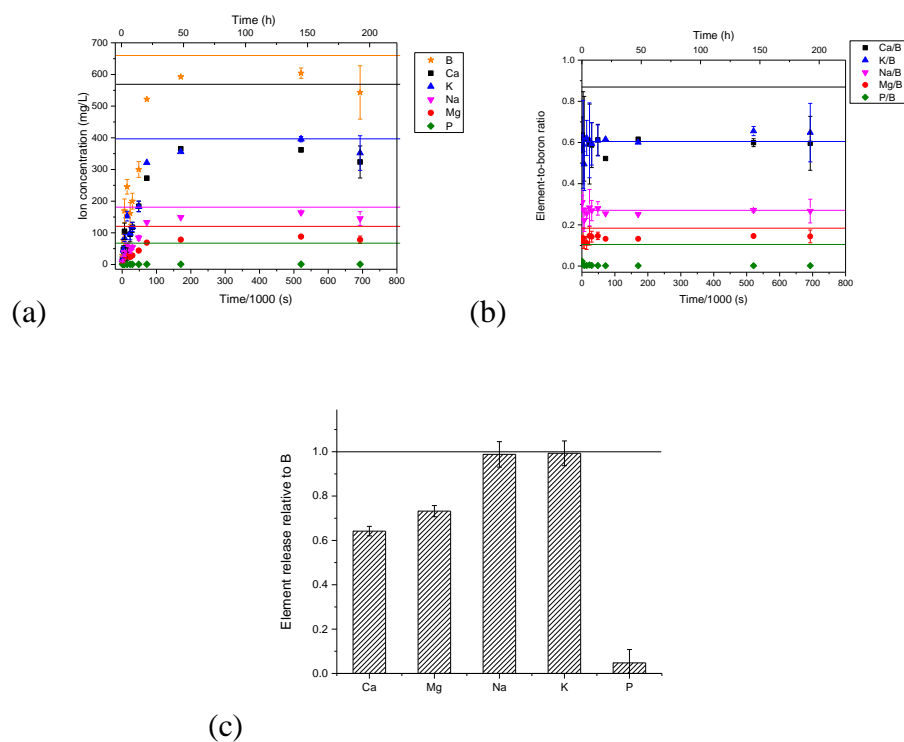
Figure 1. Elemental release for dissolution experiments. (a) Elemental release (B, Ca, Mg, K, Na, and P) as a function of time, (b) Elemental release relative to boron, and (c) elemental release relative to boron, normalized to the element-to-boron ratio in the nominal glass composition for dissolution of B3 glass in water at 39°C.
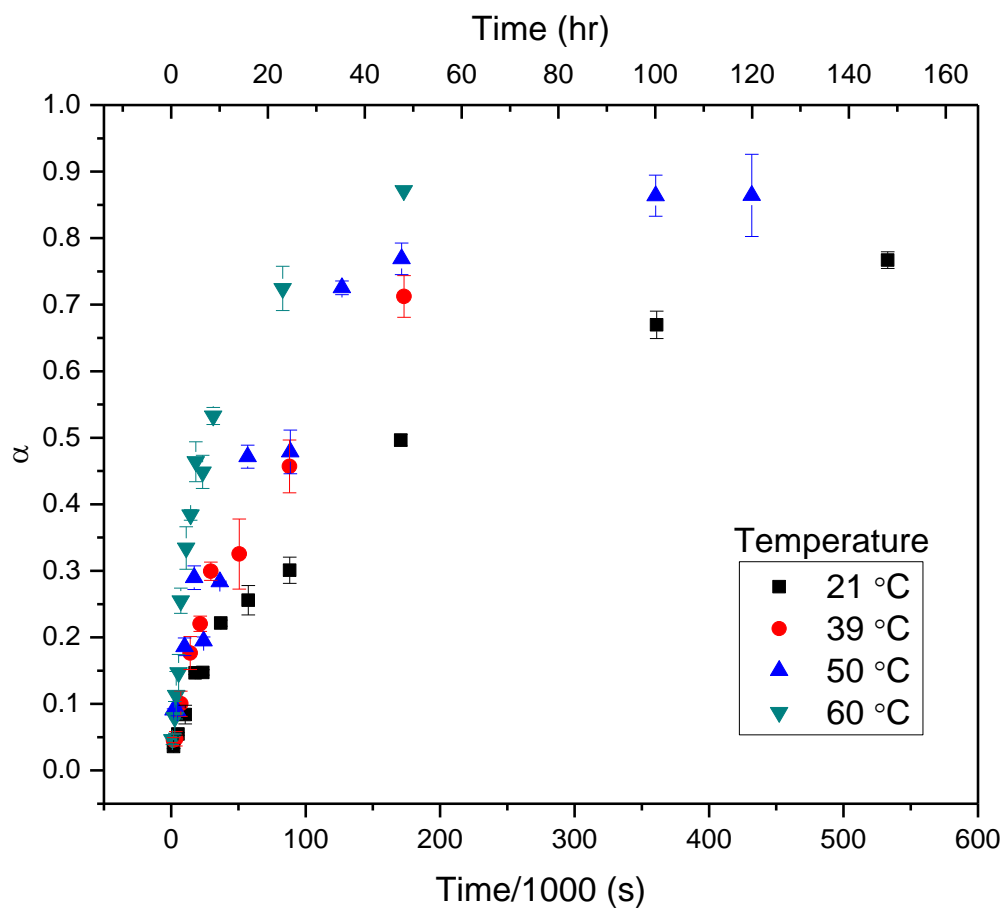
Figure 2. Extent of dissolution, α, is shown as a function of time for static dissolution of B3 glass at temperatures from 21 to 60 °C in water.
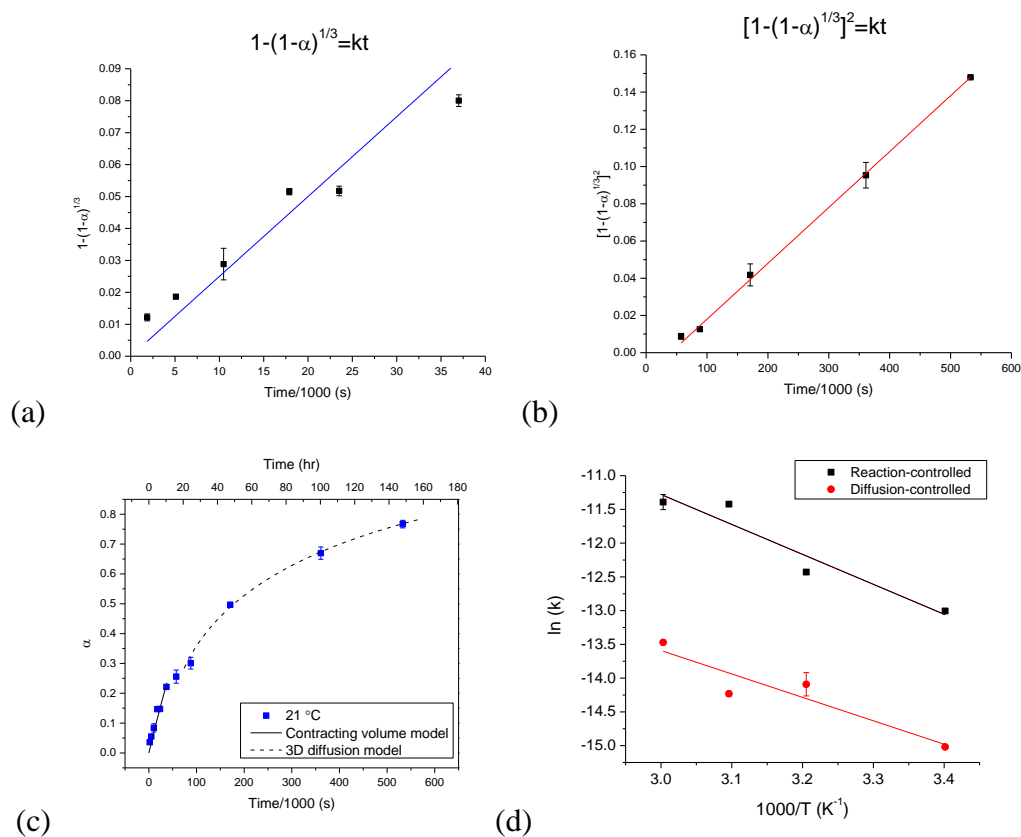
Figure 3. Kinetic analyses of boron release rates. (a) At short times, extent of dissolution follows the contracting volume model (static, 21°C) (b) At longer times, extent of dissolution follows the 3D diffusion model (static, 21°C) (c) The 21°C extent of dissolution data is shown overlaid onto the contracting volume and 3D diffusion model fits (d) Arrhenius relationship for reaction constants (k) for reaction-controlled and diffusion-controlled regimes at all temperatures.
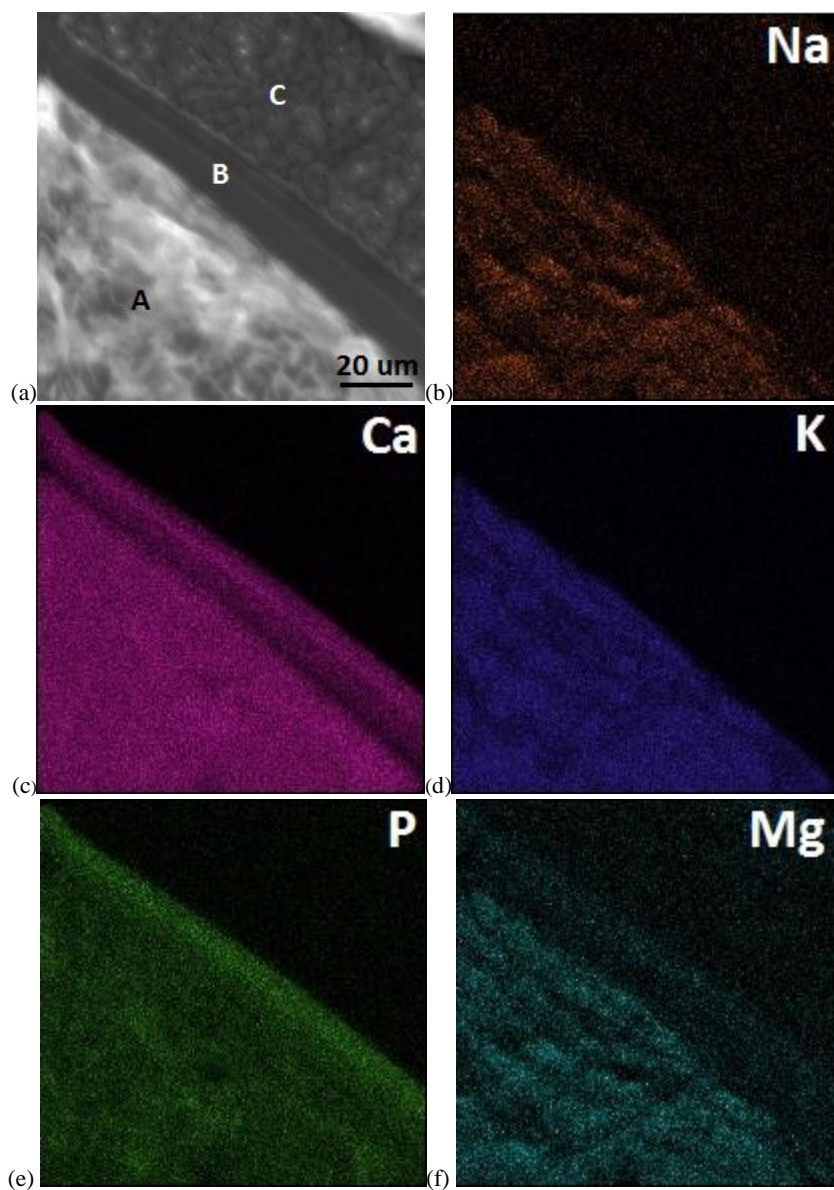
Figure 4. SEM/EDS data for partially reacted glasses. (a) Representative scanning electron microscopy image of a particle reacted for 4d at 21°C. The cross section shows unreacted glass (A), the reaction layer (B), and epoxy (C). (b-f) EDS phase maps for Na, Ca, K, P, and Mg, respectively.
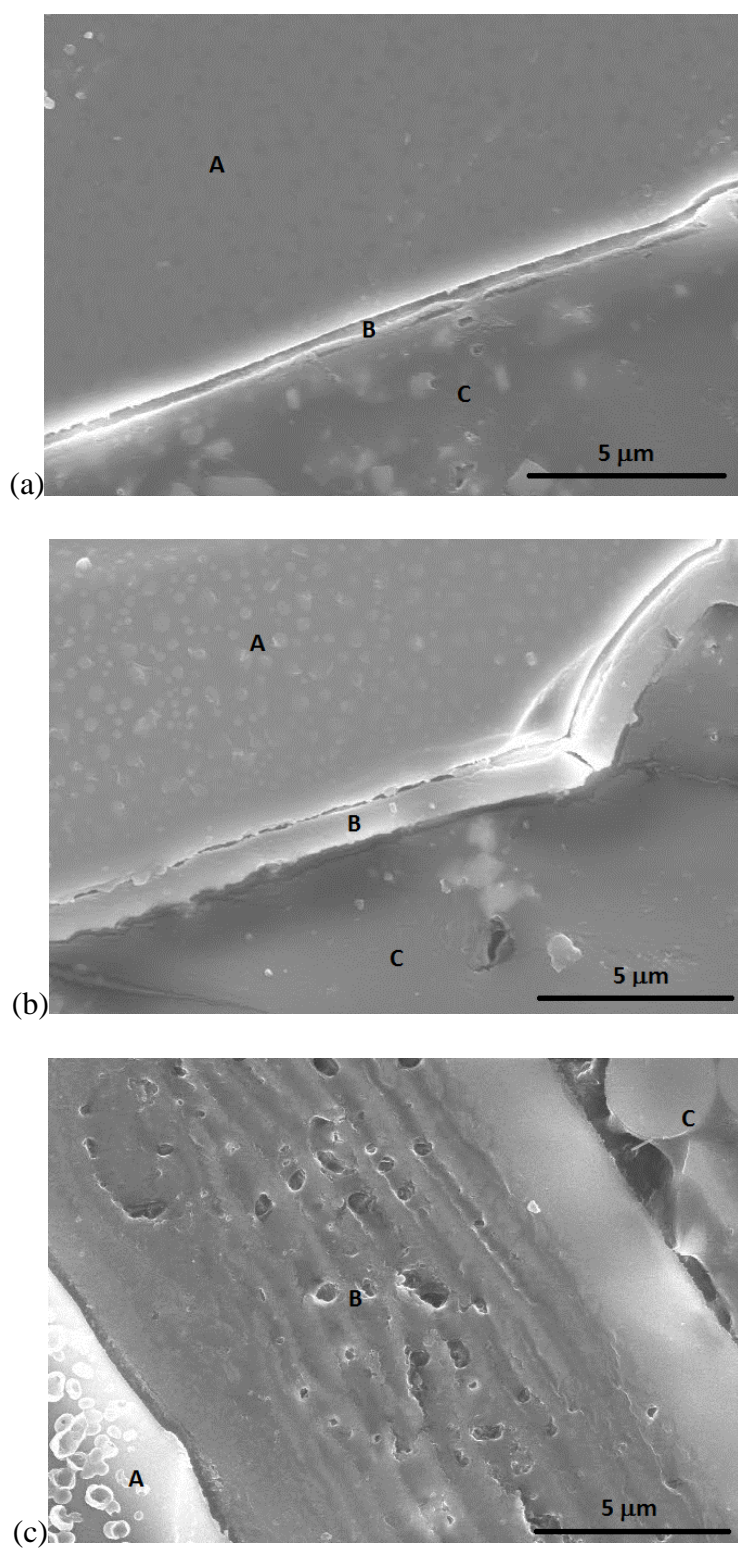
Figure 5. A higher-resolution SEM image of a reaction layer following reaction at 21°C for (a) 4h, (b) 16h, and (c) 6d. The cross section shows unreacted glass (A), the reaction layer (B), and epoxy (C).
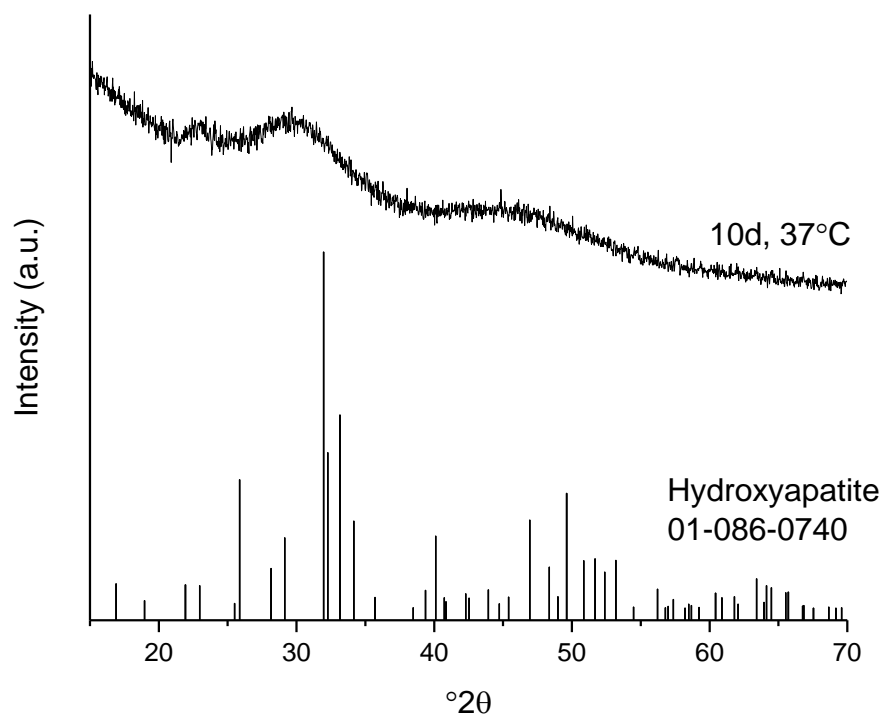
Figure 6. X-ray diffraction pattern for a sample reacted for 10d at 37°C (α=1). Reference pattern for hydroxyapatite (ICDD 01-086-0740) is shown.

REFERENCES

[1]   L. L. Hench, R. J. Splinter, W. C. Allen and T. K. Greenlee, "Bonding Mechanisms at the Interface of Ceramic Prosthetic Materials," *J. Biomed. Mater. Res.*, **5** [6] 117-41 (1971).

[2]   M. Brink, "The Influence of Alkali and Alkaline Earths on the Working Range for Bioactive Glasses," *J. Biomed. Mater. Res.*, **36** [1] 109-17 (1997).

[3]   S. Jung and D. Day, "Conversion Kinetics of Silicate, Borosilicate, and Borate Bioactive Glasses to Hydroxyapatite," *Phys. Chem. Glasses: Eur.J. Glass Sci. Technol. B*, **50** [2] 85-8 (2009).

[4]   S. Jung, "Borate Based Bioactive Glass Scaffolds for Hard and Soft Tissue Engineering"; Ph.D. Thesis. Missouri University of Science and Technology, Rolla, MO, 2010.

[5]   L. Bi, M. Rahaman, D. Day, Z. Brown, C. Samujh, X. Liu, A. Mohammadkhah, V. Dusevich, J. D. Eick and L. Bonewald, "Effect of Bioactive Borate Glass Microstructure on Bone Regeneration, Angiogenesis, and Hydroxyapatite Conversion in a Rat Calvarial Defect Model," *Acta Biomater.*, **9** [8] 8015-26 (2013).

[6]   Q. Fu, M. N. Rahaman, H. Fu and X. Liu, "Silicate, Borosilicate, and Borate Bioactive Glass Scaffolds with Controllable Degradation Rate for Bone Tissue Engineering Applications. I. Preparation and in Vitro Degradation," *J. Biomed. Mater. Res. A*, **95A** [1] 164-71 (2010).

[7]   Q. Fu, M. N. Rahaman, B. S. Bal, L. F. Bonewald, K. Kuroki and R. F. Brown, "Silicate, Borosilicate, and Borate Bioactive Glass Scaffolds with Controllable Degradation Rate for Bone Tissue Engineering Applications. II. In Vitro and in Vivo Biological Evaluation," *J. Biomed. Mater. Res. A*, **95A** [1] 172-9 (2010).

[8]   W. Huang, M. Rahaman, D. Day and Y. Li, "Mechanisms for Converting Bioative Silicate, Borate, and Borosilicate Glasses to Hydroxyapatite in Dilute Phosphate Solution," *Phys. Chem. Glasses: Eur.J. Glass Sci. Technol. B*, **47** [6] 647-58 (2006).

[9]   M. H. Velez, H. L. Tuller and D. R. Uhlmann, "Chemical Durability of Lithium Borate Glasses," *J. Non-Cryst. Solids*, **49** 351-62 (1982).

[10]   Z. Zhang, K. Hirao and N. Soga, "Water Corrosion Behavior of Densified Glass. II. Borate Glasses," *J. Non-Cryst. Solids*, **135** [1] 62-6 (1991).

[11]   P. Zapol, H. He, K. D. Kwon and L. J. Criscenti, "First-Principles Study of Hydrolysis Reaction Barriers in a Sodium Borosilicate Glass," *International Journal of Applied Glass Science*, **4** [4] 395-407 (2013).

[12]   A. Khawam and D. R. Flanagan, "Solid-State Kinetic Models: Basics and Mathematical Fundamentals," *The Journal of Physical Chemistry B*, **110** [35] 17315-28 (2006).

[13]   S. Kuslu, F. C. Disli and S. Colak, "Leaching Kinetics of Ulexite in Borax Pentahydrate Solutions Saturated with Carbon Dioxide," *J. Ind. Eng. Chem.*, **16** 673-8 (2010).

[14]   Y. Gu, W. Xiao, L. Lu, W. Huang, M. Rahaman and D. Wang, "Kinetics and Mechanisms of Converting Bioactive Borate Glasses to Hydroxyapatite in Aqueous Phosphate Solutions," *J. Mater. Sci.*, **46** [1] 47-54 (2011).

[15]   W. Liang, M. N. Rahaman, D. E. Day, N. W. Marion, G. C. Riley and J. J. Mao, "Bioactive Borate Glass Scaffold for Bone Tissue Engineering," *J. Non-Cryst. Solids*, **354** [15–16] 1690-6 (2008).

[16]   X. Liu, M. Rahaman and D. Day, "Conversion of Melt-Derived Microfibrous Borate (13-93b3) and Silicate (45S5) Bioactive Glass in a Simulated Body Fluid," *J. Mater. Sci.: Mater. Med.*, **24** [3] 583-95 (2013).

[17]   J. Zhao, Y. Liu, W.-b. Sun and H. Zhang, "Amorphous Calcium Phosphate and Its Application in Dentistry," *Chem. Cent. J.*, **5** [1] 40 (2011).

[18]   A. L. Boskey and A. S. Posner, "Magnesium Stabilization of Amorphous Calcium Phosphate: A Kinetic Study," *Mater. Res. Bull.*, **9** [7] 907-16 (1974).

[19]   H. Fu, M. Rahaman, D. Day and W. Huang, "Effect of Pyrophosphate Ions on the Conversion of Calcium–Lithium–Borate Glass to Hydroxyapatite in Aqueous Phosphate Solution," *J. Mater. Sci.: Mater. Med.*, **21** [10] 2733-41 (2010).

[20]   W. Huang, D. Day, K. Kittiratanapiboon and M. Rahaman, "Kinetics and Mechanisms of the Conversion of Silicate (45S5), Borate, and Borosilicate Glasses to Hydroxyapatite in Dilute Phosphate Solutions," *J. Mater. Sci.: Mater. Med.*, **17** [7] 583-96 (2006).

[21]   Y. Gu, W. Xiao, L. Lu, W. Huang, M. Rahaman and D. Wang, "Kinetics and Mechanisms of Converting Bioactive Borate Glasses to Hydroxyapatite in Aqueous Phosphate Solution," *J. Mater. Sci.*, **46** [1] 47-54 (2011).

[22]   J. Lowry, "Dissolution Behavior of Alkali Borate Glasses"; Master of Science Thesis. University of Missouri - Rolla, Rolla, MO, 2002.

[23]   K. L. Goetschius, "The Effect of Composition on the Viscosity, Crystallization, and Dissolution of Simple Borate Glasses and Compositional Design of Borate Based Bioactive Glasses"; Ph.D. Thesis. Missouri University of Science and Technology, Rolla, 2014.

[24]   J. L. George and R. K. Brow, "*In-Vitro* Dissolution of a Bioactive Borate Glass under Dynamic Conditions," *J. Non-Cryst. Solids*, [to be submitted] (2015).

[25]   J. L. George and R. K. Brow, "*In-Situ* Characterization of Borate Glass Dissolution Kinetics by μ-Raman Spectroscopy," *J. Non-Cryst. Solids*, [to be submitted] (2015).

[26]   X. Lu and Y. Leng, "Theoretical Analysis of Calcium Phosphate Precipitation in Simulated Body Fluid," *Biomaterials*, **26** [10] 1097-108 (2005).

III. IN-VITRO DISSOLUTION OF A BIOACTIVE BORATE GLASS UNDER DYNAMIC CONDITIONS

AUTHORS

Jaime L. George

Richard K. Brow

ABSTRACT

Single-pass flow-through experiments are employed to study the dissolution mechanism and kinetics of a borate bioactive glass 13-93B3 in water, simulated body fluid (SBF), and other solutions. The SPFT dissolution rate equation was modified to account for changes in surface area of this fast-reacting glass. Glass particles dissolved faster under faster flow rates and smaller glass volumes, conditions which reduced the local concentrations of ions released from the glass. The ion release rates ranged from 1.7×10^{-5} g/m^2/s for slow flow rates to 1.1×10^{-3} g/m^2/s for lower glass volumes. As the glass particles dissolved, a calcium phosphate phase precipitated on the particle surfaces. For the slow flow rates, amorphous calcium phosphate was present after 43 days of reaction, whereas nanocrystalline (12-23nm) hydroxyapatite formed for faster flow rate experiments. The formation of crystalline hydroxyapatite was favored with faster flow rates, longer reaction times, and increased phosphate concentration in solution.

1. INTRODUCTION

Glasses have been investigated for biomedical applications such as soft tissue repair and bone repair since Hench reported the first Bioglass composition in 1969.[1] Bioactive glasses convert to a hydroxyapatite-like material *in vivo* and bond to bone.[2, 3] Although silicate glasses have received the most attention for biomedical applications, borate glasses have also been investigated in recent years. Richard first replaced the SiO_2 component of the Bioglass 45S5 composition with B_2O_3 (designated 45S5B1) and showed that the glass promoted new bone formation at a faster rate than silicate 45S5.[4] The borate glass analogues converted to hydroxyapatite at a much faster rate than 45S5.[5-7] Other borate glass compositions have been investigated.[8-11] The borate analog of the bioactive silicate glass 13-93, again with the SiO_2 replaced with B_2O_3 (13-93B3), was used to fabricate scaffolds for tissue-engineering applications and showed a beneficial biological response.[8, 12, 13] The dissolution properties of this glass and similar borate glasses have been investigated under static *in-vitro* conditions and *in vivo* conditions.[5, 6, 14, 15]

An *in-vitro* static study examined the effects of a 13-93B3 scaffolds on murine MLO-A5 osteogeneic cells and showed that the borate scaffold was toxic to the cells.[16] However, when the same glass scaffolds were evaluated after being implanted in mice, the biological responses were favorable.[7, 8, 12, 17] The significant differences between the outcomes of the static *in-vitro* study and *in-vivo* studies were attributed to an increase in pH as glasses dissolve and ionic concentration increases in static studies.[13] An *in-vitro* study where solutions continuously flow over glass scaffolds may be a better indicator of

in-vivo bioactivity.[13] Single-pass-flow-through (SPFT) experiments are a good candidate for dynamic *in-vitro* studies of glass dissolution and have been used by those studying silicate glasses for nuclear waste encapsulation.[18-20]

In an SPFT experiment, an aqueous solution is flowed continuously over the dissolving material and this reduces the local concentrations of ions released from the glass which could produce a large change in pH.[21] Following contact with the dissolving species, solutions can be analyzed for changes in pH or ion concentration. This more closely mimics the *in-vivo* conditions where blood and body fluids are continuously pumped through the body. Blood flow rates will vary by tissue and are reported by Cowles *et al*.[22] Using reported information for blood flow rates and tissue densities in humans, we can calculate that a 1 cm^3 scaffold might experience a blood flow rate of 48mL/day in muscle or 70mL/day in subcutaneous tissue.[22]

Single-pass-flow-through experiments provide several advantages over traditional static dissolution experiments. The SPFT technique allows for the measurement of a forward dissolution rate – with which one can measure the maximum amount of any species that is released from the surface area of a glass upon dissolution. Additionally, the flowing conditions reduce the effects of concentration gradients, pH changes, and high ion concentrations. In this work, the effect of solution composition, flow rate, and surface area on dissolution rate and the formation of calcium phosphate phases on a borate bioactive glass are investigated.

2. EXPERIMENTAL PROCEDURE

2.1. GLASS PREPARATION

The borate bioactive glass, designated 13-93B3, with the nominal composition (wt%) 53 B_2O_3 – 20 CaO – 12 K_2O – 6 Na_2O – 5 MgO – 4 P_2O_5 was prepared by conventional melt quenching techniques. The raw materials H_3BO_3 (98%, Alfa Aesar), $CaCO_3$, (98%, Alfa Aesar), K_2CO_3, (99%, Alfa Aesar), Na_2CO_3 (98%, Alfa Aesar), $MgCO_3$ (USP/FCC grade, Fisher Scientific), and $NH_2H_2PO_4$ (98%, Alfa Aesar) were mixed and melted in air for one hour at 1075°C in a Pt-Rh crucible. The melt was quenched between two steel plates to form glass. The density of the glass was measured using the Archimedes technique with water. Prior to dissolution, the glass was ground to particles 150-300 μm in diameter using a porcelain mortar and pestle.

2.2. SOLUTION PREPARATION

Simulated body flulid (SBF) was prepared as outlined by Kokubo *et al.*[23] using NaCl (USP/FCC grade, Fisher Scientific), $NaHCO_3$ (99.7%, Aldrich), KCl (99%, Aldrich), K_2HPO_4•$3H_2O$ (99%, Acros Organics), $MgCl_2$•$6H_2O$ (99%, Alfa Aesar), $CaCl_2$ (USP/FCC grade, Fisher Scientific), Na_2SO_4 (99%, Alfa Aesar), $NH_2C(CH_2OH)_3$ (99%, Alfa Aesar), and 1M HCl (Fisher Scientific). The pH was adjusted to 7.4 using 1M HCl. A boron- and calcium-spiked solution (spk), described in Table I, was prepared by adding H_3BO_3 (98%, Alfa Aesar) and $Ca(OH)_2$ (95%, Alfa Aesar) to deionized water.

2.3. DYNAMIC DISSOLUTION.

A single-pass-flow-through (SPFT) experiment was designed following ASTM designation C1662-10.[21] Glass particles 150-300 μm in diameter with a weight of 1 g,

500 mg, 200 mg, or 50 mg were placed in a polystyrene Millipore monitor cassette

reaction cell, confined between two 0.45 μm polycarbonate filters. The reaction cell is 37

mm in diameter with a volume of 16 mL. The experimental configuration is described in

Fig. 1(b) of ASTM designation C1662-10. A KDS200 syringe pump (KD Scientific) was

used to control flow rate, using polycarbonate syringes to hold reaction media (deionized

water, spiked solution, or simulated body fluid). All experiments were performed with

solutions at 37°C. Pt-cured silicone tubing was used for the entire SPFT setup.

Experiments were performed with a range of constant flow rates between 5-50 mL/day. A

summary of reaction conditions is given in Table 1. Experiments are designated by the

flow rate, sample size and solution. For example, F50-1g-w, indicates a flow of water

(w) at a rate of 50mL/day over 1.0 grams of glass particles. For flow rates of 24-50

mL/day, solution samples were collected over an approximately one hour time period

daily and the weight of the resulting aliquot was measured to calculate flow rate. All flow

rates were measured to be within 3.4% of the desired value. For the 5mL/day

experiments, samples were collected over a 24 or 48 hour time period. Aliquots were

diluted with 1 vol% HNO_3 to 1:10-1:100 for elemental analysis. Following 2-6 weeks of

SPFT experiments, particles were removed, rinsed with ethanol twice, and dried

overnight at 100 °C , then stored in a desiccator prior to analysis.

2.4. SOLUTION CHARACTERIZATION

The pH values of the solutions were measured at 37°C. Solutions collected over a

24 or 48 hour time period were measured with an Accumet pH electrode (13-620-285).

For some of the SPFT experiments, pH was measured in-line with a flow-through pH cell

and Cole-Parmer micro-pH electrode (05662-48). Inductively-coupled plasma optical emission spectroscopy (ICP-OES, PerkinElmer Optima 2000 DV, Norwalk, USA) was used to measure concentrations of boron, calcium, magnesium, sodium, potassium, and phosphorus in solution.

2.5. PARTICLE CHARACTERIZATION.

Following reaction, the weight of the dried particles was measured. X-ray diffraction (XRD) was used to determine the crystallinity of the as-reacted particles using a Philips X'pert multipurpose diffractometer with PIXcel detector, using Cu K_α radiation and Ni filter, at 45 kV and 40 mA. Crystallite size was calculated from X-ray diffraction patterns using Scherrer's equation. [24] Dried particles were mounted in poly(methyl methacrylate) (PMMA), cut with a diamond ring saw, and polished to 1200 grit with SiC polishing paper. The morphology and composition of the particles were characterized with a Hitachi S4700 scanning electron microscope (SEM, Hitachi High-Tech, Tokyo, Japan) and the attached energy dispersive spectroscopy (EDS) system.

3.   RESULTS

3.1. ICP-OES.

An example of elemental release data is shown in Figure 1(a), where 37 °C water (flow rate (q) is 50mL/day) was flowed through 1.0 g of B3 glass particles. Initially, the release rate of every element is high and gradually decreases towards zero after 14 days. Figure 1(b) shows the boron release data as a function of time for several water experiments with different flow rates and glass sample sizes. The F5-1g-spk and F5-1g-w experiments produced the greatest maximum boron concentration ($[B]_{max}$) in solution, 1183±41 and 1113±24 ppm respectively. The F15-0.05g-w and F50-1g-w experiments had the lowest $[B]_{max}$ in solution at 347 and 450±69 ppm respectively. As the flow rate of the solution decreased, the concentration of boron in solution increased. At a constant flow rate, as the glass mass increased, boron concentration in solution increased.

Kinetic analyses of the boron release data were performed for all experiments. The total amount of boron released over the time period between two data points was calculated by integrating the area between the data points and the cumulative boron release for a given time was determined by summing the boron release data for the preceding time periods. To determine the extent of dissolution at a given time, α_t, the weight of boron released into solution after time t (B_t) was normalized to the weight of boron in the glass, (B_{glass}),

$$\alpha_t = \frac{B_t}{B_{glass}} \tag{1}$$

Figure 2 shows the reaction kinetics for the SPFT experiments in water. When the glass mass was held constant the particles reacted faster as flow rate increased (Figure

2a). When the flow rate was held constant, the dissolution rate increased as glass mass decreased (Figure 2b). Dissolution in SBF occurs faster than dissolution in water for otherwise identical conditions (Figure 2c). The dissolution reaction takes longer to reach completion in the B- and Ca-spiked solution than under otherwise identical conditions in water (Figure 2d). Under conditions with the same flow rate normalized to initial glass weight (q/w_0), the glass particles follow similar reaction kinetics, shown for the F5-0.2g-w and F24-1g-w experiments in Figure 2e. Reaction completion (α=1) occurs in as little as 5 days for the F15-0.05g-w experiment or as long as α=0.25 after 16 days for the F5-1g-spk experiment.

The contracting volume model (CVM) model describes the reaction rates of spherical particles[25] and is used to described the time dependence of the alpha values. The CVM assumes a surface reaction-controlled mechanism where particles react with their surroundings at the interface. As the reaction progresses, the spheres decrease in size, and the reaction kinetics can be described according to

$$1 - (1 - \alpha_t)^{1/3} = k_1 t \tag{2}$$

Figure 3 shows the fits of the CVM to the B-release data for each of the water dissolution experiments. The reaction constant, k_1, is given by the slope of the line. Every test condition followed the CVM with values of $R^2 \geq 0.991$. The reaction constant, k_1, is plotted as a function of flow rate and glass volume in Figure 4. For a constant flow rate, the rate of boron release decreases as the glass volume increases. (Figure 4a) For a constant glass volume, the rate of boron release increases as flow rate increases. (Figure 4b)

Figure 5a shows the release of calcium, magnesium, potassium, sodium, and phosphorus from the glass into solution relative to boron as a function of time for the F5-1g-w experiment. The element-to-boron ratios were constant with respect to time, and these data were representative of all reaction conditions. The average element-to-boron ratios released to solution were normalized to the element-to-boron ratios in the base glass and are shown in Figure 5b. For the F50-1g-w and F24-1g-w dissolution tests, the ratio of Na- and K-to-B in solution is equal to that in the glass. For the F5-1g-w experiment, the ratios of Na- and K-to-B in solution are greater than that in the glass. For all experimental conditions, the ratio of Ca- and Mg-to-B in solution was less than that in the glass and the P-to-B ratio in the solution was less than 5% of the P-to-B ratio in the glass.

The pH values are shown in Figure 6. For the water experiments, the pH is initially in the range of 9.4-9.7. Once the glass is mostly dissolved, the pH begins to decrease to 8-8.4. The pH decreases more quickly as the initial glass weight decreases. For the SBF experiments, the pH was initially 7.4, then remained between 7.25-7.75 for the F50-0.2g-SBF experiment, but increased to 7.75-8.25 for the F50-1g-SBF experiment.

3.2. SEM/EDS.

A representative SEM image of a cross-section of the reaction product that remained following the F50-1g-w experiment at 14d is shown in Figure 7(a). These particles were fully reacted, as determined by the total concentration of boron released to solution, and showed no evidence for residual glass at the centers of the particles. The

EDS analyses show that the reaction products contained calcium, magnesium, and phosphorus and was absent of sodium and potassium. Figure 7(b-d) show the EDS phase maps for Ca, Mg, and P, respectively, for the area outlined in red in Figure 7(a). The Mg/Ca ratio in the reaction products ranged from 0.076±0.01 (F5-0.2g-w) to 0.170±0.010 (F5-1g-w). Figure 7(e) shows a higher magnification view of the microstructure of the magnesium-calcium phosphate reaction product. The reaction products on many particles consist of many layers, each less than 1 µm wide, radiating outward from the centers of the particles. Some particles appear to have a more continuous reaction product. There is a mix of the layered structure and continuous structure throughout the sample. At the highest magnifications, the magnesium-calcium phosphate reaction product is seen to have a spherical morphology, as shown in Figure 7(f). Figure 7(g) shows images of the partially reacted (α=0.52) particles after 22 days of reaction in the F5-1g-w experiment. A calcium, magnesium, phosphate reaction layer has formed on the surface, and unreacted glass remains in the particle core. Figure 7(h) shows a cross-section of another, smaller, fully-reacted particle from the F5-1g-w experiment at 22d. The reaction product also has a layer structure, but the layers are thicker at 2-6 µm in width. Figure 7(i-j) shows images from the F5-1g-spk experiment after 22 days. The particles are partially reacted and the reaction product is comprised of many sub-micron layers. Following the F5-0.2g-w experiment, the glass particles fully reacted to form a calcium magnesium phosphate phase with no evidence of the layered structure seen under other experimental conditions.

3.3. XRD.

XRD patterns for selected reacted B3 particles and a hydroxyapatite (HAP) reference pattern are shown in Figure 8. The patterns from the reacted products either matched the HAP pattern or were dominated by a broad peak indicating an x-ray amorphous material. A summary of the phases formed for the different reaction conditions is shown in Table II. The crystallite sizes of reaction products that formed HAP were determined using the Scherrer equation for the peak at 26 °2θ,[26] and these are also summarized in Table II. The crystallite sizes increased with increases in the flow rate-to-particle surface area ratio, reaction time, and phosphate concentration in the reaction medium.

4. DISCUSSION

For SPFT studies of glasses, ion release rates are evaluated by,[21]

$$R_{i,t} = \frac{(c_{i,t} - c_{i,0}) \cdot q}{x_i \cdot S_t} \tag{3}$$

where $R_{i,t}$ is the release rate for component i at time t, $c_{i,t}$ is the concentration of component i in solution at time t, $c_{i,o}$ is initial concentration of component i in solution prior to dissolution, q is flow rate, and x_i is the mass fraction of component i in the glass.

As 13-93B3 dissolves in water, boron, calcium, magnesium, sodium, potassium, and phosphorus are released into solution. During the early stages, the greater concentrations of ions in solution, as shown in Figure 1, are attributed to a larger surface area of the glass. As the glass dissolves, the surface area of unreacted glass decreases and the corresponding release of ions into solution also decreases. Since the reaction kinetics are well-described by the contracting volume model (Figure 3), the surface area of the unreacted glass at a given time can be calculated from the α-values. The initial median particle radius, r_0, for unreacted particles is 113 μm, which leads to a median particle volume, V_0, of 5.96×10^{-12} m³, assuming spherical particles. As the glass dissolves, the residual glass decreases in volume and the new volume, V_t, can be calculated from:

$$V_t = V_0 \cdot (1 - \alpha_t) \tag{4}$$

The diameter of the partially reacted glass particle, d_t, can then be calculated from the volume and the average specific surface area of the unreacted glass at a given time, S_t, can be calculated from[19]

where the measured density of the glass, ρ, is 2.50 ± 0.01 g/cm^3. The rate equation can accommodate the change in surface area, assuming reaction-controlled kinetics and spherical particles, according to

$$R_{i,t} = \frac{(c_{i,t}-c_{i,0})\cdot q\cdot\rho\cdot r_0}{3\cdot x_i\cdot w_0\cdot(1-\alpha_t)^{2/3}} \tag{6}$$

where w_0 is the initial weight of the glass particles. The calculation of α can be incorporated into equation (6), according to

$$R_{i,m} = \frac{(c_{i,m}-c_{i,0})\cdot q\cdot\rho\cdot r_0}{3\cdot x_i\cdot w_0\cdot\left[1-\frac{q}{x_B w_0}\cdot\sum_{n=1}^{m}\left(\frac{c_{B,n}+c_{B,n-1}}{2}\right)\cdot(t_n-t_{n-1})\right]^{2/3}} \tag{7}$$

This new version of the SPFT rate equation can be used to determine the forward dissolution rates for fast reacting glasses, like B3, which follow a reaction-controlled kinetic model.

Ion release rates were calculated from equation (7) for the water and spiked solution experiments and are shown in Figure 9. The dissolution rate for a given set of experimental conditions is constant over the course of the experiment, indicating that the surface reaction between the solution and glass controls the overall dissolution kinetics. Boron release rates range from 1.7×10^{-5} g m^{-2} s^{-1} for the F5-1g-spk experiment to 1.1×10^{-3} g m^{-2} s^{-1} for the F15-0.05g-w experiment. Phosphorus release rates are about ten times lower than boron for all experiments, whereas the sodium and potassium release rates are similar to the boron release rate. For the water experiments, the magnesium and calcium release rates are 46-78% of the boron, sodium, and potassium release rates, though not as low as the phosphorus release rates. The F5-1g-spk experiment has a Ca release rate

$(2.4 \times 10^{-6}$ g m^{-2} s^{-1}) which is 12% of the boron release rate $(1.9 \times 10^{-5}$ g m^{-2} s^{-1}). The lower calcium release rate for the spiked solution experiment is attributed to the initial solution being nearly saturated with calcium. Near-saturation levels of calcium in solution had the largest effect on calcium release from the glass, but the release of all elements was affected.

For a constant flow rate (q), as the glass mass (w_0) increases, the boron release rate decreases. Similarly, as the glass mass is kept constant, boron release rate increases with increasing flow rate. Figure 10(a) shows that the average boron release rate increases systematically with q/w_0. This dependence of boron release rate on flow rate and starting glass weight indicates that the concentration of ions in solution is limiting the dissolution rate of the glass. The dissolution rate is shown plotted against the maximum boron concentration ($[B]_{max}$) measured for each experiment in Figure 10(b). As the $[B]_{max}$ increases, dissolution rate decreases. Equation 8 shows a simplified equation for the interaction between the borate glass network and water, shown below.

$$B_2O_3 \,(glass) + 3H_2O \,(liq) \rightarrow 2H_3BO_3 \,(aq) \tag{8}$$
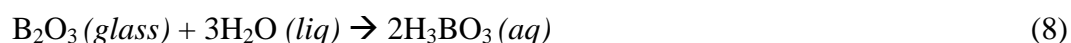
The decrease in dissolution rate as $[B]_{max}$ in solution increases (Figure 10b) is attributed to an increase in boron activity of the solution. High concentrations of H_3BO_3 in solution will lead to a decrease in the rate at which the glass network dissolves (Equation 8). Similarly, in silicate glasses, an increase in $Si(OH)_4$ concentration in solution leads to a decrease in glass dissolution rate.[27] For the borate glasses, the effect of $[B]_{max}$ decreasing glass solubility is observed far below the solubility limit (<10%) of H_3BO_3. This is of great significance for static experiments where B accumulates in solution, because as the

glass dissolves, the B activity in solution will increase, which may then cause a decrease in dissolution rate.

For the greater flow rate experiments (F50-1g-w and F24-1g-w), the Na-to-B and K-to-B ratios of 1.0 (Figure 5b) indicate that alkali ions are released congruently with respect to boron from the 13-93B3 glass. However, for the slower flow rate (F5-1g-w and F5-1g-spk) experiments, relatively more sodium and potassium are released into solution than boron. This indicates that in experimental conditions where boron concentrations are high (<~1000ppm), boron release is suppressed, although other soluble components of the glass (sodium and potassium) are still released into solution. The release of network modifying cations (potassium and sodium) without the release of network former (boron) could be a result of a borate mineral precipitating, boron being incorporated in the reaction layer, or an alkali-depleted layer in the residual glass, although no evidence for any of these processes was obtained.

The release of calcium, magnesium, and phosphorus into water is suppressed with respect to boron, but is constant (Figure 5a). This indicates that the precipitation of the calcium magnesium phosphate reaction layer occurs continuously as the glass dissolves, and that the stoichiometry of the layer remains constant. If all of the phosphorus in the glass reacts to form stoichiometric hydroxyapatite, 37% of the calcium in the B3 glass will be required to satisfy the stoichiometry if it reacts with all of the phosphate in the glass. The remaining 63% of the calcium could then be released to solution. Since a small amount of phosphorus is released into solution and some magnesium is present in the reaction layer, the amount of calcium released to the solution should be greater than 63%.

This is the case for the F24-1g-w and F50-1g-w experiments, where 70-80% of the calcium in the dissolved glass was released into solution (Figure 5b). However, for the F5-1g-w experiment, only 45% of the calcium was released into solution and for the F5-1g-spk experiment, less than 20% of the calcium was released into solution. The lower Ca:B ratios in solution for these experiments, compared to the experiments with greater flow rates, indicates that there is more calcium in the reaction product or another calcium phase is precipitating, although no precipitation was observed. EDS measurements on the reaction products from the F5-1g experiments show Ca/P ratios of 2.24±0.104 for water and 3.35±0.98 for the spiked solution.

As the glasses dissolve in water, the released calcium and phosphate react to form a magnesium-substituted amorphous calcium phosphate (ACP) reaction layer. Over time, the ACP reaction layer crystallizes to hydroxyapatite. The conversion between ACP and HAP has been hypothesized to be a dissolution-precipitation reaction.[28] The faster flow rate experiments or lower initial glass weights produce reaction layers with larger hydroxyapatite crystallite sizes in shorter times than the slower flow rate experiments or greater initial glass weights (Table II). The crystalline reaction products have Ca/P ratios (Ca/P=1.36± 0.05) below that of stoichiometric hydroxyapatite (Ca/P=1.67) while the amorphous reaction products have Ca/P ratios (Ca/P=2.25±0.104 and Ca/P=3.35±0.98) higher than stoichiometric hydroxyapatite. This indicates that that Ca^{2+} concentration in solution is affecting the conversion rate from ACP to HAP. The greater calcium concentration in solution may inhibit ACP dissolution, which would limit HAP

formation. The implication of these studies is that ion activity in solution plays a

significant role in the formation of the calcium phosphate layer.

5. CONCLUSIONS

The SPFT method has been modified to study the dissolution processes of a fast-reacting borate bio-active glass in water and SBF. The dissolution rate increased as initial glass weight decreased, flow rate increased, and boron concentration in solution decreased. As the glass particles dissolved, a calcium phosphate phase precipitated on the particle surfaces. For the slow flow rates, amorphous calcium phosphate was present after 43 days of dissolution, whereas nanocrystalline (12-23nm) hydroxyapatite formed for faster flow rate experiments. The formation of crystalline hydroxyapatite was favored with faster flow rates, longer reaction times, and increased phosphate concentration in solution. The experiments suggest that the local chemistry in solution can significantly affect both the dissolution behavior of the glass and the precipitation and structure of reaction products. This technique will provide a useful tool to study dissolution of bio-active glasses in physiological solutions to gain a better understanding of the effects of environment on the conversion of borate glasses to phosphate compounds such as hydroxyapatite.

TABLES AND FIGURES

Table 1. Parameters for single-pass flow-through dissolution tests.

Test (FlowRate-GlassAmt-Fluid)	Flow rate (F) [mL/day]	Glass weight (g)	Fluid	Time
F50-1g-w	50	1	water	14 days
F24-1g-w	24	1	water	16 days
F5-0.2g-w	5	0.2	water	22, 33 days
F5-1g-w	5	1	water	22, 43 days
F5-1g-spk	5	1	water + 560ppm B + 360ppm Ca	22, 43 days
F50-1g-SBF	50	1	SBF	8 days
F50-0.2g-SBF	50	0.2	SBF	8 days
F15-1g-w	15	1	water	13 days
F15-0.5g-w	15	0.5	water	13 days
F15-0.2g-w	15	0.2	water	13 days
F15-0.05g-w	15	0.05	water	13 days

Table 2. Resulting phases after varying times for different SPFT test parameters.

Test	Time (days)	Phase, grain size
F50-1g-w	14	HAP, 19nm
F5-0.2g-w	22	HAP, 13nm
	33	HAP, 23nm
F5-1g-w	22	amorphous
	43	amorphous
F5-1g-spk	22	amorphous
	43	amorphous
F50-1g-SBF	8	HAP, 12nm
F50-0.2g-SBF	8	HAP, 19nm
F15-1g-w	13	amorphous
F15-0.5g-w	13	HAP, 20nm
F15-0.2g-w	13	HAP,20nm
F15-0.05g-w	13	HAP
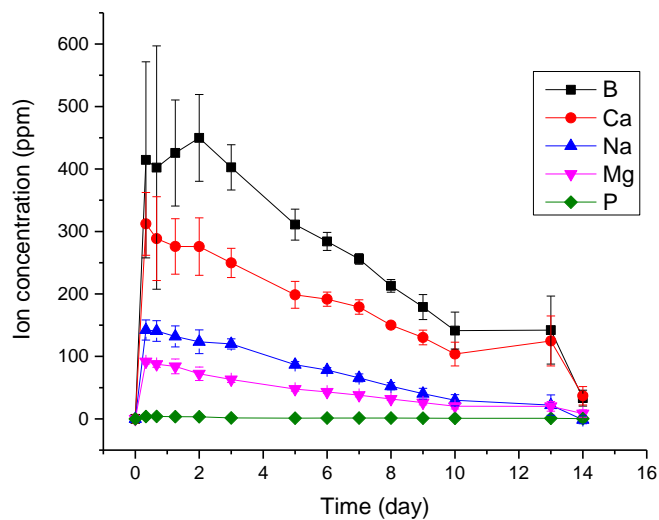
(a)
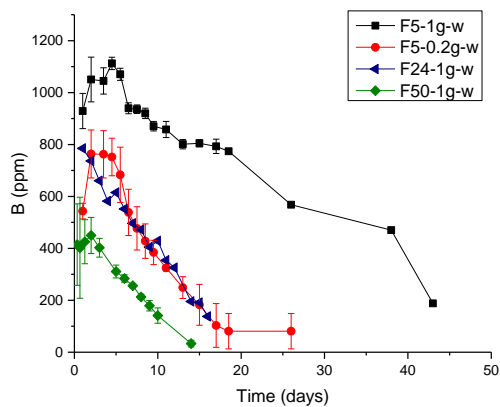
(b)

Figure 1. Elemental release for SPFT experiments. (a) Elemental release (B, Ca, Mg, Na, and P) as a function of time for dissolution of B3 glass at in water at 37°C with a flow rate of 50 mL/day (F50-1g-w). (b) Boron release as a function of time for dissolution of B3 glass in water at 37°C with varying flow rates and glass volumes.
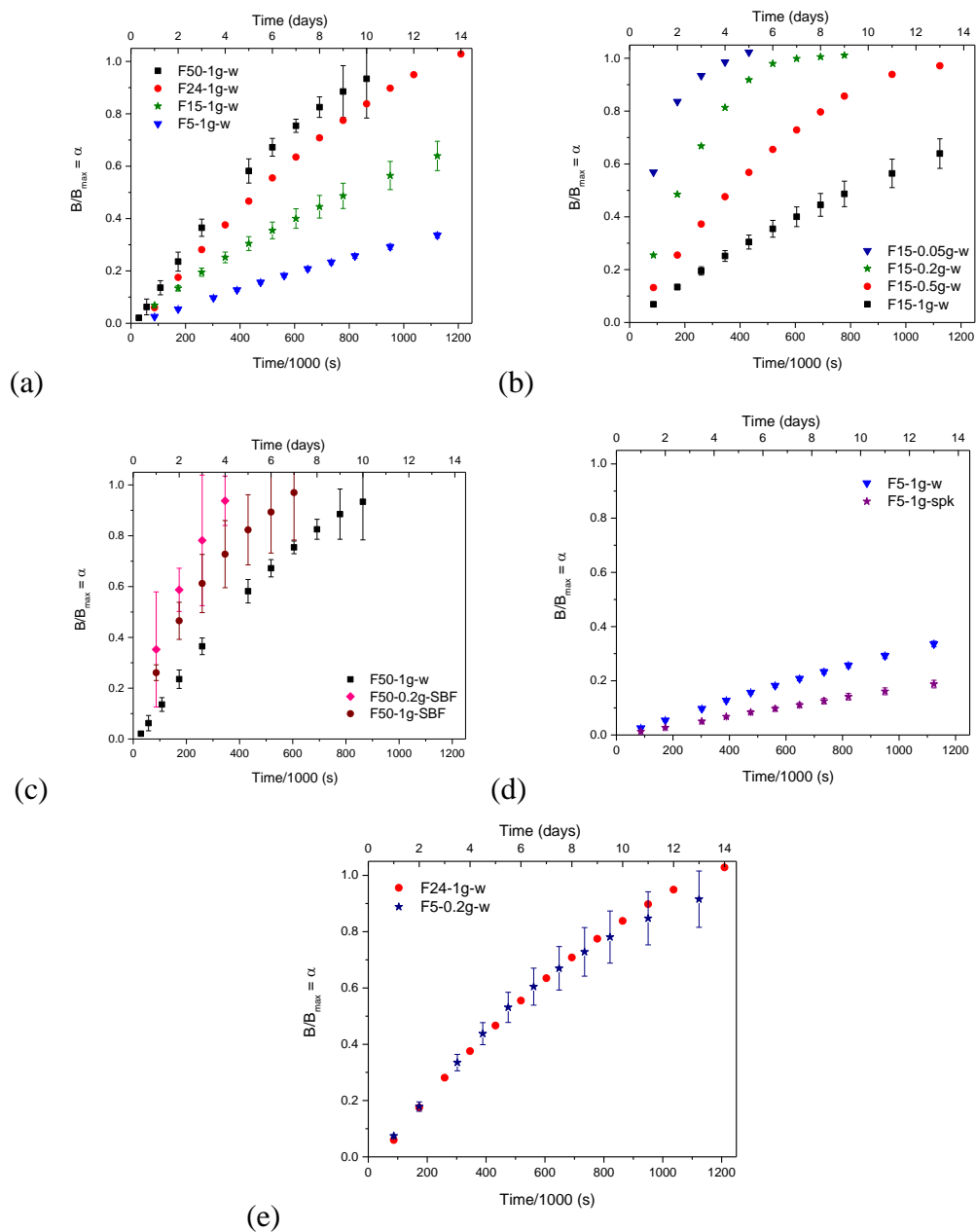
Figure 2. Extent of dissolution, α, is shown as a function of time for experiments where (a) the flow rate is varied (5-50 mL/d) and the glass volume is constant (1g), (b) the flow rate is constant (15mL/d) and the glass volume is varied (0.05-1g), (c) the flow rate is constant (50mL/d), the glass volume is varied (0.2g or 1g), and solution is changed (water or SBF), (d) the flow rate is constant (5mL/d), the glass volume is constant (1g), and the solution is changed (water or spk), (e) the flow rate and glass volume are changed. All reaction conditions are at a temperature of 37 °C.
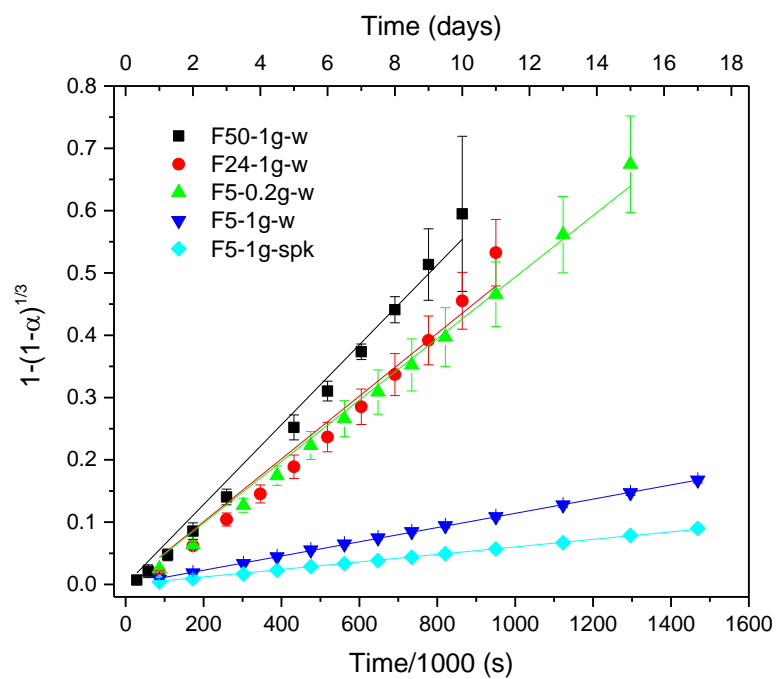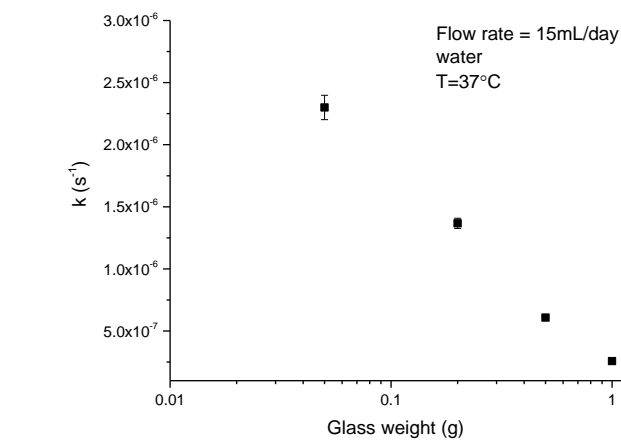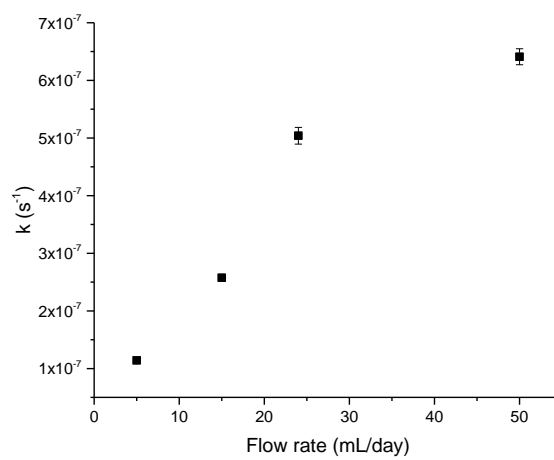
Figure 3. Contracting volume model as a function of time for selected dynamic studies at 37°C. The results shown are representative of all experiments studied in this paper.

(a)

(b)

Figure 4. Reaction constant (k_1) as a function of (a) glass weight for a constant flow rate of 15 mL/day and (b) flow rate for a constant glass weight of 1g.
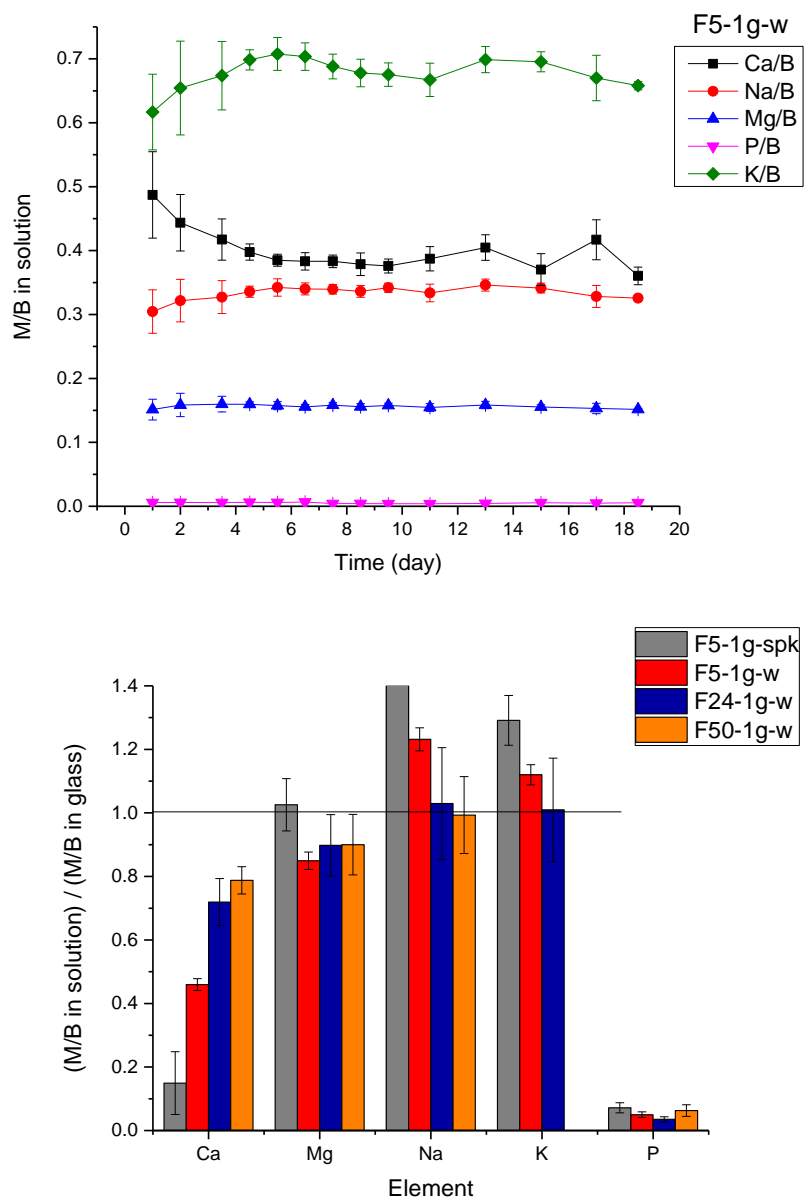
Figure 5. Elemental release relative to boron for SPFT experiments. (a) Elemental release relative to boron for the F5-1g-w experiment, shown as a function of time. (b) Elemental release relative to boron, normalized to the element-to-boron ratio in the nominal glass composition for dissolution of B3 glass in water at 37°C under all conditions.
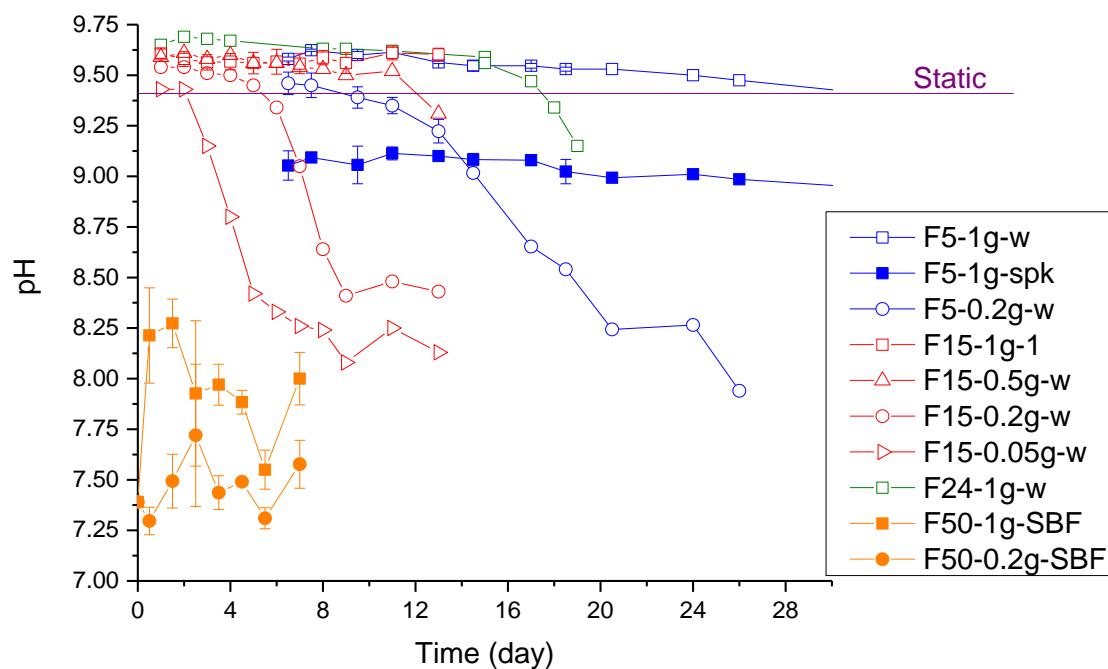
Figure 6. pH as a function of time for various SPFT experiments. (Lines are a guide for the eye. Data sets without error bars are a result of single measurements.)
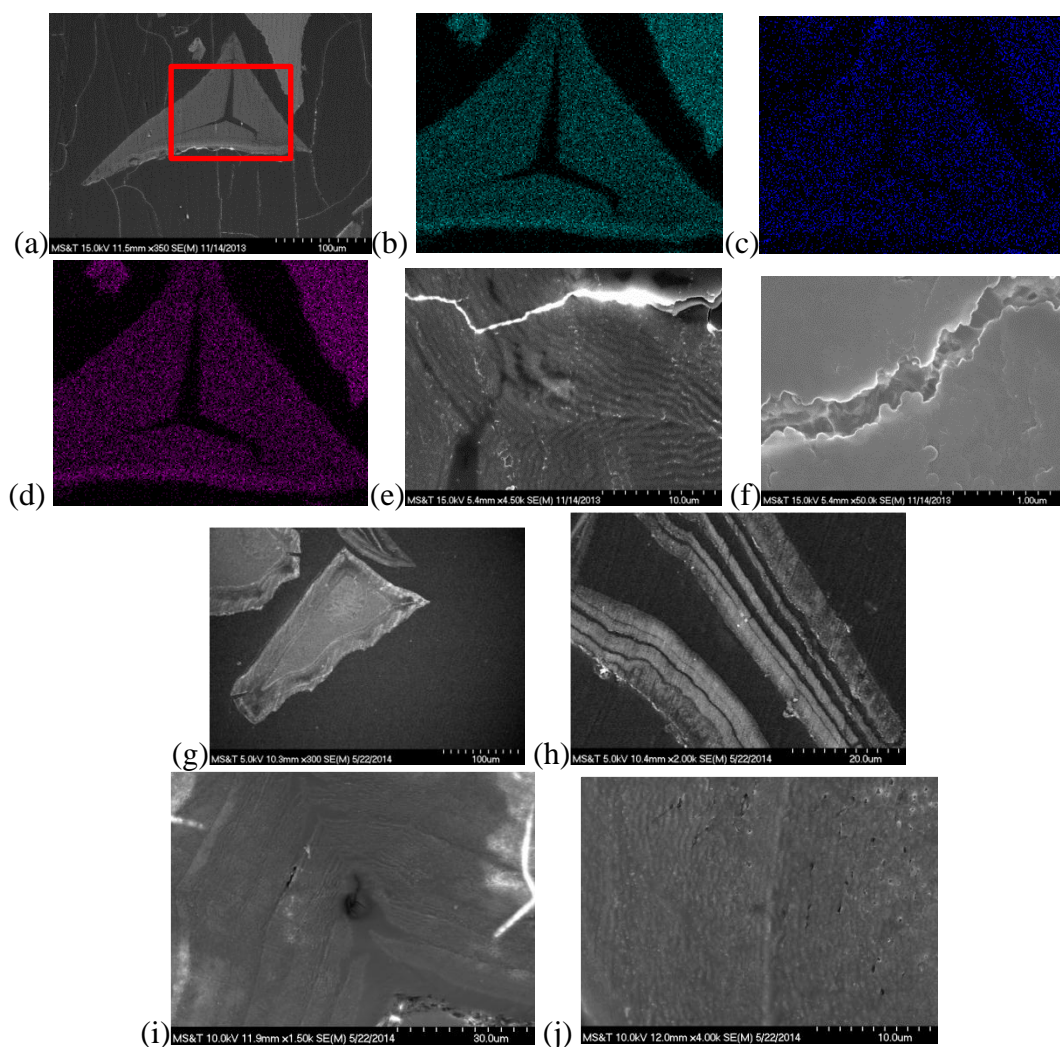
Figure 7. Scanning electron microscope images for cross sections of particles following SPFT experiments (a) A fully-reacted particle, F50-1g-w experiment at 14d. (b-d) EDS phase maps for Ca, Mg, and P (b-d, respectively) for the area outlined in red from part (a). (e-f) Magnified pictures of particles from the F50-1g-w experiment at 14d show the microstructure and morphology of the reaction layer. (g) A partially reacted particle from the F5-1g-w experiment at 22d. (h) A magnified image of the reaction layer from the F5-1g-w experiment at 22 d. (i) The reaction layer of a partially-reacted particle from the F5-1g-spk experiment at 22d. (i) A magnified image of the reaction layer from the F5-1g-spk experiment at 22d.
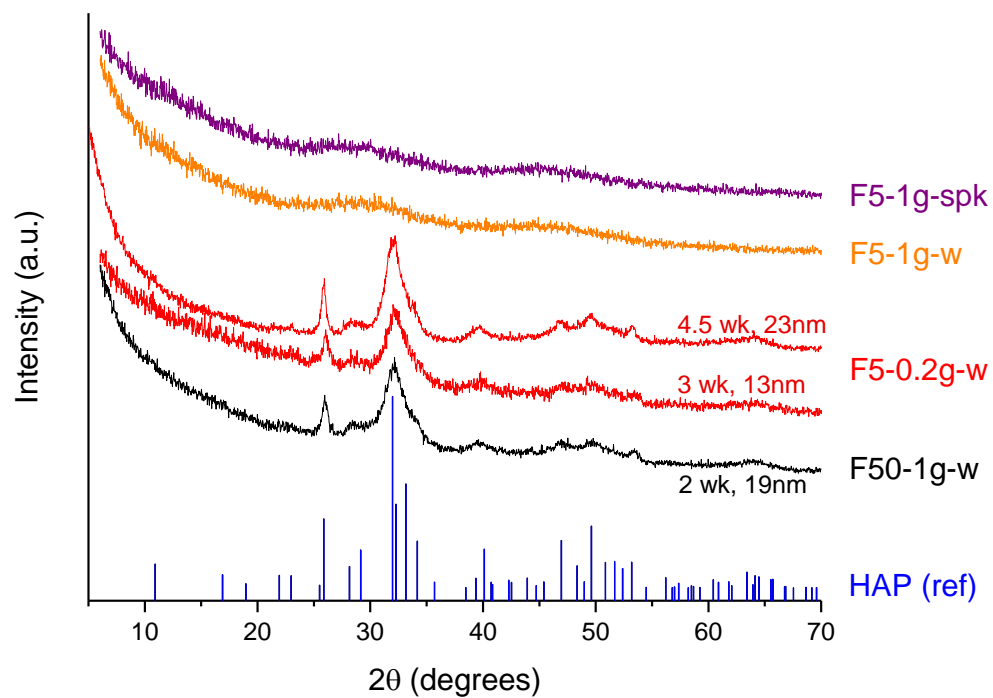
Figure 8. X-ray diffraction patterns for selected experiments following dissolution. (a) F5-1g-spk, 43d (b) F5-1g-w, 43d (c) F5-0.2g-w, 33d (d) F5-0.2g-w, 22d (e) F50-1g-w, 14d and (f) hydroxyapatite [ICDD 00-009-0432]
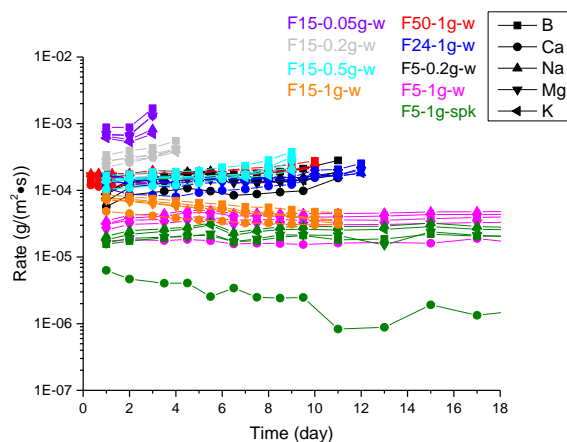
(a)
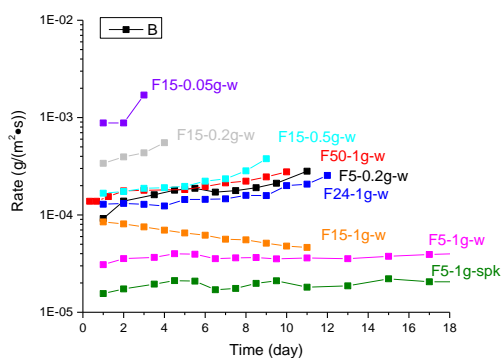
(b)
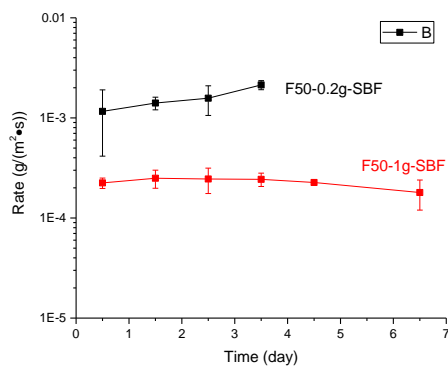
(c)

Figure 9. Normalized elemental release rates for: (a) Boron, calcium, sodium, magnesium, and potassium release rate for SPFT experiments in water, shown as a function of time. For clarity, only boron release is shown in (b). (c) Boron release rate for SPFT experiments in SBF, shown as a function of time.
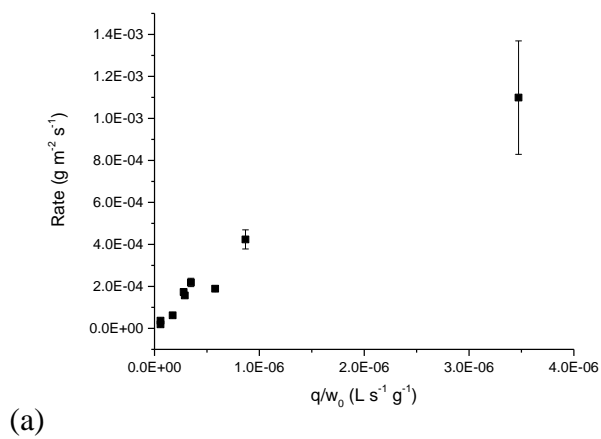
(a)
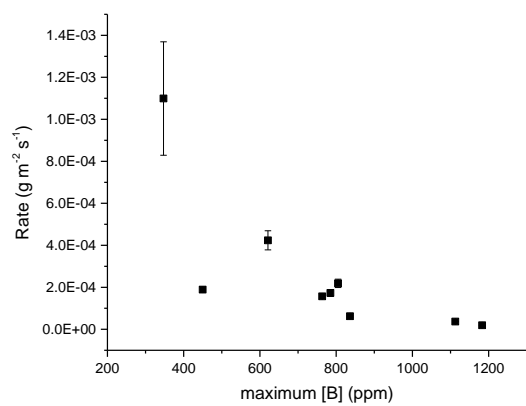
(b)

Figure 10. Boron release rate as a function of (a) flow rate, q, normalized to initial glass weight, w_0, and (b) maximum [B] observed over the course of the experiment for the water dissolution experiments.

REFERENCES

[1]   L. Hench, "The Story of Bioglass®," *J. Mater. Sci.: Mater. Med.*, **17** [11] 967-78 (2006).

[2]   J. R. Jones, "Review of Bioactive Glass: From Hench to Hybrids," *Acta Biomater.*, **9** [1] 4457-86 (2013).

[3]   M. N. Rahaman, D. E. Day, B. Sonny Bal, Q. Fu, S. B. Jung, L. F. Bonewald and A. P. Tomsia, "Bioactive Glass in Tissue Engineering," *Acta Biomater.*, **7** [6] 2355-73 (2011).

[4]   M. Richard, "Bioactive Behavior of a Borate Glass"; M.S. Thesis. University of Missouri - Rolla, Rolla, 2000.

[5]   W. Huang, D. Day, K. Kittiratanapiboon and M. Rahaman, "Kinetics and Mechanisms of the Conversion of Silicate (45S5), Borate, and Borosilicate Glasses to Hydroxyapatite in Dilute Phosphate Solutions," *J. Mater. Sci.: Mater. Med.*, **17** [7] 583-96 (2006).

[6]   S. B. Jung and D. E. Day, "Conversion Kinetics of Silicate, Borosilicate, and Borate Bioactive Glasses to Hydroxyapatite," *Physics and Chemistry of Glasses - European Journal of Glass Science and Technology Part B*, **50** [2] 85-8 (2009).

[7]   S. B. Jung, "Borate Based Bioactive Glass Scaffolds for Hard and Soft Tissue Engineering"; Ph.D. Thesis. Missouri University of Science and Technology, Rolla, 2010.

[8]   Q. Fu, M. N. Rahaman, H. Fu and X. Liu, "Silicate, Borosilicate, and Borate Bioactive Glass Scaffolds with Controllable Degradation Rate for Bone Tissue Engineering Applications. I. Preparation and in Vitro Degradation," *J. Biomed. Mater. Res. A*, **95A** [1] 164-71 (2010).

[9]   D. E. Day, J. E. White, R. F. Brown and K. D. McMenamin, "Transformation of Borate Glasses into Biologically Useful Materials," *Glass Technol.*, **44** [2] 75-81 (2003).

[10]   Q. Wang, W. Huang, D. Wang, B. Darvell, D. Day and M. N. Rahaman, "Preparation of Hollow Hydroxyapatite Microspheres," *J. Mater. Sci.: Mater. Med.*, **17** [7] 641-6 (2006).

[11]   X. Han and D. Day, "Reaction of Sodium Calcium Borate Glasses to Form Hydroxyapatite," *J. Mater. Sci.: Mater. Med.*, **18** [9] 1837-47 (2007).

[12]   Q. Fu, M. N. Rahaman, B. S. Bal, L. F. Bonewald, K. Kuroki and R. F. Brown, "Silicate, Borosilicate, and Borate Bioactive Glass Scaffolds with Controllable Degradation Rate for Bone Tissue Engineering Applications. II. In Vitro and in Vivo Biological Evaluation," *J. Biomed. Mater. Res. A*, **95A** [1] 172-9 (2010).

[13]   S. B. Jung, "Bioactive Borate Glasses"; chapter in Bio-Glasses: An Introduction; Edited by J. R. Jones and A. G. Clare. John Wiley & Sons, Ltd., 2012.

[14]   Y. Gu, W. Xiao, L. Lu, W. Huang, M. Rahaman and D. Wang, "Kinetics and Mechanisms of Converting Bioactive Borate Glasses to Hydroxyapatite in Aqueous Phosphate Solution," *J. Mater. Sci.*, **46** [1] 47-54 (2011).

[15]   Y. Li, M. N. Rahaman, Q. Fu, B. S. Bal, A. Yao and D. E. Day, "Conversion of Bioactive Borosilicate Glass to Multilayered Hydroxyapatite in Dilute Phosphate Solution," *J. Am. Ceram. Soc.*, **90** [12] 3804-10 (2007).

[16]   R. F. Brown, M. N. Rahaman, A. B. Dwilewicz, W. Huang, D. E. Day, Y. Li and B. S. Bal, "Effect of Borate Glass Composition on Its Conversion to Hydroxyapatite and on the Proliferation of Mc3t3-E1 Cells," *J. Biomed. Mater. Res. A.*, **88A** [2] 392-400 (2009).

[17]   L. Bi, M. N. Rahaman, D. E. Day, Z. Brown, C. Samujh, X. Liu, A. Mohammadkhah, V. Dusevich, J. D. Eick and L. F. Bonewald, "Effect of Bioactive Borate Glass Microstructure on Bone Regeneration, Angiogenesis, and Hydroxyapatite Conversion in a Rat Calvarial Defect Model," *Acta Biomater.*, **9** [8] 8015-26 (2013).

[18]   B. P. McGrail, D. H. Bacon, J. P. Icenhower, F. M. Mann, R. J. Puigh, H. T. Schaef and S. V. Mattigod, "Near-Field Performance Assessment for a Low-Activity Waste Glass Disposal System: Laboratory Testing to Modeling Results," *J. Nucl. Mater.*, **198** 95-111 (2001).

[19]   E. M. Pierce, E. A. Rodriguez, L. J. Calligan, W. J. Shaw and B. Pete McGrail, "An Experimental Study of the Dissolution Rates of Simulated Aluminoborosilicate Waste Glasses as a Function of pH and Temperature under Dilute Conditions," *Appl. Geochem.*, **23** [9] 2559-73 (2008).

[20]   J. P. Icenhower, B. P. McGrail, W. J. Shaw, E. M. Pierce, P. Nachimuthu, D. K. Shuh, E. A. Rodriguez and J. L. Steele, "Experimentally Determined Dissolution Kinetics of Na-Rich Borosilicate Glass at Far from Equilibrium Conditions: Implications for Transition State Theory," *Geochim. Cosmochim. Acta*, **72** [12] 2767-88 (2008).

[21]   ASTM Standard C1662-10, 2007, "Standard Practice for Measurement of the Glass Dissolution Rate Using the Single-Pass Flow-through Test Method," ASTM International, West Conshohocken, PA,

[22]   A. L. Cowles, H. H. Borgstedt and A. J. Gillies, "Tissue Weights and Rates of Blood Flow in Man for the Prediction of Anesthetic Uptake and Distribution," *Anesthesiology*, **35** [5] 523-6 (1971).

[23]   T. Kokubo, H. Kushitani, S. Sakka, T. Kitsugi and T. Yamamuro, "Solutions Able to Reproduce in Vivo Surface-Structure Changes in Bioactive Glass-Ceramic a-W3," *J. Biomed. Mater. Res.*, **24** [6] 721-34 (1990).

[24]   A. L. Patterson, "The Scherrer Formula for X-Ray Particle Size Determination," *Physical Review*, **56** [10] 978-82 (1939).

[25]   A. Khawam and D. R. Flanagan, "Solid-State Kinetic Models: Basics and Mathematical Fundamentals," *The Journal of Physical Chemistry B*, **110** [35] 17315-28 (2006).

[26]   A. Patterson, "The Scherrer Formula for X-Ray Particle Size Determination</Title>," *Physical Review*, **56** [10] 978-82 (1939).

[27]   B. P. McGrail, D. H. Bacon, J. P. Icenhower, F. M. Mann, R. J. Puigh, H. T. Schaef and S. V. Mattigod, "Near-Field Performance Assessment for a Low-Activity Waste Glass Disposal System: Laboratory Testing to Modeling Results," *J. Nucl. Mater.*, **298** [1–2] 95-111 (2001).

[28]   J. Zhao, Y. Liu, W.-b. Sun and H. Zhang, "Amorphous Calcium Phosphate and Its Application in Dentistry," *Chem. Cent. J.*, **5** [1] 40 (2011).

IV. NANOCRYSTALLINE RARE-EARTH PHOSPHATES FROM GLASS DISSOLUTION AND PRECIPITATION REACTIONS

AUTHORS

Jaime George
Colin Ryan
Richard K. Brow

Department of Materials Science and Engineering
Missouri University of Science and Technology
Rolla, MO
65409

ABSTRACT

A novel method is employed for the formation of rare-earth phosphate solid solution compounds with unique mesoscopic structures. Europium- and lanthanum-doped sodium borate glass microspheres and particles, ranging in sizes from 50-300 μm, were reacted in 0.25 M K_2HPO_4 solution to form hollow spheres of nanocrystalline rare-earth phosphate compounds by dissolution-precipitation reactions. The initially x-ray amorphous precipitated rare-earth phosphate materials were heat-treated at 700 °C for two hours to form nanocrystalline compounds. Differential thermal analysis (DTA) experiments yield an average activation energy for crystallization of 394±26 kJ/mol. X-ray diffraction (XRD) data indicates that samples crystallized to the monazite structure (monoclinic $P2_1/n$) with unit cell volumes ranging from 306.5 $Å^3$ for $LaPO_4$ to 282.5 $Å^3$ for $EuPO_4$ and with crystallite grain sizes of 56±14 nm. Compositions containing both rare-earth elements formed solid solutions with the composition $La_{(1-x)}Eu_xPO_4$. Raman spectroscopy indicates that the P-O symmetric stretching vibrations (ν_1) change systematically from 963 cm^{-1} for $LaPO_4$ to 986 cm^{-1} for $EuPO_4$, consistent with a

systematic decrease in average P-O bond length. Photoluminescence measurements show maximum emission intensity for the $La_{0.65}Eu_{0.35}PO_4$ composition.

1. INTRODUCTION

Rare-earth orthophosphate (REPO$_4$) materials have been used in many optical applications including fluorescent lamps, plasma display panels, and phosphors for LEDs.[1-3] Rare earth orthophosphates are typically formed by precipitating nanoparticles from lanthanide- and phosphate-containing acidic (pH ~ 2) solutions, and heat treating to elevated temperatures (< 1000 °C) where P$_2$O$_5$ volatility and lanthanide clustering are concerns.[1, 2, 4, 5] Conzone developed a different method to form hollow dysprosium phosphate (DyPO$_4$) microspheres by dissolving Dy-containing borate glasses in phosphate-containing solutions.[6] The DyPO$_4$ material precipitates onto the glass surface, thus retaining the initial shape of the glass. Hollow spheres of optically-active rare earth phosphates could be beneficial for optical applications because the fluorescing lanthanide elements are concentrated at the surface of the sphere, which prevents the material from absorbing photons emitted deeper in the sample.[7]

Low atomic number lanthanide (La-Gd) orthophosphate compounds crystallize to form the monoclinic P2$_1$/n structure, monazite, whereas greater atomic number lanthanide (Tb-Lu) orthophosphate compounds crystallize to form the tetragonal I4$_1$/amd structure, xenotime.[8] The crystal structures of the single-phase monazite lanthanide orthophosphates have been determined by x-ray diffraction [8-11] and have been characterized by Raman spectroscopy.[2, 12, 13] The monazite structure consists of alternating phosphate tetrahedra and nine-coordinated lanthanide polyhedra.[10, 14] Begun *et al.* showed that the Raman shift of the P-O symmetric stretching vibrational mode (v_1) increases linearly with atomic number of the lanthanide element in the monazite

structure.[12] Popović *et al.* found a linear relationship between ν_1 and P-O bond length for monovalent and divalent phosphate crystals.[15]

In this study, the borate glass dissolution/re-precipitation method is used to form novel rare-earth phosphate solid solution materials for optical applications. XRD and Raman spectroscopy are used to correlate ν_1 to P-O bond length for single phase lanthanide orthophosphates and $(La,Eu)PO_4$ solid solution compounds and this structural information is used to interpret trends in the fluorescence spectra from the Eu^{3+}-doped samples.

2. EXPERIMENTAL PROCEDURE

2.1. SYNTHESIS OF REPO$_4$ MATERIALS.

Glasses with the nominal compositions (mol %) $xEu_2O_3 \cdot (2-x)La_2O_3 \cdot 24.5Na_2O \cdot 73.5B_2O_3$, where $0 \leq x \leq 2$, were prepared by conventional melt quenching techniques. The raw materials H_3BO_3 (98%, Alfa Aesar), Na_2CO_3 (98%, Alfa Aesar), La_2O_3 (99.99%, Research Chemicals), and Eu_2O_3 (99.99%, Research Chemicals), were mixed, and each batch was melted in air for one hour at 1100 °C in a Pt-Rh crucible. Glasses were quenched onto a steel plate and ground to particles between 50-300 μm using a mortar and pestle. Some glass particles were made into microspheres by using a vibrating spatula to drop particles into a propane-oxygen flame. Microspheres were then collected and examined with optical microscopy to confirm a spherical shape.

Conversion of glass particles to phosphate compounds was done by reacting 0.5 g of glass particles or microspheres in 50 mL of 0.25 M K_2HPO_4 ($K_2HPO_4 \cdot 3H_2O$, 99%, Acros Organics) aqueous solution at 40 °C for 2 days. During this time, the glass dissolves and releases La^{3+} and Eu^{3+} ions into solution, where they react with phosphate anions to form a hydrated REPO$_4$ compound that precipitates on the glass surface.[6] The reacted particles were filtered from the solution, ultrasonically rinsed twice with deionized water and twice with ethanol, then dried at 100 °C for at least 12 hours. Reacted particles or microspheres will be referred to as "as-reacted REPO$_4$." As-reacted REPO$_4$ particles and microspheres were then heat-treated in a Pt-Rh crucible in air at temperatures up to 700 °C for up to two hours to crystallize the materials and these are referred to as "heat treated" samples.

2.2. CHARACTERIZATION.

Analytical scanning electron microscopy (SEM) was performed using an FEI

Helios NanoLab 600 FIB/FESEM with an Oxford energy dispersive spectrometer (EDS)

attachment to characterize the morphology and compositions of both the as-reacted and

heat-treated samples. Crystallization behavior was investigated by differential thermal

analysis (DTA). DTA experiments were performed using a Perkin-Elmer DTA7 on 27±3

mg of as-reacted $REPO_4$ in Pt crucibles and under flowing nitrogen with heating rates of

5-20 °C/min. Other DTA experiments were performed using fixed heating (10 °C/min)

and cooling (-10 °C/min) cycles. Sample weights were measured before and after DTA

experiments to characterize weight losses after heating. Thermal gravimetric analysis

(TGA) was performed on the sample Eu/(Eu+La)=0.5 with a heating rate of 10 °C/min

using a Netzsch STA 409 CD DTA/TGA. Crystal structure, unit cell lattice parameters,

and grain size were determined by X-ray diffraction (XRD). Diffraction patterns were

collected from 10 to 90° 2θ with a Philips X'pert multipurpose diffractometer with

PIXcel detector, using Cu $K_α$ radiation and Ni filter, at 45 kV and 40 mA. A Rietveld

refinement was performed using RIQAS software by Material Data Inc. Initial starting

structures of $LaPO_4$ and $EuPO_4$, calculated by Ni,[8] were used for the refinement and fit

with a Pearson VII shape function. Raman spectra were collected using a 100 mW, 785

nm diode laser on a HORIBA Jobin Yvon LabRAM ARAMIS micro-Raman

spectrometer. For each sample, ten spectra were collected through a 10x microscope

objective from the surfaces of the particles and averaged. Fluorescence spectra were

collected with a HORIBA FL3-22 spectrometer with xenon arc lamp light source. All

emission spectra were collected under the same conditions, with an excitation wavelength

of 394 nm and an average of three spectra from each sample was used for reported

emission intensities.

3. RESULTS

3.1. SEM/EDS.

An example of an SEM image collected from heat-treated, hollow microspheres is shown in Figure 1. EDS data averaged over 25 measurements indicates the presence of predominantly oxygen, phosphorus, europium, and lanthanum in the heat-treated product, with small amounts (<3 at%) of sodium or potassium. There is no evidence for sodium or potassium presence in the final rare-earth phosphate crystals. The relative concentrations of Eu, determined by EDS, for the heat-treated samples are shown in Figure 2, where they are compared to the nominal compositions of the initial borate glasses. For all samples, the relative Eu-content of the heat-treated samples is equivalent to the relative Eu-content of the original glass.

3.2. DTA/TGA.

Figure 3(a) shows the DTA and TGA curves for the as-reacted sample where Eu/(Eu+La)=0.5 and the heating rate is 10 ˚C/min, along with the DTA curves above 400 °C for heating rates of 5, 15, and 20 °C/min. A large endothermic transition is seen in the DTA data below 300 °C, accompanied in the TGA scan by a weight loss of about 9% between 100 and 400 °C. An exothermic peak is present above 500 °C for all DTA scans. The peak temperature, T_p, of the exotherm systematically increases from 569 to 589 °C with increasing heating rates. The heating rate dependence of T_p is summarized in Figure 3(b). The TGA experiment shows a weight loss of 9.2% below 400 °C and no mass loss at higher temperatures. For the DTA experiments, average mass losses of 12.0±1.7%, 15.7±1.3%, and 13.5±2.6% are observed for Eu/(Eu+La)= 0, 0.5 and 1, respectively, after

heating to 1000°C. Upon cooling and reheating to 1000°C, no features, endothermic or exothermic, are evident on the DTA curves.

3.3. XRD.

Figure 4 shows XRD patterns for the sample Eu/(Eu+La)=0.5, heat-treated for two hours at 200, 500, and 700 ˚C. Samples are initially x-ray amorphous and remain amorphous after heat treatment at 500 ˚C for two hours. When heated at 700 ˚C for two hours, the samples crystallized to from the monazite structure. Figure 5 shows the diffraction patterns for all compositions heat-treated for two hours at 700 ˚C. For clarity, data is only shown for 2θ between 10 and 60 °. Reference patterns for monoclinic $LaPO_4$ and $EuPO_4$ are shown for comparison.[8] All compositions formed the monoclinic monazite crystal structure, space group $P2_1/n$. As Eu replaces La, all peaks are shifted to a greater 2θ. A Rietveld lattice parameter refinement was performed on all samples to determine the monoclinic unit cell dimensions (a, b, and c) and angle (β); these lattice parameters are shown in Figure 6. Unit cell dimensions decrease linearly and the angle β increases linearly as Eu-content increases. Lattice parameters for the two end members of the series, $LaPO_4$ and $EuPO_4$, are consistent with literature values.[8]

3.4. RAMAN.

Figure 7 shows the Raman spectra for the Eu/(Eu+La)=0.5 particles: as-prepared glass, as-reacted $REPO_4$, and after heat treatment for two hours at 700 ˚C. Peaks are present in the spectrum from the unreacted glass predominantly in the range from 700 to 850 cm^{-1}. After the initial reaction in the phosphate solution, these peaks disappear and are replaced by broad peaks below 600 cm^{-1} and in the range from 900 to 1100 cm^{-1}. After heat-treatment, the same peaks have become more sharp and narrow. Raman

spectra for all heat-treated (700 °C, two hours) compositions are shown in Figure 8. The spectra are consistent with previous Raman studies of lanthanide orthophosphates.[12, 13, 16] Phosphate tetrahedra in orthophosphate materials are characterized by four Raman active modes: symmetric P-O stretching (v_1), antisymmetric stretching (v_3), and two bending modes (v_2 and v_4).[13] The frequency of each of these PO_4 vibrational modes increases as Eu replaces La in the $REPO_4$. These trends are most pronounced for the symmetric stretching mode, as shown as a function of Eu-content in Figure 9.

3.5. FLUORESCENCE.

Fluorescence emission spectra for as-reacted and heat-treated samples where Eu/(Eu+La) = 0.35 are given in Figure 10; the excitation wavelength for all emission experiments was 394 nm. Peaks are observed for all $^5D_0$ - ^7F_j transitions of Eu^{3+}, where j = 0-4, for all Eu-containing samples.[17] For the heat-treated samples of all compositions, the emission peaks were sharper and more defined than for the as-reacted samples. For Eu/(Eu+La) < 0.35, the intensity of the as-reacted sample is about 10% that of the heat-treated sample and above Eu/(Eu+La) = 0.35, the intensity of the as-reacted sample increases gradually, relative to the heat-treated sample, until at Eu/(Eu+La) = 1, the intensity of the as-reacted sample is 75% of the heat-treated sample. Emission peaks for all $^5D_0$ - ^7F_j transitions were integrated to determine peak areas and normalized to the maximum value. These normalized areas are shown as a function of composition for both as-reacted and heat-treated samples in Figure 11. The emission intensities for all electronic transitions increase as a function of Eu-content until they reach a maximum at Eu/(Eu+La) = 0.5-0.65 for the as-reacted samples and at Eu/(Eu+La) = 0.35 for the heat-treated samples. After reaching a maximum, the emission intensities gradually decrease

with increasing Eu-content, reaching a final intensity of about 20% of the maximum for both as-reacted and heat treated samples at Eu/(Eu+La) = 1.

The asymmetric ratio (A_{21}) is the ratio of the areas of the $^5D_0$ - $^7F_2$ to $^5D_0$ - $^7F_1$ transitions and is shown in Figure 12 for both as-reacted and-heat treated samples. In both series, the asymmetric ratio is lowest at Eu/(Eu+La) = 0.05 and increases as the Eu-content increases to a maximum value at Eu/(Eu+La) $\geq$ 0.35. The asymmetric ratios for the as-reacted samples are approximately double those for the heat-treated samples.

4.   DISCUSSION

The dissolution process of a soluble rare-earth sodium borate glass in a phosphate-containing solution begins at the surface of the sample. The Na_2O and B_2O_3 components of the glass dissolve into solution and the RE_2O_3 component reacts with HPO_4^{2-} anions in solution to form a rare-earth phosphate reaction layer surrounding the unreacted glass core.[6] As dissolution time increases, glass from the core continues to dissolve and the reaction layer increases in thickness as more $REPO_4$ is precipitated. EDS data in Figure 2 shows that the relative fraction of Eu in the final product is equal to the relative fraction of Eu in the as-batched glass, demonstrating that there is no preference for the precipitation of one rare-earth ion over the other. Since the initially amorphous phosphate precipitates on the surface of the glass microsphere or particle, the as-reacted $REPO_4$ microspheres/particles have similar sizes and shapes as the original glass. Due to the relatively low concentration of rare-earth oxide in the base glass, a hollow core is formed once the glass is fully dissolved. With greater concentrations of rare earth oxides in the base glass (> 30 wt%), a porous, solid rare earth particle can be formed.[6]

Mass loss and an endothermic peak below 400 °C from DTA/TGA experiments (Figure 3) are attributed to water loss from the initially amorphous, as-reacted samples. From the weight loss measurements made on the DTA samples, an average of 2.1±0.5 mol H_2O is lost per mol $REPO_4$, indicating that the initial precipitated material is $La_{(1-x)}Eu_xPO_4 \bullet 2H_2O$.

The exothermic peak in the DTA scans near 570-590 ˚C (Figure 3) is attributed to crystallization of the amorphous precipitated phase to the monazite form of $La_{(1-x)}Eu_xPO_4$ (Figure 4). The possibility of a reversible polymorphic phase transition was eliminated

because no endothermic features upon cooling or exothermic features upon a second heating were observed by DTA. A Kissinger analysis of the effect of heating rate (ø) on the DTA peak temperature (T_p in Kelvins) was applied to determine the activation energy, E_a, for crystallization,[18]

$$\ln\left(\frac{\phi}{T_p^2}\right) = \ln(k) + \frac{-E_a}{RT_p} \tag{1}$$

where k is the pre-exponential factor, and R is the gas constant. Figure 3(b) provides a plot of $\ln(\phi/T_p^2)$ vs. $1/T_p$ for four heating rates (ø=5, 10, 15, and 20 K^{-1}) for the as-reacted samples where Eu/(Eu+La)= 0.5. Activation energies, which are determined from the slopes of the data, were calculated for Eu/(Eu+La) = 0, 0.5, and 1. The activation energies are independent of the Eu-content and their average is 394±26 kJ/mol. This activation energy is similar to the activation energies for diffusion of Ln^{3+} (Ln=Yb, Dy, Sm) in orthophosphate structures, which are 362±13, 349±16, and 441±12 kJ/mol respectively.[19] This similarity in activation energies indicates that crystallization of the amorphous as-reacted phosphate may be controlled by diffusion of the Eu^{3+} and/or La^{3+} ions.

As the initially amorphous $La_{(1-x)}Eu_xPO_4 \cdot 2H_2O$ is heated, it loses water, which is fully removed by 400 °C. Following heat treatment at 500 °C for 2 hours, the REPO$_4$ compound is still amorphous, indicating that crystallization is independent of the water loss process. Following crystallization at 700 °C, the decrease in the unit cell lattice parameters as Eu/(Eu+La) increases (Figure 6) is consistent with smaller Eu^{3+} ions replacing larger La^{3+} ions in the crystal structure. Vegard's law, which describes the

relationship between unit cell volume and substitutional solid solution composition, is given by,[20]

$$X_{i,j} = f_i * X_i + f_J * X_j \qquad (2)$$

where X_{ij} is the lattice parameter of the solid solution, f is the atom fraction of component i or j, and X is a lattice parameter of component i or j. Throughout the entire compositional range, lattice parameters decrease linearly as described by Vegard's law, represented by the solid lines in Figure 6. Thus, the heat-treated samples are solid solutions with the monazite structure and a stoichiometry of $La_{(1-x)}Eu_xPO_4$.

Scherrer's equation can be applied to determine grain size (τ) based on the full width at half max (B) of the XRD peaks by the equation,[21]

$$\tau = \frac{K\lambda}{B \cos\theta} \qquad (3)$$

where λ is the x-ray wavelength, θ is the Bragg angle of the peak and K is a dimensionless shape factor. Since peak broadening occurs with the formation of solid solution compounds, the Scherrer analysis was applied only to the $La_{1-x}Eu_xPO_4$ (x = 0 and 1) end member materials. After accounting for broadening of the diffractometer using a NIST-SRM 660a LaB_6 standard, Equation 3 was used with a value of K=0.9,[22] to determine an average grain size for these two samples of 56±14 nm.

In the Raman spectrum from the as-prepared glass (Figure 7), the peak at 778 cm⁻¹ is attributed to the breathing mode of a six-membered borate ring with one tetrahedral boron, following Konijnendijk's Raman studies of alkali borate glasses of similar composition.[23] This peak is no longer present in the Raman spectra from the as-reacted samples, indicating that the glass has fully dissolved into solution. The as-reacted samples show broad peaks in the region of the P-O symmetric stretching (950-1000 cm⁻¹)

and bending (450-500 cm^{-1}) modes.[13] The sharpening of these peaks upon heat treatment is attributed to crystallization of the amorphous, as-reacted $La_{(1-x)}Eu_xPO_4 \cdot 2H_2O$ material.

Popović[15] has shown that an inverse correlation exists between the frequencies of the P-O stretching modes in the Raman spectra and the average P-O bond distance in crystalline monovalent and divalent phosphates. For the single phase monazite rare-earth phosphates (Ln=La, Pr, Nd, Sm, Eu, Gd), a linear relationship also exists. P-O bond lengths were determined by Mullica from XRD data[9-11] and the Raman shift of ν_1 was reported by Begun.[12] This relationship is shown in the inset of Figure 9 and the trend of the line is given by,

$$\nu_1 = 170.7 - 0.01795 * R \qquad (4)$$

where R is the P-O bond length in pm and ν_1 is the Raman shift of the P-O symmetric stretch in cm^{-1}. The shift of Raman peaks to greater frequencies as Eu^{3+} replaces La^{3+} in the solid solution structure implies that the average P-O bond length decreases with increasing Eu-content. Using this empirically derived formula, the average P-O bond lengths over the compositional range decrease linearly from 153.4 to 153.0 pm, shown as a secondary y-axis in Figure 9. This decrease in average P-O bond length is consistent with the decrease in unit cell parameters noted from the XRD data in Figure 6.

The emission spectra (e.g., Figure 10) show every $^5D_0$ - ^7F_j transition for Eu^{3+}, including the forbidden $^5D_0$ - $^7F_0$ transition, for all samples. The lower emission intensity from the as-reacted samples relative to the heat-treated samples is attributed to the presence of OH^- groups, which are known to quench Eu^{3+} luminescence through multiphonon relaxation.[24-26] The maximum in emission intensity, followed by the decrease of intensity (Figure 11) is attributed to concentration quenching related to Eu^{3+}-

Eu^{3+} interactions. For the heat treated samples, the composition with maximum emission intensity, $La_{0.65}Eu_{0.35}PO_4$, is equivalent to 5.8 at% Eu^{3+}. For the as-reacted samples, the maximum emission intensity occurs at $La_{0.35}Eu_{0.65}PO_4 \cdot 2H_2O$, or 5.4 at% Eu^{3+}. These values are consistent with reported maximum Eu-concentrations (5-6 at%) in other phosphate systems ($LaPO_4$, $TbPO_4$, YPO_4, and $Sr_3Bi(PO_4)_3$) before concentration quenching occurs.[24, 26-28] Blasse proposed[29] and Dong *et al.* reported[28] that the critical distance between Eu^{3+} ions for energy transfer (R_c) can be calculated by,

$$R_c = 2 * \left(\frac{3*V}{4*\pi*x_c*N} \right)^{1/3} \tag{5}$$

where V is the unit cell volume, N is the number of host cations in the unit cell, and x_c is the critical concentration of the activator ion. For the heat treated samples with a critical Eu^{3+} concentration of 5.8 at%, the critical Eu^{3+}-Eu^{3+} distance for this system is calculated to be 13.5 Å. These calculations assume that Eu^{3+} randomly substitutes for La^{3+} in the monazite crystal structure, and are consistent with the formation of $La_{(1-x)}Eu_xPO_4$ solid solution compounds.

The $^5D_0$ - $^7F_2$ electric dipole transition intensity is greater than the $^5D_0$ - $^7F_1$ magnetic dipole transition intensity in the spectra from all of the as-reacted samples and the heat-treated samples where $Eu/(Eu+La) \geq 0.35$ (Figure 12). The ratio of these two intensities, the asymmetric ratio, is a measure of Eu^{3+} site symmetry.[30] The $^5D_0 \rightarrow {}^7F_2$ electric dipole transition is a hypersensitive transition which depends on site symmetry and is only allowed when Eu^{3+} occupies a site without an inversion center.[5, 31] The $^5D_0 \rightarrow {}^7F_1$ magnetic dipole is not as sensitive to local symmetry and is independent of environment.[30] When the asymmetric ratio is small, the point of symmetry is closer to an

inversion center.[27, 30] In both the as-reacted and heat-treated samples, Eu^{3+} ions have symmetries closer to inversion centers as the Eu-content of the samples decrease. However, all of the as-reacted samples have an asymmetric ratio greater than the heat-treated samples (Figure 12), meaning that Eu^{3+} ions in the heat-treated samples are in relatively more symmetric environments.

5. CONCLUSIONS

Novel nanocrystalline rare earth phosphate solid solutions were prepared by dissolution-precipitation reactions between soluble rare earth-doped borate glasses and a phosphate solution. The nanocrystalline material formed a hollow mesoscopic structure based on the size and shape of the initial glass particles. This is the first reported instance of solid solution phosphate materials being formed by this glass dissolution-precipitation method. As-reacted, the precipitated materials are x-ray amorphous and they crystallize following heat-treatment. The $La_{(1-x)}Eu_xPO_4$ materials form solid solutions across the entire compositional series and as the Eu-content increases, unit cell volume and P-O bond lengths decrease. Emission spectra indicate that the Eu^{3+} ions are in a more centro-symmetric environment when Eu-contents are low.

ACKNOWLEDGMENTS
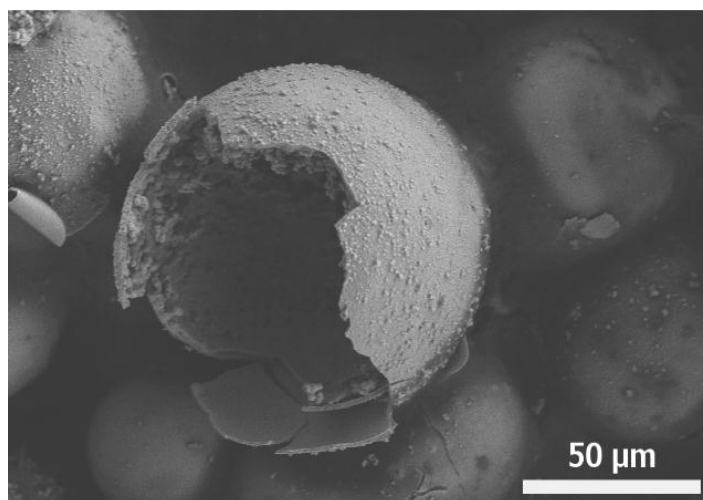
FIGURES

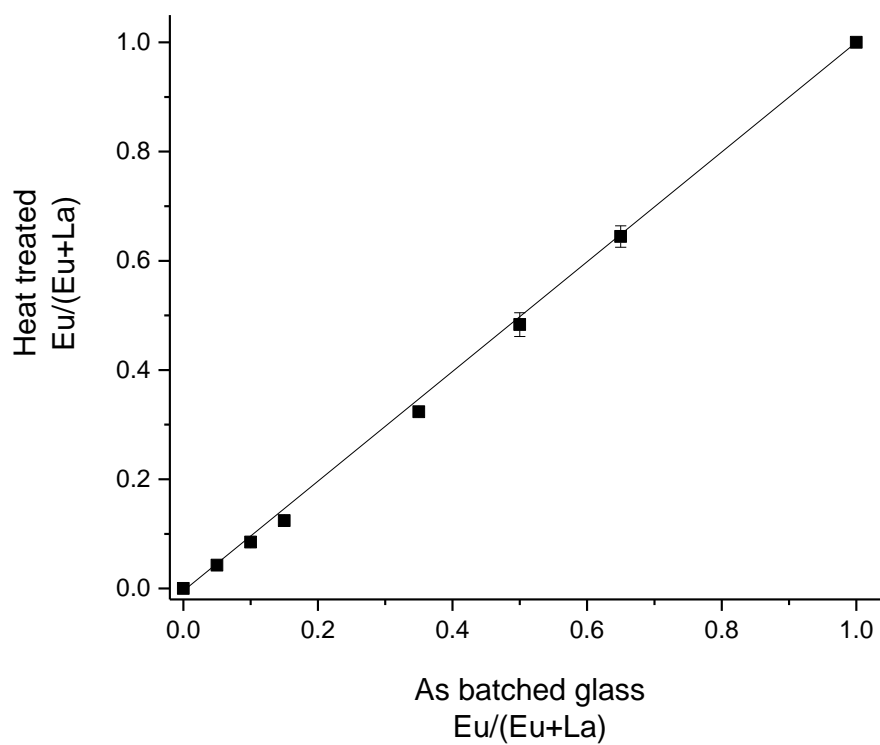Figure 1. Representative scanning electron microscopy image of a fractured, heat-treated La$_{(1-x)}$Eu$_x$PO$_4$ microsphere, x=1.

Figure 2. Compositional data (atom fraction) for the $La_{(1-x)}Eu_xPO_4$ particles heat-treated to 700 °C for 2 hours, measured by EDS, compared to the nominal compositions of the respective, as-batched glasses. A 1:1 atomic ratio is indicated by the straight line. Error bars not shown are within the size of the data marker.
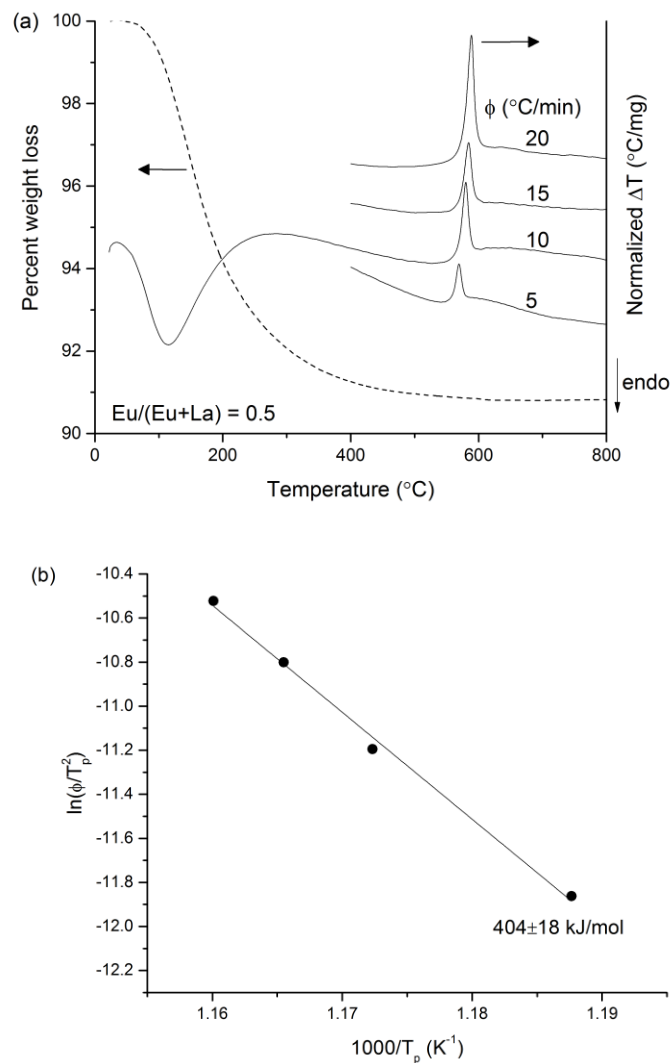
Figure 3. DTA curves of the as-reacted $La_{(1-x)}Eu_xPO_4 \cdot 2H_2O$ samples. (a) Weight loss from TGA is overlaid with normalized ΔT curve for a heating rate of 10 °C/min, x=0.5. Normalized ΔT is also shown above 400 °C for heating rates of 5, 15, and 20 °C/min. (b) Kissinger analysis for crystallization of as-reacted $La_{(1-x)}Eu_xPO_4 \cdot 2H_2O$, x=0.5. The solid line was determined by linear least-squares regression analysis and the resulting activation energy calculated from Equation 1 is given.
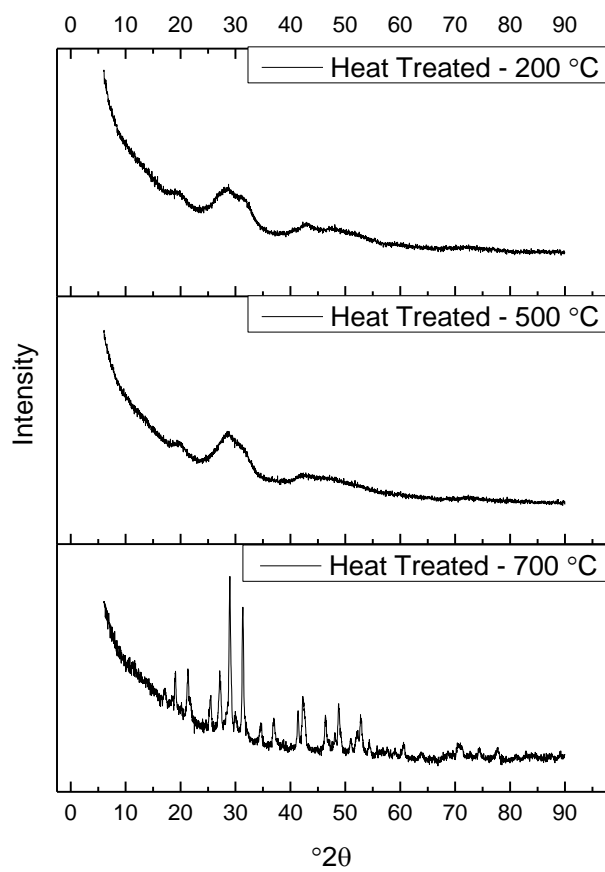
Figure 4. X-ray diffraction patterns of a $La_{o.5}Eu_{0.5}PO_4$ sample, heat treated for 2 hours at 200 °C, 500 °C, and 700 °C.

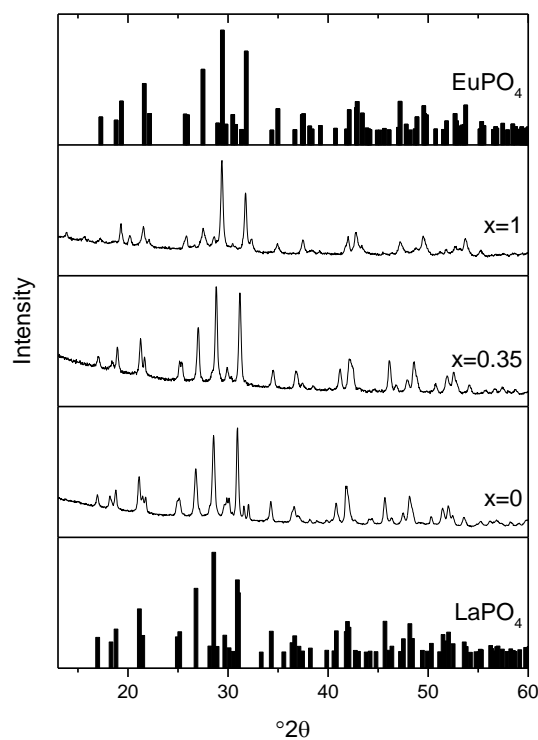Figure 5. X-ray diffraction patterns for La$_{(1-x)}$Eu$_x$PO$_4$ samples heat treated to 700 °C for 2 hours. Legend values represent values of 'x' for each composition. The EuPO$_4$ and LaPO$_4$ patterns are provided from Ni, et al.[8]
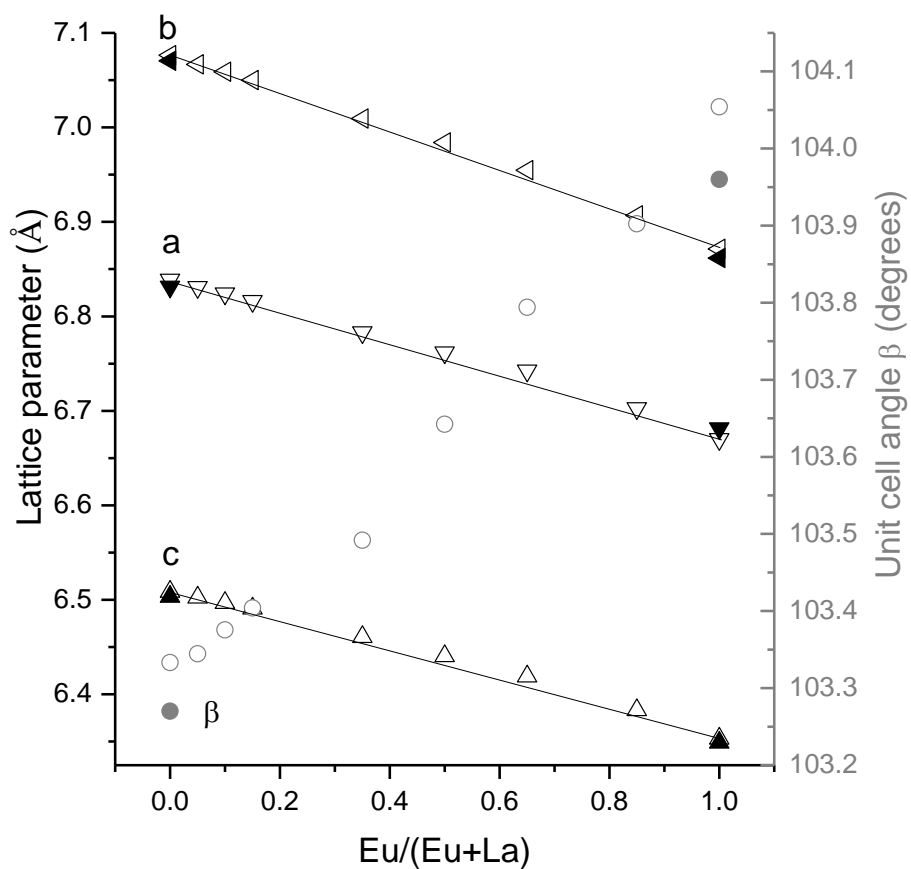
Figure 6. Lattice parameters a, b, and c and unit cell angle (β) for $La_{(1-x)}Eu_xPO_4$ samples after heat-treatments for two hours at 700 °C, shown as a function of x, Eu/(Eu+La) (open symbols). Closed symbols show lattice parameters from the literature.[8] Solid lines indicate the trends according to Vegard's law (Equation 2).
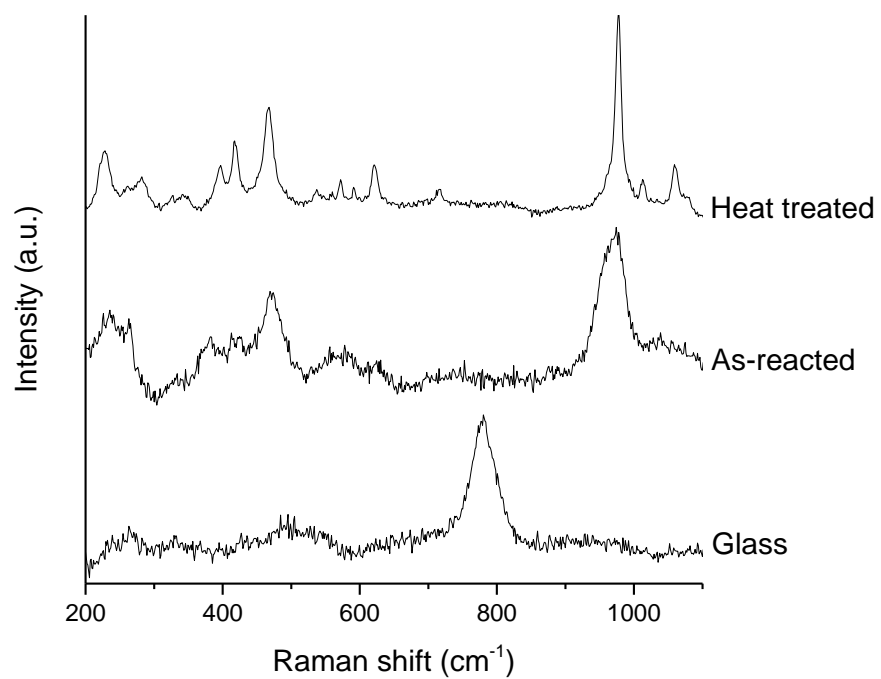
Figure 7. Raman spectra of the as-prepared glass (bottom), as-reacted
$La_{0.5}Eu_{0.5}PO_4 \cdot 2H_2O$ sample (middle), and $La_{0.5}Eu_{0.5}PO_4$ sample after heat treatment at
700 °C for two hours (top). Intensity is provided as arbitrary units (a.u.).

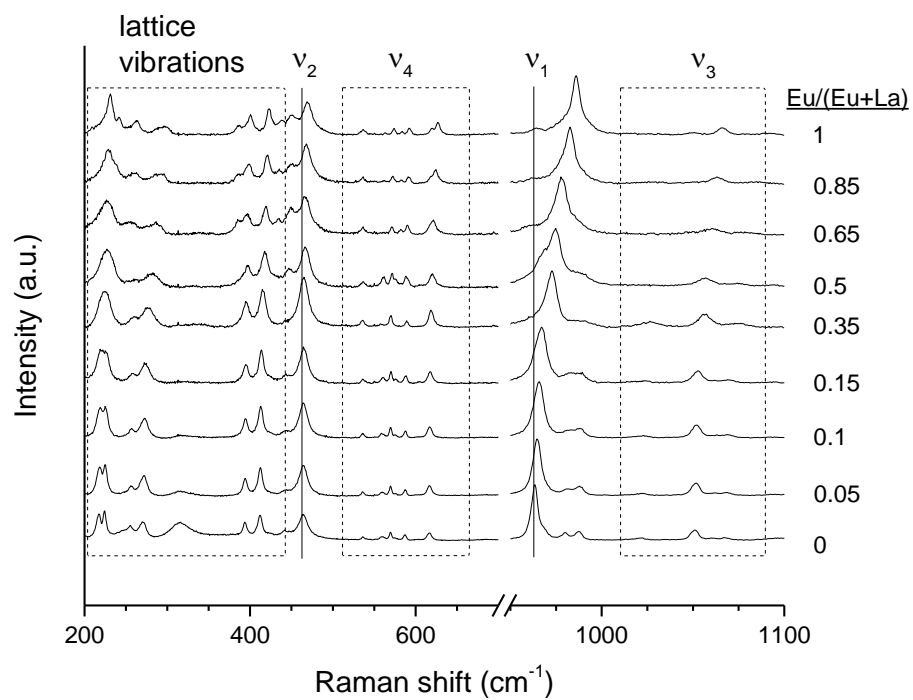Figure 8. Raman spectra of La$_{(1-x)}$Eu$_x$PO$_4$ samples after heat-treatment for two hours at 700 °C.
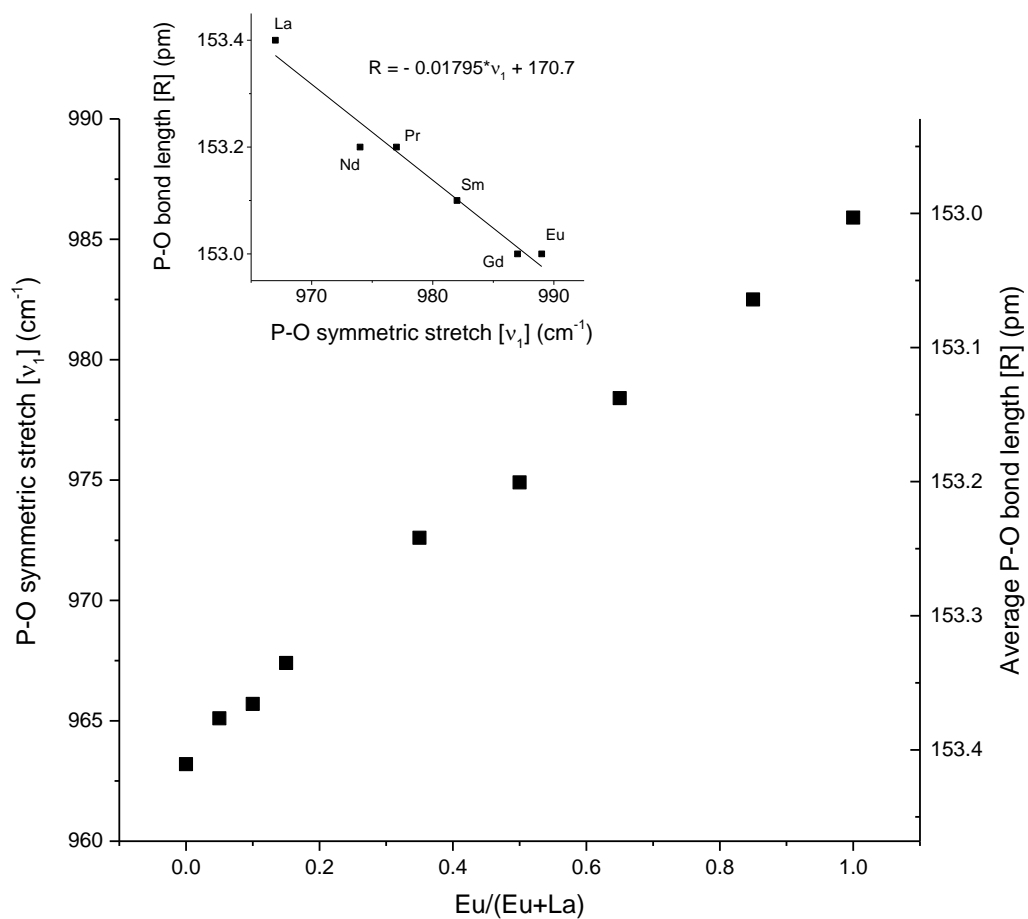
Figure 9. Raman shift of the P-O symmetric stretching mode for $La_{(1-x)}Eu_xPO_4$ samples after heat-treatment for two hours at 700 °C (left y-axis). The inset shows P-O bond length data collected from XRD[9-11] as a function of Raman shift of P-O symmetric stretching mode[12] for single phase $REPO_4$ compounds. Using the trend from the inset (Equation 4), a right y-axis is added showing average P-O bond length as a function of composition.

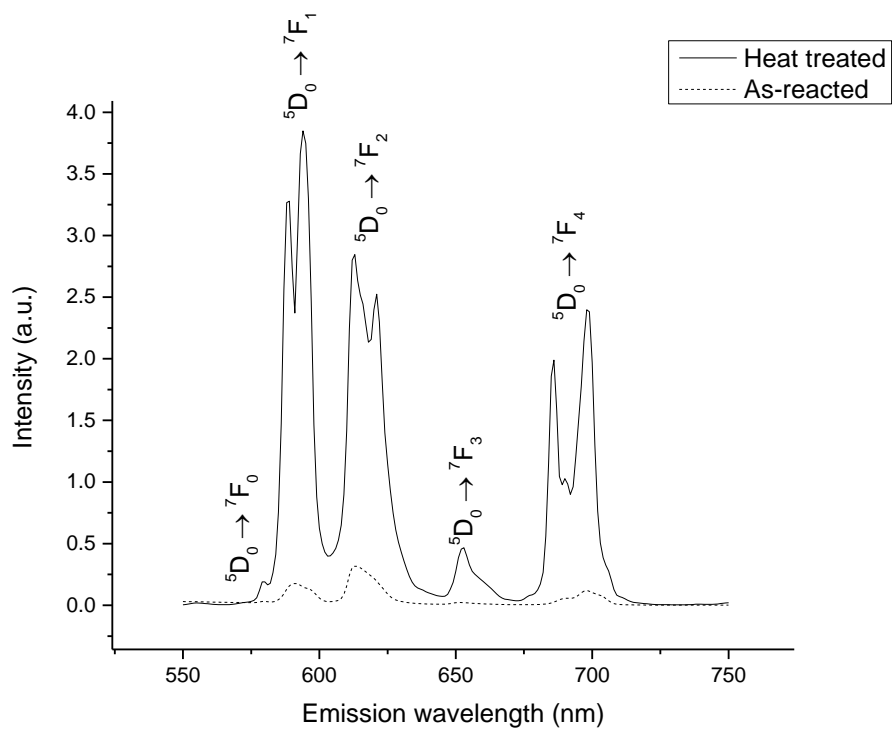Figure 10. Emission spectra for the as-reacted $La_{0.65}Eu_{0.35}PO_4 \cdot 2H_2O$ sample (dashed line) and the $La_{0.65}Eu_{0.35}PO_4$ sample after heat-treatment at 700 °C for two hours (solid line). (λ_{ex} = 394 nm)
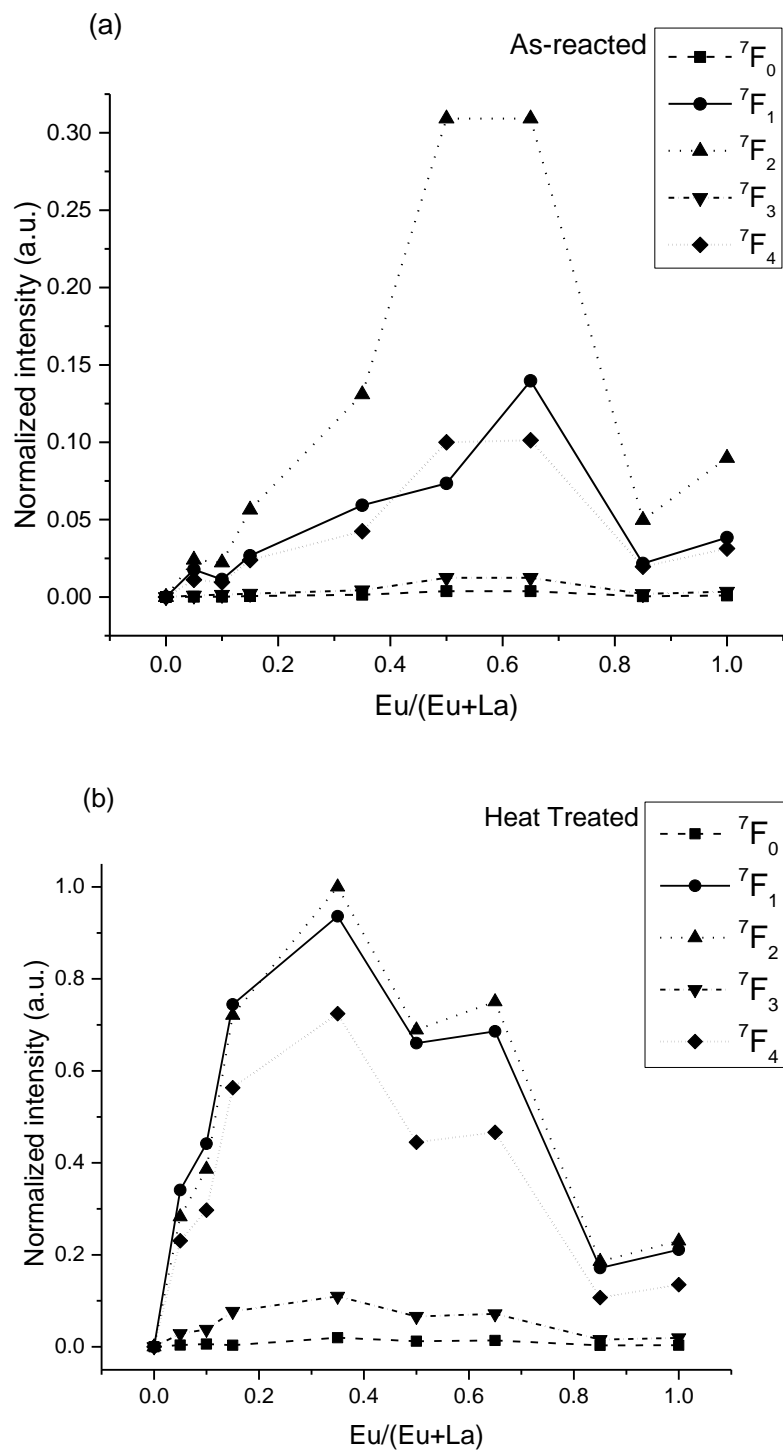
Figure 11. Relative peak areas for the (a) as-reacted and (b) heat treated $La_{(1-x)}Eu_xPO_4$ samples, normalized to most intense peak for the heat-treated samples.
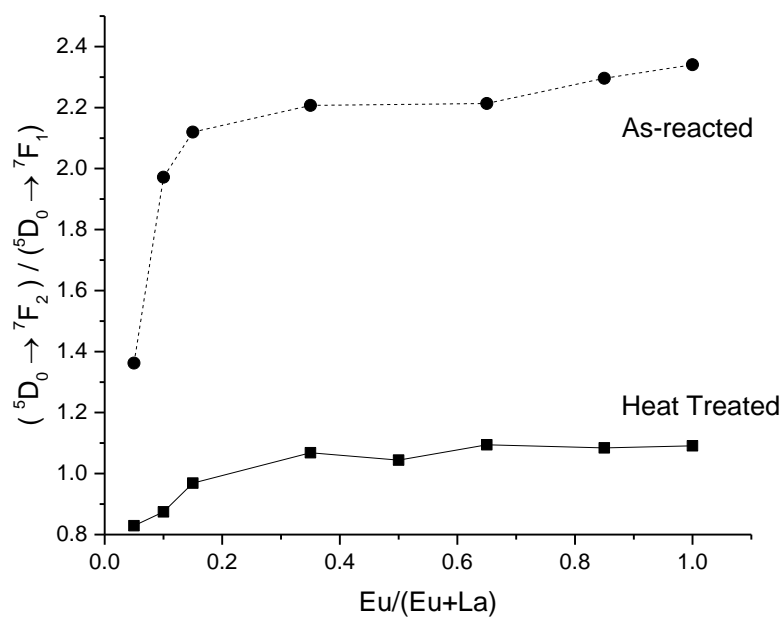
Figure 12. Ratios of the areas of the peaks due to the $^5D_0 \rightarrow {}^7F_2$ and $^5D_0 \rightarrow {}^7F_1$ transitions for as-reacted and heat treated $La_{(1-x)}Eu_xPO_4$ samples. The lines are guides for the eye.

REFERENCES

[1]   J. Dexpert-Ghys, R. Mauricot and M. D. Faucher, "Spectroscopy of Eu3+ Ions in Monazite Type Lanthanide Orthophosphates LnPO$_4$, Ln = La or Eu," *J. Lumin.*, **69** 203-15 (1996).

[2]   C. T. Dinh, P. V. Huong, R. Olazcuaga and C. Fouassier, "Syntheses, Structures, and Raman Spectra of Luminescent Gadolinium Phosphates," *J. Optoelectron. Adv. M.*, **2** [2] 159-69 (2000).

[3]   B. Damien, A. Fabienne, C. Thibault, S. Dimitri and B.-A. Didier, "Solid-State Synthesis of Monazite-Type Compounds LnPO$_4$ (Ln=La to Gd)," *Solid State Sci.*, **9** 432-9 (2007).

[4]   R. Kijkowska, "Ca-Substituted Europium(III) Phosphate Monohydrate Obtained through Crystallisation from Phosphoric Acid Solution," *J. Alloys Compd.*, **363** 138-42 (2004).

[5]   N. Yaiphaba, R. S. Ningthoujam, N. S. Singh, R. K. Vatsa, N. R. Singh, S. Dhara, N. L. Misra and R. Tewari, "Luminescence, Lifetime, and Quantum Yield Studies of Redispersible Eu^{3+}-Doped GdPO$_4$ Crystalline Nanoneedles: Core-Shell and Concentration Effects," *J. Appl. Phys.*, **107** [3] (2010).

[6]   S. D. Conzone and D. E. Day, "Preparation and Properties of Porous Microspheres Made from Borate Glass," *J. Biomed. Mater. Res. A*, **88A** [2] 531-42 (2009).

[7]   P. R. Ehrmann and J. H. Cambell, "Nonradiative Energy Losses and Radiation Trapping in Neodymium-Doped Phosphate Laser Glasses," *J. Am. Ceram. Soc.*, **85** [5] 1061-9 (2002).

[8]   Y. Ni, J. M. Hughes and A. N. Mariano, "Crystal Chemistry of the Monazite and Xenotime Structures," *Am. Mineral.*, **80** 21-6 (1995).

[9]   D. F. Mullica, D. A. Grossie and L. A. Boatner, "Coordination Geometry and Structural Determinations of SmPO$_4$, EuPO$_4$, and GdPO$_4$," *Inorg. Chim. Acta*, **109** 105-10 (1985).

[10]   D. F. Mullica, W. O. Milligan, D. A. Grossie, G. W. Beall and L. A. Boatner, "Ninefold Coordination in LaPO$_4$: Pentagonal Interpenetrating Tetrahedral Polyhdron," *Inorg. Chim. Acta*, **95** 231-6 (1984).

[11]   D. F. Mullica, D. A. Grossie and L. A. Boatner, "Structural Refinements of Praseodymium and Neodymium Orthophosphate," *J. Solid State Chem.*, **58** [71-77] (1985).

[12]   G. M. Begun, G. W. Beall, L. A. Boatner and W. J. Gregor, "Raman Spectra of the Rare Earth Orthophosphates," *J. Raman Spectrosc.*, **11** [4] 273-8 (1981).

[13]   E. N. Silva, A. P. Ayala, I. Guedes, C. W. A. Paschoal, R. L. Moreira, C. K. Loong and L. A. Boatner, "Vibrational Spectra of Monazite-Type Rare-Earth Orthophosphates," *Opt. Mater.*, **29** 224-30 (2006).

[14]   N. Clavier, R. Podor and N. Dascheux, "Crystal Chemistry of the Monazite Structure," *J. Eur. Ceram. Soc.*, **31** 941-76 (2011).

[15]   L. Popović, D. DeWaal and J. C. A. Boeyens, "Correlations between Raman Wavenumbers and P-O Bond Lengths in Crystalline Inorganic Phosphates," *J. Raman Spectrosc.*, **36** 2-11 (2005).

[16]   C. W. A. Paschoal, A. P. Ayala, I. Guedes, C. K-Loong and L. A. Boatner, "Raman Phonons in RPO_4 Crystals," The XVIIIth International Conference on Raman Spectroscopy, (2002).

[17]   U. Rambabu and S. Buddhudu, "Optical Properties of $LnPO_4 : Eu^{3+}$ (Ln = Y, La and Gd) Powder Phosphors," *Opt. Mater.*, **17** 401-8 (2001).

[18]   R. L. Blaine and H. E. Kissinger, "Homer Kissinger and the Kissinger Equation," *Thermochim. Acta*, **540** 1-6 (2012).

[19]   D. J. Chermiak, "Pb and Rare Earth Element Diffusion in Xenotime," *Lithos*, **88** 1-14 (2006).

[20]   A. R. Denton and N. W. Ashcroft, "Vegard's Law," *Phys. Rev. A*, **43** [6] 3161-4 (1991).

[21]   A. L. Patterson, "The Scherrer Formula for X-Ray Particle Size Determination," *Physical Review*, **56** [10] 978-82 (1939).

[22]   F. W. Jones, "The Measurement of Particle Size by the X-Ray Method," *Proceedings of the Royal Society of London. Series A, Mathematical and Physical Sciences*, **166** [924] 16-43 (1938).

[23]   W. L. Konijnendijk and J. M. Stevels, "The Structure of Borate Glasses Studied by Raman Scattering," *J. Non-Cryst. Solids*, **18** 301-31 (1975).

[24] H. Lai, H. Yang, C. Tao and X. Yang, "Preparation, Characterization and Luminescence Property of YPO$_4$:Eu Nanocrystals," *Physica status solidi (a)*, **204** [4] 1178-84 (2007).

[25] V. Buissette, M. Moreau, T. Gacoin, J.-P. Boilot, J.-Y. Chane-Ching and T. LeMercier, "Colloidal Synthesis of Luminescent Rhabdophane LaPO$_4$:Ln^{3+}–xH$_2$O (Ln: Ce, Tb, Eu; X ≈ 0.7) Nanocrystals," *Chem. Mater.*, **16** 3767-73 (2004).

[26] W. Di, X. Wang, P. Zhu and B. Chen, "Energy Transfer and Heat-Treatment Effect of Photoluminescence in Eu^{3+}-Doped Tbpo$_4$ Nanowires," *J. Solid State Chem.*, **180** 467-73 (2007).

[27] Z. Xiu, S. Liu, M. Lu, H. Zhang and G. Zhou, "Photoluminescence of Eu^{3+}-Doped LaPO$_4$ Nanocrystals Synthesized by Combustion Method," *Mater. Res. Bull.*, **41** 642-6 (2006).

[28] G. Dong, H. Ma, Y. Liu, Z. Yang and Q. Liu, "Synthesis and Photoluminescence Properties of the High-Brightness Eu^{3+}-Doped Sr$_3$Bi(PO$_4$)$_3$ Phosphors," *Opt. Commun.*, **285** 4097-101 (2012).

[29] G. Blasse, "Energy Transfer between Inequivalent Eu^{2+} Ions," *J. Solid State Chem.*, **62** [2] 207-11 (1986).

[30] H. Lai, A. Bao, Y. Yang, Y. Tao and H. Yang, "Correlation of Photoluminescence of (La,Ln)PO$_4$:Eu^{3+} (Ln = Gd and Y) Phosphors with Their Crystal Structures," *J Nanopart Res*, **10** 1355-60 (2008).

[31] M. Ferhi, K. Horchani-Naifer and M. Férid, "Combustion Synthesis and Luminescence Properties of LaPO$_4$: Eu (5%)," *J. Rare Earth*, **27** [2] 182-6 (2009).

SECTION

3.   **AFTERWORDS**

This section provides a summary of the conclusions drawn from the work in this dissertation. Additionally, recommendations for future experiments are provided.

1. A technique for using μ-Raman spectroscopy to analyze borate glass dissolution kinetics was developed. Glass dissolution exhibited linear kinetics for binary $Na_2O-B_2O_3$ glasses and parabolic kinetics for ternary $Na_2O-CaO-B_2O_3$ glasses. The formation of a calcium phosphate layer on the glass surface contributed to diffusion-controlled dissolution. The coordination of boron in the solution was determined to be dependent on solution pH. A relationship between Raman peak areas associated with stretching modes of three- and four-coordinated boron and pH was determined, and can be used to measure the solution pH in the range of 8-10. The pH, and therefore the fraction of four-coordinated boron in solution, increased as the modifier content of the glass increased. Dissolution of the borate glass was affected by the network modifier. Dissolution rate does not directly correlate with the fraction of four-coordinated boron in the glass.

2. Static dissolution kinetics of 13-93B3 in water were determined to initially follow a reaction-controlled kinetic model. As the glass dissolved, an ACP layer precipitated on the glass surface, and after the glass was ~25% reacted, the boron release kinetics transitioned to a diffusion-controlled model. This work suggests that an amorphous precipitation layer may cause diffusion of either water species to the glass surface or glass components into solution.

3. Formation of calcium phosphate phases following glass dissolution was found to be heavily dependent on solution chemistry. A high Ca/P ratio in solution leads to an ACP layer with a Ca/P ratio higher than stoichiometric HAP. Under the high Ca/P solution conditions, recrystallization from ACP to HAP was unlikely to occur. In-vitro experimental conditions can be altered to achieve the desired precipitation phase

4. Dissolution kinetics of 13-93B3 were studied under dynamic conditions in water and SBF. The glass dissolution rate decreased as flow rate decreased and glass volume increased. As the boron concentration in solution increases, the dissolution of the borate network is suppressed, even at <10% of the B solubility limit. This negative effect on dissolution rate is similar to those seen in silicate glasses, though in those cases, Si is much closer to the solubility limit. Calcium addition to the water slows the dissolution rate of the glass. The calcium release from the glass is suppressed the most, but an effect is seen on all elements. Dissolution in SBF is faster than in water. The presence of phosphate in the SBF allows for the precipitation of more calcium phosphate and therefore lessens the effect of [Ca].The lower pH of SBF contributes to the faster dissolution rate in SBF than water.

5. Nanocrystalline rare earth phosphate solid solutions were prepard by dissolution-precipitation reactions between soluble rare earth-doped borate glasses and a phosphate solution. The nanocrystalline material formed a hollow mesoscopic structure based on the size and shape of the initial glass particles. This is the first reported instance of solid solution phosphate materials being formed by this

glass dissolution-precipitation method. The precipitated materials are x-ray amorphous and they crystallize following heat-treatment. A negative correlation is observed between P-O bond length and Raman shift. Emission spectra indicate that the Eu^{3+} ions are in a more centro-symmetric environment when Eu-contents are low.

Recommendations for future work:

1. While this work provided valuable information for characterizing borate glass dissolution by μ-Raman spectroscopy, there is opportunity for expanding this technique. The concentration dependence of the borate peak areas was determined at only one pH value and may vary greatly at different pH values. Quantitative NMR performed on these solutions would provide quantitative information on the contribution of each $B(OH)_3$ and $B(OH)_4^-$ species to the total peak area. Having quantitative speciation information and pH dependence of the Raman cross-sections would allow characterization of boron release at a wider range of pH values. The pH dependence of phosphate and other anion speciation in solution would also allow for pH measurement at a wider range of pH values. In particular, the speciation between HPO_4^{2-} and $H_2PO_4^-$ anions or H_2CO_3 and HCO_3^- anions would be useful at biological pH values. A reaction cell that is designed for dissolution in the Raman spectrometer and the use of a high magnification immersion microscope objective would allow *in-situ* characterization under flowing environments. Additionally, a higher magnification objective would allow accurate measurements of ion concentration or pH away from a glass surface and in conjunction with Raman confocality, can determine the thickness of precipitated phosphate layers. There is also the potential opportunity to characterize changes in glass structure near the surface during dissolution.

2. SPFT experiments performed at a faster flow rate should eliminate the effects of ion concentration on glass dissolution rate. The forward dissolution rate could provide insight into how fast hydrolysis of a borate network can occur. SPFT

experiments at multiple temperatures would determine the true activation energy for dissolution of a glass. Additionally, forward dissolution rates measured for other glasses could provide more insight into the compositional dependence of borate glass dissolution. SPFT dissolution testing of new glass compositions in SBF can provide information which will accurately reflect how such glasses will behave *in-vivo*.

APPENDIX A:
STATIC DISSOLUTION OF 13-93B3 IN SIMULATED BODY FLUID

INTRODUCTION

During this study, there was evidence that solution B and Ca concentrations could affect dissolution rate and formation of calcium phosphate phases. The data presented in papers 2 and 3 suggested that an increase in solution [B] concentration would suppress dissolution rate. Additionally, data suggests that when there is an excess of Ca in solution relative to P that reacted calcium phosphate layers may have a Ca/P ratio higher than that of stoichiometric HAP. The reaction layers with higher Ca/P ratios remain x-ray amorphous rather than crystallize to HAP. Based on the results of Paper 2 and Paper 3, experiments with a high glass-to-solution volume ratio should dissolve slower than experiments with low glass-to-solution volume ratios. Additionally, high glass-to-solution ratios will release more Ca into solution, which may result in an ACP reaction product rather than HAP. A static dissolution experiment was designed where particle size and glass-volume-to-solution-volume was systematically varied.

EXPERIMENTAL PROCEDURE

Glass preparation: A glass, designated 13-93B3, with the nominal composition (wt%) 12 K_2O – 6 Na_2O – 20 CaO –5 MgO – 53 B_2O_3 –4 P_2O_5 was prepared by conventional melt quenching techniques. The raw materials, H_3BO_3 (98%, Alfa Aesar), $CaCO_3$, (98%, Alfa Aesar), K_2CO_3, (99%, Alfa Aesar), Na_2CO_3 (98%, Alfa Aesar), $MgCO_3$ (USP/FCC grade, Fisher Scientific), and $NH_2H_2PO_4$ (98%, Alfa Aesar), were mixed and melted in air for one hour at 1075°C in a Pt-Rh crucible. The melt was quenched between two steel plates to form glass that was stored in a desiccator. Prior to dissolution experiments, glass was crushed to particles with a porcelain mortar and pestle.

Three ranges of particle sizes are used for this experiment: 75-150 μm, 150-300 μm, and 425-500 μm.

Static dissolution experiments: Glass particles with weights of 30, 200, and 500 mg were rinsed in ethanol to remove fines, added to a polypropylene conical tube with 50 mL of simulated body fluid (SBF), and placed on their side in a Lab-Line Orbit Microprocessor shaker bath at 37 °C. SBF was prepared as described in Paper III. Particles were distributed along the bottom of the container to ensure maximum exposure to solution. At times 0.5, 1, 2, 4, 6, 8, 12, 16, 24, 48, 96, and 240 h the aliquots of 100 μL were sampled from the vials and added to 10-15 mL 1% HNO_3. Samples were removed from the oven and particles were collected with 8 μm filter paper from solutions at 6, 12, 24, 38, 96, and 240 h. Particles were rinsed twice with deionized water and twice with ethanol, then dried overnight at 100 °C. The dilute solution (1:100-1:150 with 1 vol% HNO_3) was used for elemental analysis using inductively-coupled plasma optical emission spectroscopy (ICP-OES, PerkinElmer Optima 2000 DV, Norwalk, USA). X-ray diffraction (XRD) was used to characterize the as-reacted particles using a Philips X'pert multipurpose diffractometer with PIXcel detector, with Cu K_α radiation and Ni filter, at 45 kV and 40 mA.

RESULTS AND DISCUSSION

All reaction products were x-ray amorphous at 1 d and 4 d. At 10 d, all 30 mg glass samples were crystalline hydroxyapatite (HAP) while the 200 mg and 500 mg glass samples were x-ray amorphous, shown in Figure A.1. For the 30 mg samples, as the particle size increased, the diffraction peak was more intense and had a smaller full-width half-max (FWHM), shown in Figure A.2, which indicates larger HAP crystals.

Figure A.3 shows the fraction of glass reacted as a function of time for all experiments. The 30 mg samples dissolved faster than the 200 mg or 500 mg samples, which were equally slow.

Figure A.4 shows the phosphorus and calcium concentration as a function of time for all experiments. The initial ion concentrations in SBF were measured and are 89.3±5.9 ppm Ca, 35.3±1.8 ppm Mg, and 34.1±2.4 ppm P. Following dissolution of 30 mg glass, there should be enough phosphorus in SBF to react with all of the calcium in the SBF and the calcium in the glass to form hydroxyapatite. For the 200 mg and 500 mg dissolution studies, all of the phosphorus should react with calcium to form HAP and once the phosphorus is depleted, an excess of calcium will be released from the glass into solution. The 30 mg samples all showed a minimum in calcium concentration at the 4 d mark, which also coincides with a near-depletion fo the phosphate in the SBF. The calcium concentration then increases to approximately 100 ppm for the 10 d samples. This suggests that the calcium in SBF and the calcium released from the glass are reacting with the phosphate in the solution to form amorphous calcium phosphate. By 4d, the remainder of the calcium in the glass is released into solution, which accounts for the increase. Assuming all of the phosphate reacts with calcium to form HAP, the residual calcium concentration will be 80 ppm. The solutions still contain ~ 10 ppm phosphate at 4 d. Accounting for this residual phosphate, the calcium release assuming stoichiometric HAP formation will be 96 ppm, which is consistent with the data shown in Figure A.4.

Figure A.5 compares the boron release from this experiment to the data collected and shown in Paper II, (200 mg, 150-300 μm, 37°C SBF or water). For the SBF

experiments, the boron is released to solution faster than the water experiments. This is

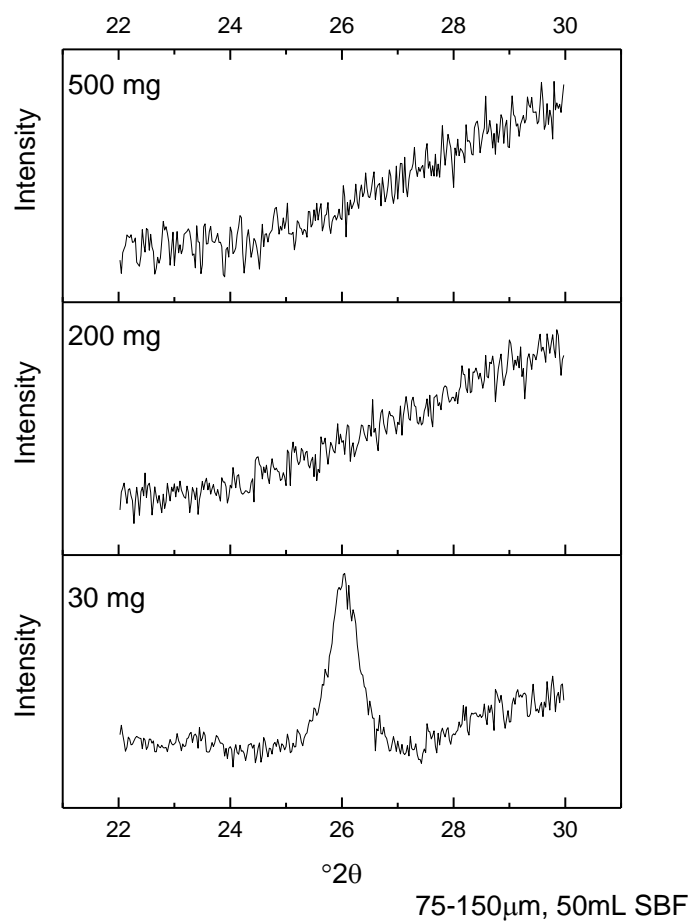consistent with the results seen between water and SBF in Paper III.

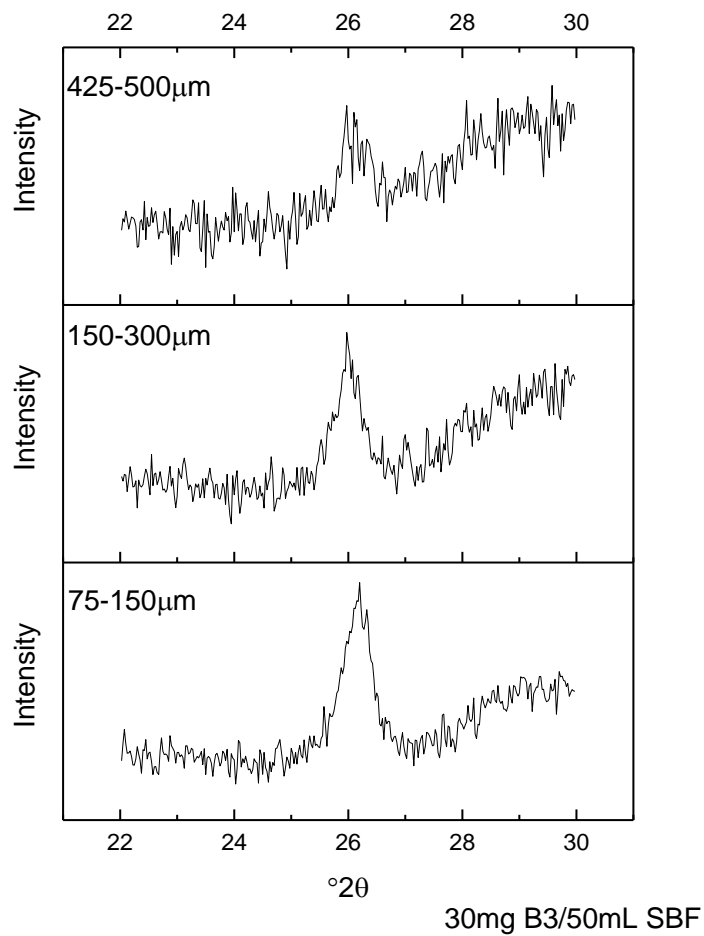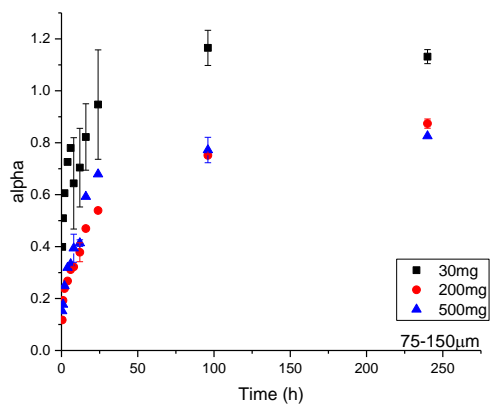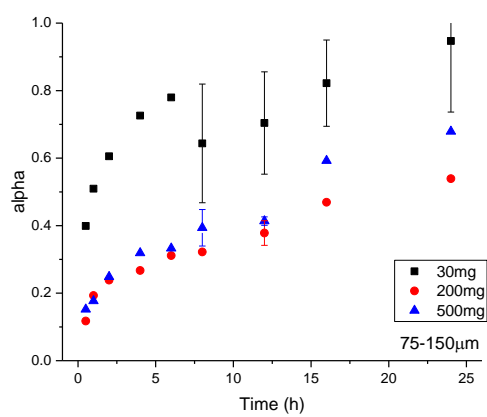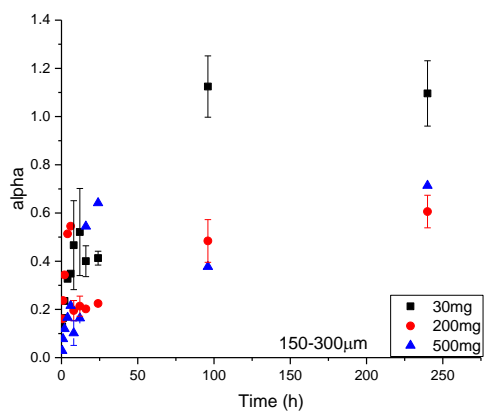Figure A.1. X-ray diffraction pattern for 13-93B3 glass dissolved in SBF for 10d.

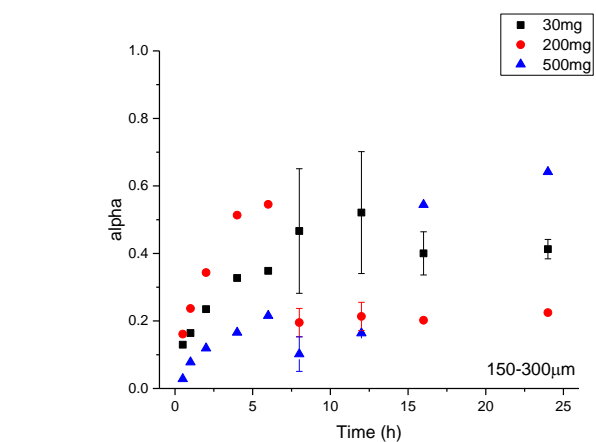Figure A.2. X-ray diffraction pattern for 30 mg 13-93B3 glass samples at 10d.
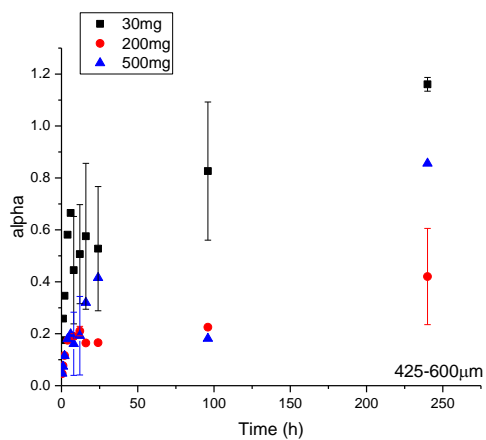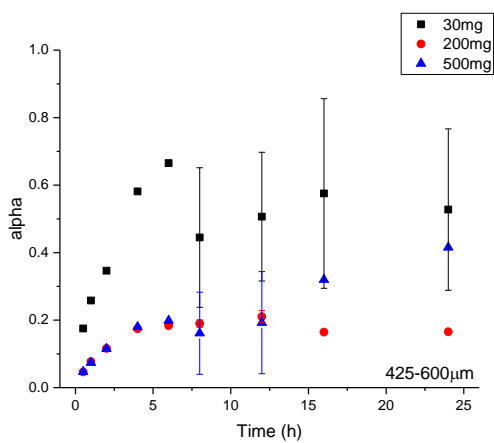
(a)

(b)

(c)

(d)

(e)

(f)

Figure A.3. Fraction of glass reacted, alpha, as a function of time for 75-150 μm particles at all times (a) and short times (b), 150-300 μm particles at all times (c) and short times (d), and 425-600 μm particles at all times (e) and short times (f)
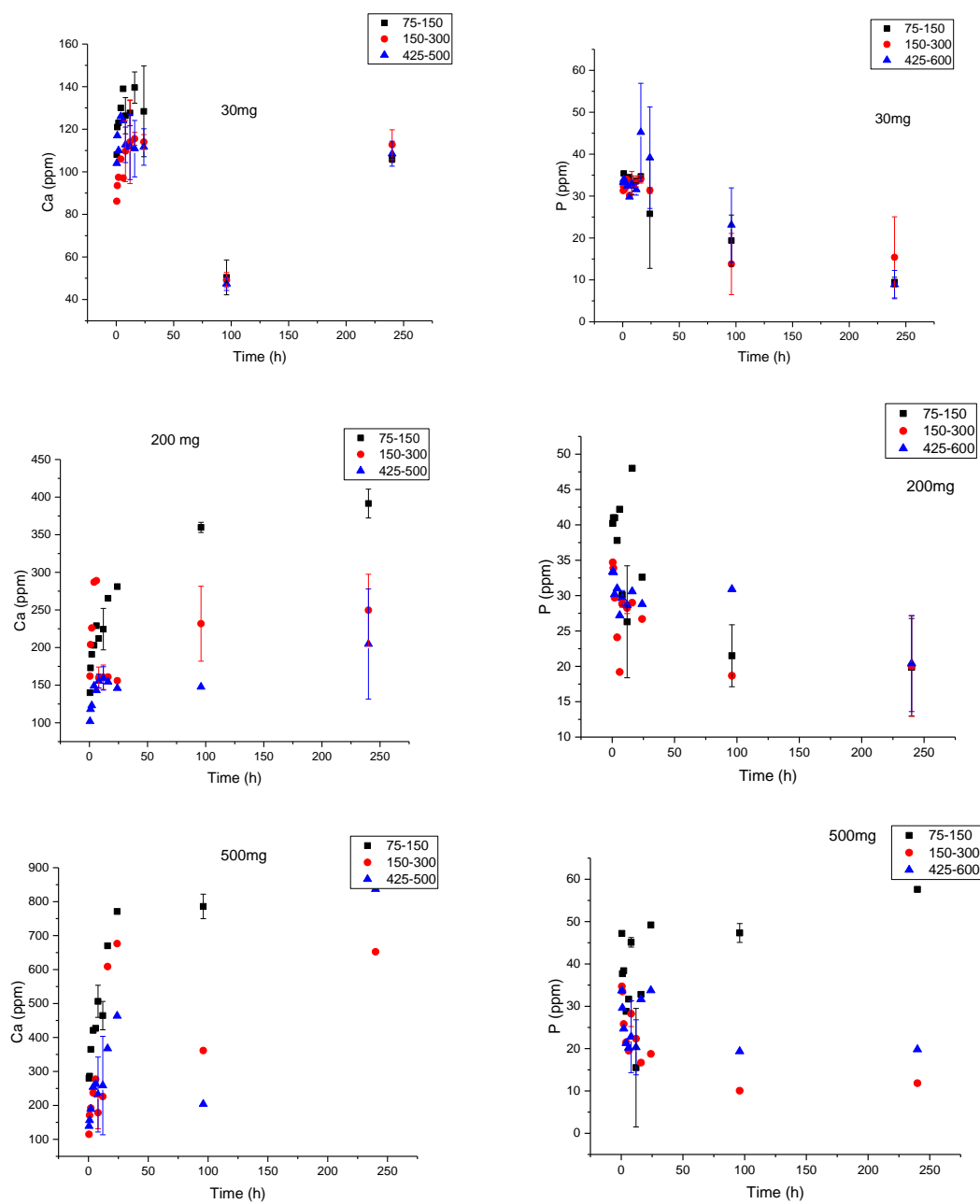
Figure A.4. Phosphorus concentration following dissolution of (a) 30mg, (b) 200mg, and (c) 500mg of 13-93B3 in SBF.
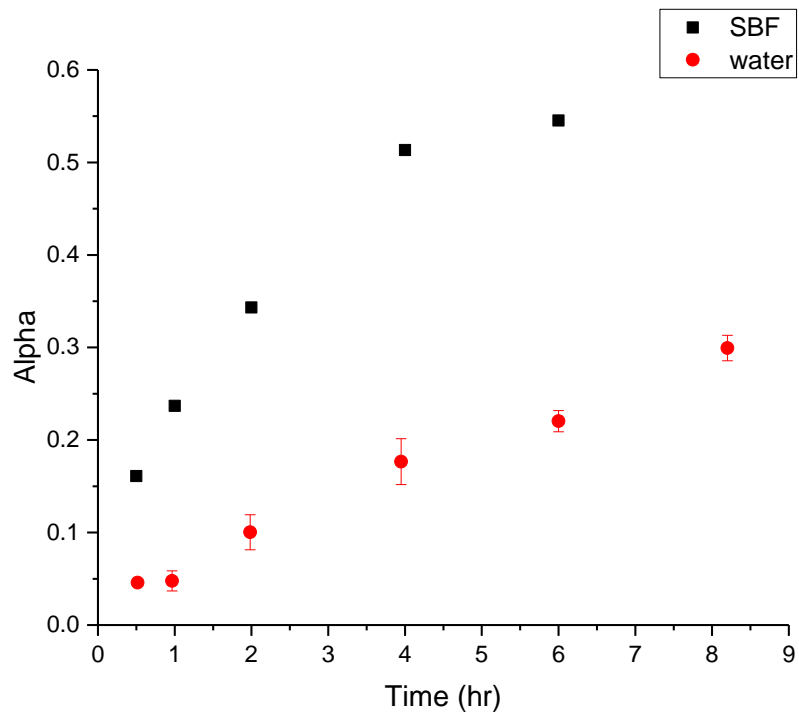
Figure A.5. Comparison of glass dissolution in SBF in water (200 mg, 150-300 μm, 37°C)

APPENDIX B:
RAMAN MEASUREMENTS OF BORON CONCENTRATIONS AS A
FUNCTION OF DISTANCE FROM THE GLASS SURFACE

One of the goals of this work was to measure boron concentration gradients as a function of distance from the surface of a dissolving glass. The Raman microscope is equipped with a motorized stage which allows controlled movement of the sample in 1 μm increments in the x, y, or z directions. In Paper I, Raman spectra were collected on solutions at distances of 30-1000 μm from the dissolving glass surface. This appendix highlights the results of two glasses which were studied in Paper I, $20Na_2O-80B_2O_3$ and $5Na_2O-15CaO-80B_2O_3$.

Figure B.1 shows the area of the peaks for $B(OH)_3$ (A_{876}) and $B(OH)_4^-$ (A_{745}) normalized to the area for HPO_4^{2-} (A_{989}) at distances of 30-1000 μm for the $20Na_2O-80B_2O_3$ and $5Na_2O-15CaO-80B_2O_3$ glasses studied in Paper I. For the sodium calcium borate glass, the spectra collected at 30 μm from the surface had larger borate peak areas relative to phosphate peak area than the spectra collected at 120-1000 μm at all time points. The spectra collected at 120 μm, 500μm, and 1000 μm were constant. This suggests that at 30 μm from the glass surface, the boron concentration is higher than at 120 μm or further from the glass surface. A similar trend is observed for the $20Na_2O-80B_2O_3$ glass. At the earlier time points (<1 h), the boron concentration is the highest at 30 μm and then steadily decreases. At the later time points, there is less of an effect on distance from the surface, as evidenced by the shallower slopes. For the $5Na_2O-15CaO-80B_2O_3$ glass, the peak areas ratios are summarized in Figure B.2. The 30 μm distance consistently has a higher boron concentration than the 120 μm spot.

Based on the results of these experiments, any ion concentration away from a dissolving glass surface occurs within the first ~100 μm away from the surface. Since all spectral measurements were made through a 10x microscope objective, the spatial

resolution is limited to ~50 μm. With a higher magnification (63x) immersion objective,

the spatial resolution can be increased to a few microns.

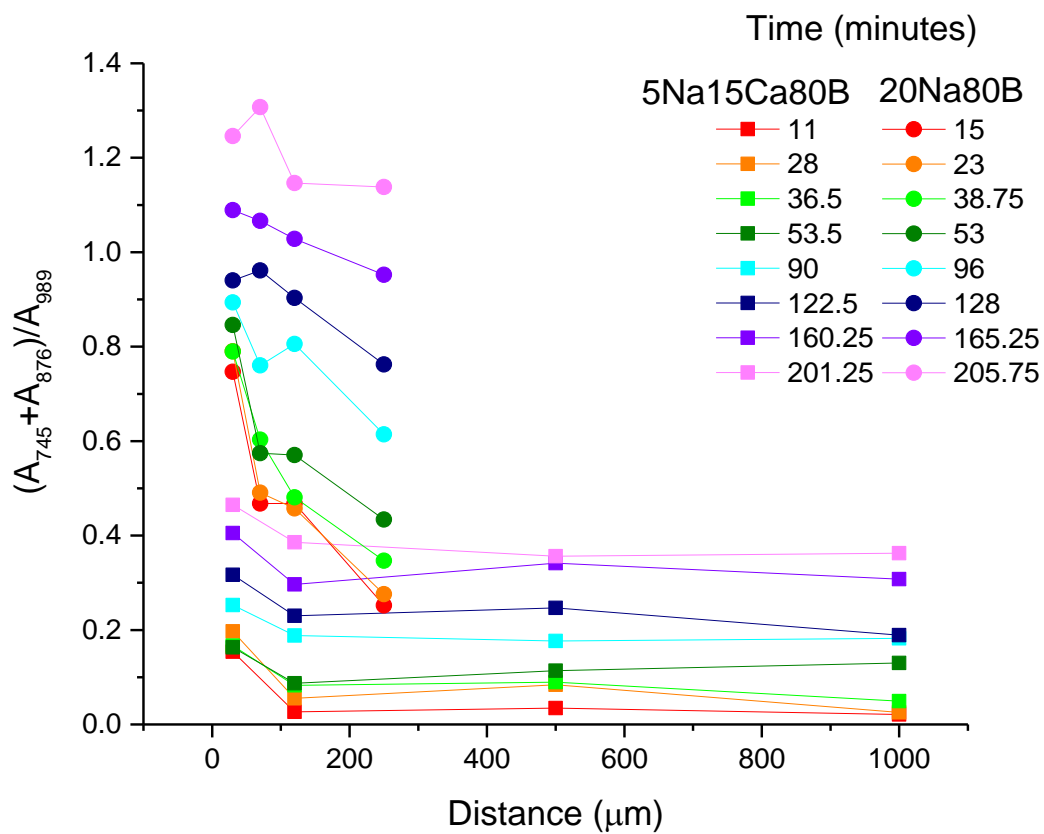Figure B.1. Boron peak areas normalized to phosphate peak areas as a function of distance away from the surface for $20Na_2O-80B_2O_3$ and $5Na_2O-15CaO-80B_2O_3$ glasses.
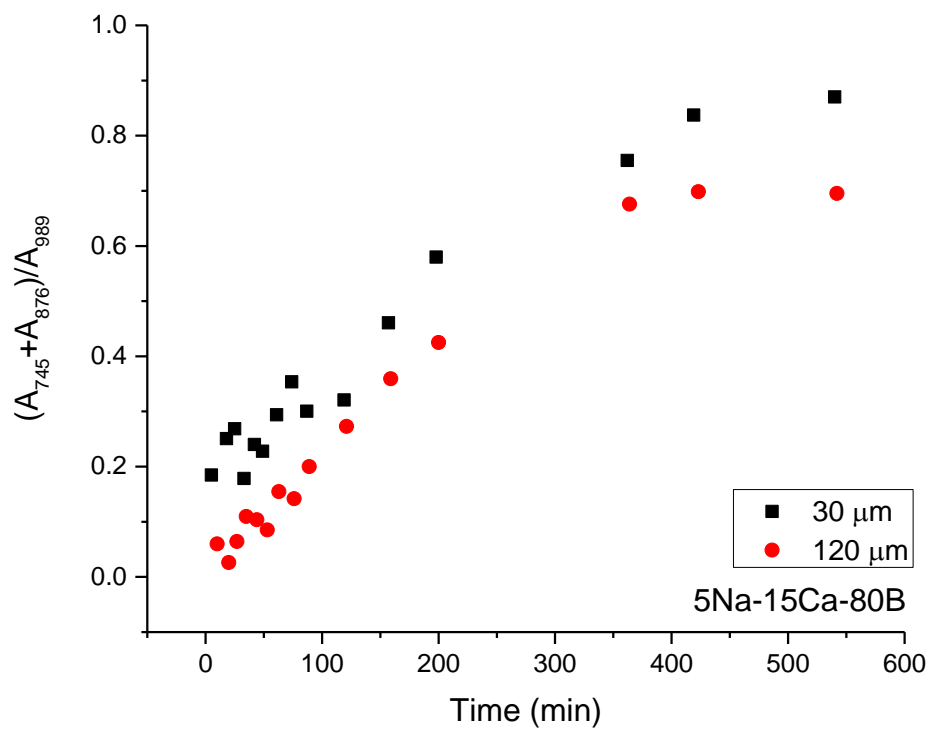
Figure B.2. Boron peak areas normalized to phosphate peak areas as a function of time, collected at 30 and 120 μm from the surface, for 5Na$_2$O-15CaO-80B$_2$O$_3$ glass dissolved in 0.1 M K$_2$HPO$_4$.

APPENDIX C:
SOLUTION COMPOSITION AND PH FOR CALIBRATION SOLUTIONS IN
PAPER I

This appendix provides a summary of the solutions used to prepare the concentration and pH calibration curves in Paper I. Table C.1 summarizes the solutions used for the concentration calibration curve. The phosphate concentration and pH are held relatively constant and the boron concentration is varied. Table C.2 summarizes the solutions used for the pH calibration curve. Either deionized water or 0.1 M K_2HPO_4 are used as the base solution and either 300, 1000, or 2000 ppm B is added from H_3BO_3. The pH was adjusted with NaOH or an H_3PO_4/H_3BO_3 mixture.

Table C.1. Boron concentrations (ppm) and pH values for series 1 solutions containing 0.1 M K_2HPO_4, H_3BO_3, and NaOH.

Series 1	
0.1 M K_2HPO_4	
[B]	**pH**
100	8.82
250	8.81
500	8.82
750	8.76
1000	8.82
1250	8.78
1500	8.73
2000	8.77

Table C.2. Boron concentrations (ppm) and pH values for series 2 solutions containing H_3BO_3; 0.1 M K_2HPO_4 or water; and NaOH or H_3BO_3/H_3PO_4 mixture.

Series 2		Series 3		Series 4		Series 5	
0.1 M K_2HPO_4		0.1 M K_2HPO_4		0.1 M K_2HPO_4		deionized water	
[B]	pH	[B]	pH	[B]	pH	[B]	pH
300	7.42	1000	7.34	2000	7.25	1000	11.83
300	7.95	1000	7.71	2000	7.62	1000	10.51
300	8.25	1000	8.06	2000	8.01	1000	9.78
300	8.67	1000	8.78	2000	8.58	1000	8.86
300	8.97	1000	9.09	2000	9.16	1000	7.74
300	9.45	1000	9.45	2000	9.64	1000	5.67
300	9.88	1000	9.78	2000	10.09	1000	4.86
300	11.11	1000	10.48	2000	10.89		

VITA

Jaime Lynn George was born to Michael and Patricia George on October 28, 1987 in Hornell, NY. She graduated from Hornell Senior High School in June 2005. She enrolled at Alfred University in August 2005. During her undergraduate career she served as President of the New York Chapter of Keramos. She graduated in May 2009 magna cum laude with a B.S. in Biomedical Materials Engineering Science and a minor in Chemistry. She served on the American Ceramic Society's President's Council of Student Advisors from 2009-2011. She received her Ph.D. in Materials Science and Engineering in May 2015 under the supervision of Dr. Richard K. Brow.